ONE-DIMENSIONAL PLASMONS CONFINED IN BILAYER GRAPHENE P-N JUNCTIONS

by

Nora M. Hassan

A thesis submitted to the faculty of
The University of Utah
in partial fulfillment of the requirements for the degree of

Master of Science

in

Physics

Department of Physics and Astronomy

The University of Utah

August 2012

The University of Utah Graduate School

STATEMENT OF THESIS APPROVAL

The thesis of Nora M. Hassan
has been approved by the following supervisory committee members:

Eugene Mishchenko	, Chair	August 17th, 2011 Date Approved
Mikhail Raikh	, Member	August 15th, 2011 Date Approved
John Belz	, Member	August 22nd, 2011 Date Approved

and by David B. Kieda, Chair of
the Department of Physics and Astronomy

and by Charles A. Wight, Dean of The Graduate School.

ABSTRACT

We investigated one-dimensional plasmon propagation in bilayer graphene under the effect of in-plane electric field $\mathbf{E_0}$. Because of the gapless nature of graphene spectrum the applied electric field can induce separation of charges creating a p-n junction that split the width of the flake into positively and negatively charged halves. The fluctuations of the induced charge density and nonhomogeneity of charge distribution across the width of the flake underlie the propagation of one-dimensional plasmon along the p-n junction. The flake dimensions and electric field were chosen large enough to allow semiclassical treatment through the approximation of charge carriers as 2D fluid and the use of hydrodynamic model to obtain the dispersion relations. In the limit of short wavelength, even modes had higher energies than odd ones. Surprisingly, that behavior was reversed with the first even mode becoming the lowest mode in the limit of long wavelengths. In all cases the plasmon spectra were proportional to $\sqrt{E_0}$. We considered a second case where an additional perpendicular electric field was applied through a gate. In that case, the additional field created a gap in the spectrum of graphene resulting in a neutral strip along the flake. The spectrum was linear in electric field E_0 indicating more sensitivity to the applied field in gated bilayer than in gapless case.

CONTENTS

LIST OF FIGURES

ACKNOWLEDGEMENTS

I would like to express deep gratitude and appreciation to my supervisor, Professor Mishchencko, for his patience in teaching me and sincerity in advising and guiding me. I am grateful that he agreed to spend the time and effort to teach me quantum field theory as a reading course. I was very fortunate to get the opportunity to work with him on a research project as I got the chance to learn from him skills I would not have been able to acquire from textbooks; I learned techniques to approach and solve problems, and methods to interpret the mathematical results into physics phenomena. It was a pleasure to work with such a supportive and dedicated supervisor. Without his offering to work on this project and his constant feedback, I would not have been able to finish with a degree from the University of Utah or publish my first paper. I am grateful that Professor Mishchencko supported my decision to study particle physics at a different university and I am indebted to him for the chance I got at Johns Hopkins and other opportunities I might get in the future.

In addition, I would like to thank Professor Mkhitaryan for his great contribution to the current work; without his input this project would not have taken its current final form. His ideas and discussion with Professor Mishchencko helped us gain more understanding of the problem and expand the project. I am grateful for his dedication to the project and his sincerity in helping me with the difficulties I had.

I would like to express my appreciation and respect to Professor Raikh whom I met during my first year at the University of Utah. I asked his advice on a few occasions and he was kind and sincere in offering his advice. I was lucky to attend the common exam preparation session he taught and his class where he showed great passion in teaching students. From my experience the best in-class courses I have taken were the ones where the teacher lectures with passion for the material and love for teaching; the course I took with Professor Raikh was one of those very few classes.

Last but not least, I owe my mother everything. I would not have gone anywhere without her encouragement, support and belief in me. I am lucky to have such an unconventional and strong mother. Also, I would like to express my appreciation to my late father for his

encouragement and progressiveness and to my friends at the University of Utah, especially Shirin Jamali and Song, for their help and support during my studies here.

CHAPTER 1

INTRODUCTION

Graphene, a one-atom thick 2D layer of carbon atoms arranged in honeycomb lattice, is under extensive theoretical [4] and experimental [12, 10, 1] investigation due to its unique electronic properties that make it a very promising material for nanoelectronics [9]. It also exhibits exotic physical phenomena like quantum hall effect [19, 21] making it a good material for fundamental research. Its exceptional transport and optical properties are due to its unusual band structure. Because of the linearity of energy in momentum, charge carriers in graphene exhibit relativistic behavior, a new realm in condensed matter. As a result, electrons, under the effect of periodic potential of nuclei, behave as if they have velocities that may reach 10^6 m/s, making graphene a good candidate for small and faster electronics. The gapless nature of graphene spectrum makes it metal-like with high conductivity. This also adds to its versatility due to the relative easiness of inducing charges on its surface by applying electric fields. Even though the gapless nature of its spectrum limits its applications to semiconductor technology, it enabled experimentalists to induce a tunable band gap in bilayer graphene, by adding one [18] or two gates [22], and thus opening new grounds in transistor technology.

The recent success of graphene extraction by micromechanical exfoliation of graphite [11] has opened new grounds for research and made graphene based applications possible in the near future. In that spirit our work investigates plasmon propagation in bilayer graphene, a practical study for plasmon transistor technology. This work is an extension of the study done in [6] that investigated the spectrum of plasmon propagating along p-n junction in monolayer graphene. Unlike previous research, applying electric field to graphene allows tune-ability of plasmon spectrum because eigenfrequencies proved to depend on the amplitude of the electric field. The objective of this study is to understand the behavior of plasmon spectrum and its dependence on the applied field in bilayer graphene. We studied two cases of gapless and bandgapped bilayer graphene. The quadratic dispersion of bilayer graphene made it possible to treat the system as two-dimensional electron gas (2DEG) and

use hydrodynamics equations for eigenfrequency calculations.

In this work a brief introduction is given to the different methods or theories used in developing our solutions. An introduction to the band structure of monolayer and bilayer graphene is presented in Chapter 2 to conclude with the dispersion relation used in subsequent calculations. Plasmons and plasma oscillations were explained briefly in Chapter 3. Thomas-Fermi method is discussed in Chapter 4 to prove the Thomas-Fermi integral equation used in calculating the induced equilibrium charge density in bilayer graphene. One of the three equations used in the hydrodynamics approximation of charge carriers in graphene is derived in Chapter 5 to give way to the main work discussed in Chapters 6 and 7. The first case of plasmon spectra propagating along gapless bilayer graphene is treated in Chapter 6. The calculation starts with finding induced charged density under the effect of applied in-plane electric field by solving the Thomas-Fermi integral equations. The calculated charge density is substituted into hydrodynamic equations to reach an integro-differential equation that is partially solved and analyzed. Eigenfrequencies in band gapped bilayer graphene are worked out in Chapter 7. A summary of our results is given in Chapter 8.

CHAPTER 2

GRAPHENE ELECTRONIC BAND STRUCTURE

2.1 Band Structure for Single Layer Graphene

Graphene is a one-atom-thick layer of carbon atoms that are arranged in a 2D honeycomb crystal. Because the lattice is not invariant under translation from one lattice point to another in every direction, the honeycomb crystal is not a Bravais lattice. The crystal, however, is composed of two hexagonal lattices with one carbon atom on each lattice site, see Fig. 2.1. Also, it can be considered one hexagonal lattice with a basis of two carbon atoms located at each lattice point. The primitive vectors of the hexagonal lattice are:

$$\mathbf{a}_1 = \frac{3\,a_0}{2}\hat{\mathbf{x}} + \frac{\sqrt{3}\,a_0}{2}\hat{\mathbf{y}};\;\; \mathbf{a}_2 = -\sqrt{3}\,a_0\,\hat{\mathbf{y}} \tag{2.1}$$

where a_0 is the distance between two adjacent carbon atoms ($\approx 1.42\ ^o$A) and the magnitude of the primitive vectors $|a_1| = |a_2| \equiv a = \sqrt{3}\,a_0 = 2.46\ ^o$A. Any translation between sites **A** can be achieved by vectors of the form

$$\mathbf{R} = n\,\mathbf{a}_1 + m\,\mathbf{a}_2$$

where n and m are integers. Using the definition $a_i.b_j = \delta_{ij}$, we obtain the following reciprocal lattice vectors, see Fig. 2.2,

$$\mathbf{b}_1 = \frac{2}{3\,a_0}\hat{\mathbf{x}}\;\;;\;\; \mathbf{b}_2 = (\frac{1}{3\,a_0}\hat{\mathbf{x}} - \frac{1}{\sqrt{3}\,a_0}\hat{\mathbf{y}}) \tag{2.2}$$

The most important aspect of the reciprocal lattice is the first Brillouin zone, defined as the region bounded by lines bisecting vectors drawn from origin to nearest reciprocal lattice points, because we consider only wave vectors inside this region. The six corners of the first Brillouin zone are divided into two sets such that each set has three equivalent points. In other words, the equivalent points are those that can be translated to one another through a combination of reciprocal lattice vectors $\mathbf{b}_1$ and $\mathbf{b}_2$. Therefore, we can recognize two unique sites, one from each set, **K** and $\mathbf{K}'$, see Fig. 2.3.

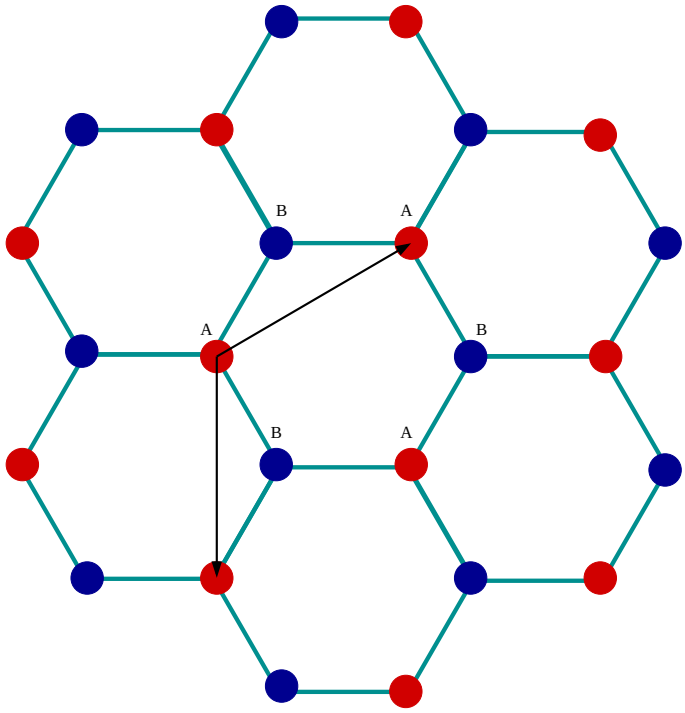

Figure 2.1: Honeycomb lattice of graphene. Atoms of a single color form a hexagonal lattice, and the two superimposed hexagonal lattices make a honeycomb structure or equivalently a hexagonal lattice with each unit cell consisting of two atoms. Black arrows show the primitive vectors $\mathbf{a}_1$ and $\mathbf{a}_2$.

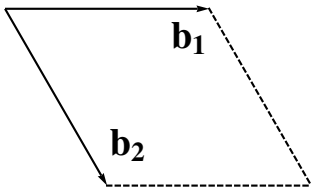

Figure 2.2: Reciprocal lattice vectors of a two-dimensional hexagonal lattice

In a honeycomb lattice each carbon atom bonds with three other carbon atoms. However, carbon has four valence electrons, two in $2s$ orbital and two unpaired ones in $2p_x$ and $2p_y$ orbitals. Thus, in its ground state, a carbon atom can only form two bonds through the unpaired electrons in the $2p$ state. Nonetheless, in the honeycomb lattice, one of the electrons in the $2s$ orbital is excited to the $2p_z$ orbital under the effect of the neighboring atoms. The $2s$, $2p_x$ and $2p_y$ states mix to form three hybrid orbitals called sp^2, arranged at angles of 120^o in the plane of the graphene layer, and leaving one unpaired electron in the $2p_z$ state. The three sp^2 orbitals are responsible for the formation of bonds among the

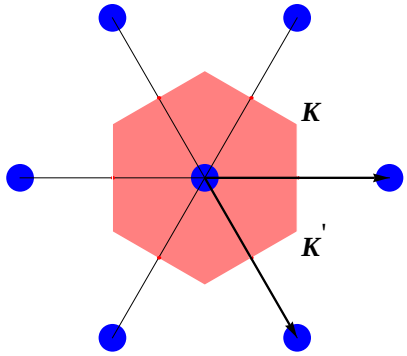

Figure 2.3: First Brillouin zone is shown in pink and lattice sites of the reciprocal lattice are shown in blue. Reciprocal lattice vectors are represented by the thick arrows. Two unique points, $\mathbf{K}$ and $\mathbf{K}^{'}$ cannot be connected with reciprocal lattice vectors, $\mathbf{b}_1$ and $\mathbf{b}_2$.

carbon atoms to assemble into a graphene sheet. The $2p_z$ electron is responsible for the conductivity and other electronic properties of graphene. The sp^2 wave function that solves the Schrödinger equation is a linear combination of the $2s$ and $2p$ orbitals [17],

$$\psi_{sp^2}(\mathbf{r}) = \frac{1}{\sqrt{3}}\psi_{2s}(\mathbf{r}) + \sqrt{\frac{2}{3}}\psi_{2p}(\mathbf{r})$$

To study the electronic properties of graphene, we need to compute the energy spectrum. In other words, the eigenvalues of the Schrödinger equation are derived to get a dispersion relation between the energy and wavenumber of electrons. All the calculations are done on the $2p_z$ orbital following the same procedure presented in Ref. [17], the first paper about graphene. Let the wave function of the unpaired $2p_z$ electron be the p orbital of hydrogen atom $\chi(\mathbf{r})$; this assumption introduces an approximation by ignoring the screening effects of the other carbon electrons, i.e., treating the multi-electron carbon like a hydrogen atom. The wave function of one electron in a graphene layer at position $\mathbf{r}$ is,

$$\Psi(\mathbf{r}) = A\psi_1 + B\psi_2 = A\sum_A e^{2\pi i \mathbf{k}.\mathbf{r}_A}\chi\left(\mathbf{r}-\mathbf{r}_A\right) + B\sum_B e^{2\pi i \mathbf{k}.\mathbf{r}_B}\chi\left(\mathbf{r}-\mathbf{r}_B\right) \qquad (2.3)$$

where $\mathbf{k}$ is the wave vector and $\mathbf{r}_A = n\mathbf{a}_1 + m\mathbf{a}_2$. The wave function is normalized, i.e., $A^2 + B^2 = 1$. The term $e^{2\pi i \mathbf{k}.\mathbf{r}}$ is due to the periodicity of the potential. According to Bloch's theorem, the wave function of a particle in a periodic potential is,

$$\psi_{n\mathbf{k}}(\mathbf{r}) = e^{2\pi i \mathbf{k}.\mathbf{r}} u_{n\mathbf{k}}\left(\mathbf{r}\right)$$

where $u_{n\mathbf{k}}\left(\mathbf{r}\right)$ is the wave function of a particle in a certain potential and $\mathbf{k}$ is the wave vector. In Eq. 2.3, ψ_1 is the wave function of an electron under the effect of the periodic

potential due to lattice points **A** and ψ_2 is the wave function of an electron under the effect of the periodic potential due to lattice points **B**. Therefore, $\Psi(\mathbf{r})$, the wave function of an electron at position $\mathbf{r}$ from the origin, is just the summation of χ orbitals of all carbon atoms in the bilayer graphene flake.

To find the energy spectrum, substitute the wave function Ψ into the the Schrödinger equation,

$$\hat{H}\Psi(\mathbf{r}) = E\,\Psi(\mathbf{r}), \tag{2.4}$$

Multiply both sides by ψ_1^* and integrate over volume,

$$\begin{aligned}
&\int d\tau\,\psi_1^*\,\hat{H}\Psi(\mathbf{r}) = \int d\tau\,\psi_1^*\,E\,\Psi(\mathbf{r}) \\
&\Rightarrow \int d\tau\,\psi_1^*\,\hat{H}\,[A\psi_1 + B\psi_2] = \int d\tau\,\psi_1^*\,E\,[A\psi_1 + B\psi_2] \\
&\Rightarrow A\int d\tau\,\psi_1^*\,\hat{H}\psi_1 + B\int d\tau\,\psi_1^*\,\hat{H}\psi_2 = A\int d\tau\,\psi_1^*\,E\,\psi_1 + B\int d\tau\,\psi_1^*\,E\,\psi_2
\end{aligned} \tag{2.5}$$

Let $\int d\tau\,\psi_1^*\,\hat{H}\psi_1 = H_{11}$, $\int d\tau\,\psi_1^*\,\hat{H}\psi_2 = H_{12}$ and $\int d\tau\,\psi_1^*\,\psi_1 = S$, and substitute for ψ_1 and ψ_2 from Eq. 2.3 into Eq. 2.5 to obtain,

$$A\,H_{11} + B\,H_{12} = A\,E\,S + B\,E\sum_A\sum_B e^{-2\pi i\mathbf{k}.(\mathbf{r}_A-\mathbf{r}_B)}\int d\tau\,\chi^*\,(\mathbf{r}-\mathbf{r}_A)\,\chi\,(\mathbf{r}-\mathbf{r}_B) \tag{2.6}$$

Because it is assumed that $2p_z$ orbitals centered on atoms at sites **A** do not overlap with orbitals centered on atoms at sites **B**, i.e.,

$$\int d\tau\,\chi^*\,(\mathbf{r}-\mathbf{r}_A)\,\chi\,(\mathbf{r}-\mathbf{r}_B) = 0 \tag{2.7}$$

Eq. 2.6 simplifies to,

$$A\,H_{11} + B\,H_{12} = A\,E\,S \tag{2.8}$$

Similarly, multiply Eq. 2.4 by ψ_2^* and integrate over volume to get the second equation,

$$A\,H_{21} + B\,H_{22} = B\,E\,S \tag{2.9}$$

where $\int d\tau\,\psi_2^*\,\hat{H}\psi_2 = H_{22}$, $\int d\tau\,\psi_2^*\,\hat{H}\psi_1 = H_{21}$ and $\int d\tau\,\psi_2^*\,\psi_2 = \int d\tau\,\psi_1^*\,\psi_1 = S$ due to symmetry between lattice sites **A** and **B**. Therefore, we can write Eq. 2.8 and Eq. 2.9 in the following matrix form,

$$\begin{pmatrix} H_{11} & H_{12} \\ H_{21} & H_{22} \end{pmatrix}\begin{pmatrix} A \\ B \end{pmatrix} = E\,S\begin{pmatrix} A \\ B \end{pmatrix} \tag{2.10}$$

The above equation is an eigenvalue problem that must be solve to find E. For A and B to have nontrivial solutions, the determinant of $\mathbf{H} - ES\mathbf{I}$, where $\mathbf{I}$ is the identity matrix, must be zero,

$$\begin{vmatrix} H_{11} - E\,S & H_{12} \\ H_{21} & H_{22} - E\,S \end{vmatrix} = 0$$
$$\Rightarrow (H_{11} - E\,S)\,(H_{22} - E\,S) - H_{12}H_{21} = 0$$

By solving the above equation, we get the following expression for the energy of electrons in graphene,

$$E = \frac{1}{2S}\left[H_{11} + H_{22} \pm \sqrt{(H_{11} - H_{22})^2 + 4H_{12}H_{21}}\right] \tag{2.11}$$

Because the Hamiltonian is hermitian, $\left(\int d\tau\, \psi_1^*\, \hat{H} \psi_2\right)^* = \int d\tau\, \psi_2^*\, \hat{H} \psi_1 \Rightarrow H_{21} = H_{12}^*$, we can simplify Eq. 2.11 to,

$$E = \frac{1}{2S}\left[H_{11} + H_{22} \pm \sqrt{(H_{11} - H_{22})^2 + 4|H_{12}|^2}\right] \tag{2.12}$$

To find the total energy, the terms S, H_{11}, H_{22} and H_{12} must be calculated. The constant S is,

$$S = \int d\tau\, \psi_1^*\, \psi_1 = \int d\tau \sum_A \sum_{A'} e^{2\pi i \mathbf{k}.(\mathbf{r}_{A'} - \mathbf{r}_A)} \chi^*\,(\mathbf{r} - \mathbf{r}_A)\,\chi\,(\mathbf{r} - \mathbf{r}_{A'})$$

where lattice sites $\mathbf{A}^{'}$ and $\mathbf{A}$ are positions on the same hexagonal lattice colored red in Fig. 2.1. Assuming no overlap of orbitals at different crystal sites, see Eq. 2.7, we get,

$$S = \sum_A \sum_{A'} e^{2\pi i \mathbf{k}.(\mathbf{r}_{A'} - \mathbf{r}_A)} \delta_{A\,A'} = N \tag{2.13}$$

where N is the number of unit cells in the crystal. The crystal sites at $\mathbf{A}$ and $\mathbf{B}$ are equivalent because both sets of points form hexagonal lattices. Therefore, the integrals $\int d\tau\, \psi_1^*\, \hat{H} \psi_1 = H_{11}$ and $\int d\tau\, \psi_2^*\, \hat{H} \psi_2 = H_{22}$ are equal, and Eq. 2.12 becomes,

$$E = \frac{1}{2S}\left[2H_{11} \pm \sqrt{4|H_{12}|^2}\right] = \frac{1}{N}\left[H_{11} \pm |H_{12}|\right] \tag{2.14}$$

From Eq. 2.14 it is obvious that H_{11} and H_{12} should be computed to obtain the spectrum of electrons in graphene. Starting with H_{11}, we obtain,

$$H_{11} = \int d\tau\, \psi_1^*\, \hat{H} \psi_1 = \sum_A \sum_{A'} e^{2\pi i \mathbf{k}.(\mathbf{r}_{A'} - \mathbf{r}_A)} \underbrace{\int d\tau\, \chi^*\,(\mathbf{r} - \mathbf{r}_A)\, \hat{H} \chi\,(\mathbf{r} - \mathbf{r}_{A'})}_{I}$$

The term denoted by I is the energy needed for an electron to hop from one $2p_z$ orbital at site $\mathbf{A}$ to another $2p_z$ orbital at site $\mathbf{A}^{'}$ of the same hexagonal lattice. For tight binding

approximation, only hopping between first and second nearest neighbors is considered. For one atom at site **A**, the summation is taken over sites $\mathbf{r}_{A'} = \mathbf{r}_A \pm \mathbf{a}_1$, $\mathbf{r}_{A'} = \mathbf{r}_A \pm \mathbf{a}_2$ and $\mathbf{r}_{A'} = \mathbf{r}_A \pm (\mathbf{a}_1 + \mathbf{a}_2)$ in addition to the case $\mathbf{r}_{A'} = \mathbf{r}_A$. Therefore, H_{11} expands to,

$$\begin{aligned}
H_{11} = &\sum_A \Bigg[\int d\tau\, \chi^* (\mathbf{r} - \mathbf{r}_A)\, \hat{H} \chi (\mathbf{r} - \mathbf{r}_A) \\
&+ e^{2\pi i \mathbf{k}.(\mathbf{r}_A \pm \mathbf{a}_1 - \mathbf{r}_A)} \int d\tau\, \chi^* (\mathbf{r} - \mathbf{r}_A)\, \hat{H} \chi (\mathbf{r} - (\mathbf{r}_A \pm \mathbf{a}_1)) \\
&+ e^{2\pi i \mathbf{k}.(\mathbf{r}_A \pm \mathbf{a}_2 - \mathbf{r}_A)} \int d\tau\, \chi^* (\mathbf{r} - \mathbf{r}_A)\, \hat{H} \chi (\mathbf{r} - (\mathbf{r}_A \pm \mathbf{a}_2)) \\
&+ e^{2\pi i \mathbf{k}.(\mathbf{r}_A \pm (\mathbf{a}_1 + \mathbf{a}_2) - \mathbf{r}_A)} \int d\tau\, \chi^* (\mathbf{r} - \mathbf{r}_A)\, \hat{H} \chi (\mathbf{r} - (\mathbf{r}_A \pm \mathbf{a}_1 \pm \mathbf{a}_2))] \Bigg] \\
= &\sum_A \Bigg[\int d\tau\, \chi^* (\mathbf{r} - \mathbf{r}_A)\, \hat{H} \chi (\mathbf{r} - \mathbf{r}_A) + e^{\pm 2\pi i \mathbf{k}.\mathbf{a}_1} \int d\tau\, \chi^* (\mathbf{r} - \mathbf{r}_A)\, \hat{H} \chi (\mathbf{r} - \mathbf{r}_A \mp \mathbf{a}_1) \\
&+ e^{\pm 2\pi i \mathbf{k}.\mathbf{a}_2} \int d\tau\, \chi^* (\mathbf{r} - \mathbf{r}_A)\, \hat{H} \chi (\mathbf{r} - \mathbf{r}_A \mp \mathbf{a}_2) \\
&+ e^{\pm 2\pi i \mathbf{k}.(\mathbf{a}_1 + \mathbf{a}_2)} \int d\tau\, \chi^* (\mathbf{r} - \mathbf{r}_A)\, \hat{H} \chi (\mathbf{r} - \mathbf{r}_A \mp \mathbf{a}_1 \mp \mathbf{a}_2)] \Bigg] \\
= &\sum_A \Bigg[\int d\tau\, \chi^* (\mathbf{r} - \mathbf{r}_A)\, \hat{H} \chi (\mathbf{r} - \mathbf{r}_A) + e^{2\pi i \mathbf{k}.\mathbf{a}_1} \int d\tau\, \chi^* (\mathbf{r} - \mathbf{r}_A)\, \hat{H} \chi (\mathbf{r} - \mathbf{r}_A - \mathbf{a}_1) \\
&+ e^{-2\pi i \mathbf{k}.\mathbf{a}_1} \int d\tau\, \chi^* (\mathbf{r} - \mathbf{r}_A)\, \hat{H} \chi (\mathbf{r} - \mathbf{r}_A + \mathbf{a}_1) \\
&+ e^{2\pi i \mathbf{k}.\mathbf{a}_2} \int d\tau\, \chi^* (\mathbf{r} - \mathbf{r}_A)\, \hat{H} \chi (\mathbf{r} - \mathbf{r}_A - \mathbf{a}_2) \\
&+ e^{-2\pi i \mathbf{k}.\mathbf{a}_2} \int d\tau\, \chi^* (\mathbf{r} - \mathbf{r}_A)\, \hat{H} \chi (\mathbf{r} - \mathbf{r}_A + \mathbf{a}_2) \\
&+ e^{2\pi i \mathbf{k}.(\mathbf{a}_1 + \mathbf{a}_2)} \int d\tau\, \chi^* (\mathbf{r} - \mathbf{r}_A)\, \hat{H} \chi (\mathbf{r} - \mathbf{r}_A - \mathbf{a}_1 - \mathbf{a}_2) \\
&+ e^{-2\pi i \mathbf{k}.(\mathbf{a}_1 + \mathbf{a}_2)} \int d\tau\, \chi^* (\mathbf{r} - \mathbf{r}_A)\, \hat{H} \chi (\mathbf{r} - \mathbf{r}_A + \mathbf{a}_1 + \mathbf{a}_2) \Bigg]
\end{aligned} \tag{2.15}$$

The last six integrals in Eq.2.15 are equivalent because the second nearest neighbors are at the same distance to site **A**. Therefore, the vectors $\mathbf{a}_1$, $\mathbf{a}_2$ and $(\mathbf{a}_1 + \mathbf{a}_2)$ can be replaced with the vector $\mathbf{\Lambda}_1 = \mathbf{a}_1$ or $\mathbf{a}_2$, and the integrals, $\int d\tau\, \chi^* (\mathbf{r} - \mathbf{r}_A)\, \hat{H} \chi (\mathbf{r} - \mathbf{r}_A \pm ...)$, can be written as,

$$\int d\tau\, \chi^* (\mathbf{r} - \mathbf{r}_A)\, \hat{H} \chi (\mathbf{r} - \mathbf{r}_A - \mathbf{\Lambda}_1)$$

Because the different sites in the graphene layer are equivalent due to symmetry, the second summation over atoms at sites **A** can be replaced by N, the number of unit cells

in the crystal. The origin can be taken arbitrarily at any carbon atom site to simplify the integrals to $\int d\tau\, \chi^*(\mathbf{r})\, \hat{H} \chi(\mathbf{r} - \mathbf{\Lambda}_1)$. Therefore, Eq. 2.15 simplifies to,

$$
\begin{aligned}
H_{11} &= N \int d\tau\, \chi^*(\mathbf{r})\, \hat{H} \chi(\mathbf{r}) + N \int d\tau\, \chi^*(\mathbf{r})\, \hat{H} \chi(\mathbf{r} - \mathbf{\Lambda}_1) \\
&\times \left(e^{2\pi i \mathbf{k}.\mathbf{a}_1} + e^{-2\pi i \mathbf{k}.\mathbf{a}_1} + e^{2\pi i \mathbf{k}.\mathbf{a}_2} + e^{-2\pi i \mathbf{k}.\mathbf{a}_2} + e^{2\pi i \mathbf{k}.(\mathbf{a}_1 + \mathbf{a}_2)} + e^{-2\pi i \mathbf{k}.(\mathbf{a}_1 + \mathbf{a}_2)} \right) \\
&= N \int d\tau\, \chi^*(\mathbf{r})\, \hat{H} \chi(\mathbf{r}) + N \int d\tau\, \chi^*(\mathbf{r})\, \hat{H} \chi(\mathbf{r} - \mathbf{\Lambda}_1) \\
&\times \Big[2\cos(2\pi \mathbf{k}.\mathbf{a}_1) + 2\cos(2\pi \mathbf{k}.\mathbf{a}_2) + 2\cos(2\pi \mathbf{k}.(\mathbf{a}_1 + \mathbf{a}_2)) \Big] \\
&= N \int d\tau\, \chi^*(\mathbf{r})\, \hat{H} \chi(\mathbf{r}) + N \int d\tau\, \chi^*(\mathbf{r})\, \hat{H} \chi(\mathbf{r} - \mathbf{\Lambda}_1) \\
&\times \Big[2\cos(2\pi(k_x a_{1x} + k_y a_{1y})) + 2\cos(2\pi(k_y a_{2y})) + 2\cos(2\pi(k_x a_{1x} + k_y a_{1y} + k_y a_{2y})) \Big] \\
&= N \int d\tau\, \chi^*(\mathbf{r})\, \hat{H} \chi(\mathbf{r}) + N \int d\tau\, \chi^*(\mathbf{r})\, \hat{H} \chi(\mathbf{r} - \mathbf{\Lambda}_1) \Big[2\cos(2\pi(k_x \frac{\sqrt{3}a}{2} + k_y \frac{a}{2})) \\
&+ 2\cos(2\pi(-k_y a)) + 2\cos(2\pi(k_x \frac{\sqrt{3}a}{2} + k_y \frac{a}{2} - k_y a)) \Big] \\
&= N \int d\tau\, \chi^*(\mathbf{r})\, \hat{H} \chi(\mathbf{r}) + N \int d\tau\, \chi^*(\mathbf{r})\, \hat{H} \chi(\mathbf{r} - \mathbf{\Lambda}_1) \\
&\times \Big[4\cos(\pi k_x \sqrt{3}a) \cos(\pi k_y a) + 2\cos(2\pi k_y a) \Big]
\end{aligned}
$$

where we have used the trigonometric identity $\cos(\theta \pm \phi) = \cos(\theta)\cos(\phi) \mp \sin(\theta)\sin(\phi)$ in the first and third terms in the fourth equality.

let $\int d\tau\, \chi^*(\mathbf{r})\, \hat{H} \chi(\mathbf{r} - \mathbf{\Lambda}_1) = -\gamma_0^{'}$, the experimentally measured in-plane hopping energy between second nearest neighbors, and $\int d\tau\, \chi^*(\mathbf{r})\, \hat{H} \chi(\mathbf{r}) = E_0$ is the energy of an electron in the $2p_z$ state. Therefore, H_{11} becomes,

$$
H_{11} = N \left[E_0 - 2\gamma_0^{'} \Big(2\cos(\pi k_x \sqrt{3}a) \cos(\pi k_y a) + \cos(2\pi k_y a) \Big) \right] \tag{2.16}
$$

To evaluate H_{12}, the same procedure is followed and we get,

$$
H_{12} = \int d\tau\, \psi_1^*\, \hat{H} \psi_2 = \sum_A \sum_B e^{2\pi i \mathbf{k}.(\mathbf{r}_B - \mathbf{r}_A)} \underbrace{\int d\tau\, \chi^*(\mathbf{r} - \mathbf{r}_A)\, \hat{H} \chi(\mathbf{r} - \mathbf{r}_B)}_{I}
$$

where the term I is the energy needed for an electron to hop from one $2p_z$ orbital at site **A** to another at site **B** and vice versa. For tight binding approximation, only hopping to nearest **B** sites is taken into account. Thus, for one atom at site **A**, the summation is taken only over

sites $\mathbf{r}_B = \mathbf{r}_A - a_0\hat{\mathbf{x}}$, $\mathbf{r}_B = \mathbf{r}_A + (a_0/2)\hat{\mathbf{x}} + (\sqrt{3}a_0/2)\hat{\mathbf{y}}$ and $\mathbf{r}_B = \mathbf{r}_A + (a_0/2)\hat{\mathbf{x}} - (\sqrt{3}a_0/2)\hat{\mathbf{y}}$. By substituting these values for $\mathbf{r}_B$, H_{12} becomes,

$$\begin{aligned} H_{12} = \sum_A \Bigg[& e^{2\pi i \mathbf{k}.(\mathbf{r}_A - a_0\hat{\mathbf{x}} - \mathbf{r}_A)} \int d\tau\, \chi^*(\mathbf{r}-\mathbf{r}_A)\, \hat{H}\chi(\mathbf{r}-\mathbf{r}_A+a_0\hat{\mathbf{x}}) \\ & + e^{2\pi i \mathbf{k}.(\mathbf{r}_A + (a_0/2)\hat{\mathbf{x}} + (\sqrt{3}a_0/2)\hat{\mathbf{y}} - \mathbf{r}_A)} \int d\tau\, \chi^*(\mathbf{r}-\mathbf{r}_A)\, \hat{H}\chi\left(\mathbf{r}-\mathbf{r}_A - \frac{a_0}{2}\hat{\mathbf{x}} - \frac{\sqrt{3}a_0}{2}\hat{\mathbf{y}}\right) \\ & + e^{2\pi i \mathbf{k}.(\mathbf{r}_A + (a_0/2)\hat{\mathbf{x}} - (\sqrt{3}a_0/2)\hat{\mathbf{y}} - \mathbf{r}_A)} \int d\tau\, \chi^*(\mathbf{r}-\mathbf{r}_A)\, \hat{H}\chi\left(\mathbf{r}-\mathbf{r}_A - \frac{a_0}{2}\hat{\mathbf{x}} + \frac{\sqrt{3}a_0}{2}\hat{\mathbf{y}}\right) \Bigg] \end{aligned}$$

The last three integrals are equivalent because the hopping energy of an electron from site **A** to any of its nearest neighbors is the same. Hence, the integrals can be written as $\int d\tau\, \chi^*(\mathbf{r})\, \hat{H}\chi(\mathbf{r}-\mathbf{\Lambda}_2)$ where $\mathbf{\Lambda}_2 = a_0\hat{\mathbf{x}}$, and the summation over atoms at sites **A** are replaced with N, the number of unit cells in the crystal. Let's denote the hopping energy $\int d\tau\, \chi^*(\mathbf{r})\, \hat{H}\chi(\mathbf{r}-\mathbf{\Lambda_2})$ by $-\gamma_0$. Therefore, H_{12} becomes,

$$\begin{aligned} H_{12} &= -N\gamma_0 \left[e^{-2\pi i \mathbf{k}.a_0\hat{\mathbf{x}}} + e^{2\pi i \mathbf{k}.((a_0/2)\hat{\mathbf{x}} + (\sqrt{3}a_0/2)\hat{\mathbf{y}})} + e^{2\pi i \mathbf{k}.((a_0/2)\hat{\mathbf{x}} - (\sqrt{3}a_0/2)\hat{\mathbf{y}})} \right] \\ &= -N\gamma_0 \left[e^{-2\pi i \mathbf{k}.a_0\hat{\mathbf{x}}} + 2\cos(\pi\, k_x a_0)\cos(\pi\, k_y\sqrt{3}a_0) + 2\, i \sin(\pi\, k_x a_0)\cos(\pi\, k_y\sqrt{3}a_0) \right] \\ &= -N\gamma_0 \left[e^{-2\pi i k_x a_0} + 2\cos(\pi\, k_y\sqrt{3}a_0) e^{i\,\pi\, k_x a_0} \right] \end{aligned}$$

By substituting $a_0 = a/\sqrt{3}$ the modulus of H_{12} becomes,

$$\Rightarrow |H_{12}| = \sqrt{H_{12}^* H_{12}} = N\,\gamma_0 \sqrt{\left[1 + 4\cos^2(\pi\, k_y a) + 4\cos(\pi\, k_y a)\cos(\sqrt{3}\pi k_x a)\right]}$$

From Eq. 2.14, the energy of an electron in a graphene layer is

$$\begin{aligned} E = E_0 - 2\gamma_0^{'} & \left(2\cos(\pi k_x\sqrt{3}a)\cos(\pi k_y a) + \cos(2\pi k_y a) \right) \\ & \pm \gamma_0 \sqrt{\left[1 + 4\cos^2(\pi\, k_y a) + 4\cos(\pi\, k_y a)\cos(\sqrt{3}\pi k_x a)\right]} \end{aligned}$$

Because hopping to the second nearest neighbor is much less probable than hopping to the nearest neighbor, i.e., $\gamma_0^{'} \approx 0.1\, eV \ll \gamma_0 \approx 2.8\, eV$, we can ignore the second term and write the energy as :

$$E - E_0 = \pm\gamma_0 \sqrt{\left[1 + 4\cos^2(\pi\, k_y a) + 4\cos(\pi\, k_y a)\cos(\sqrt{3}\pi k_x a)\right]} \tag{2.17}$$

where we are interested in the energy difference $E - E_0$. Eq. 2.17 is plotted in Fig.2.4 which shows the electronic band structure of graphene within the tight binding approximation. The spectrum exhibits very interesting behavior at certain points in k-space.

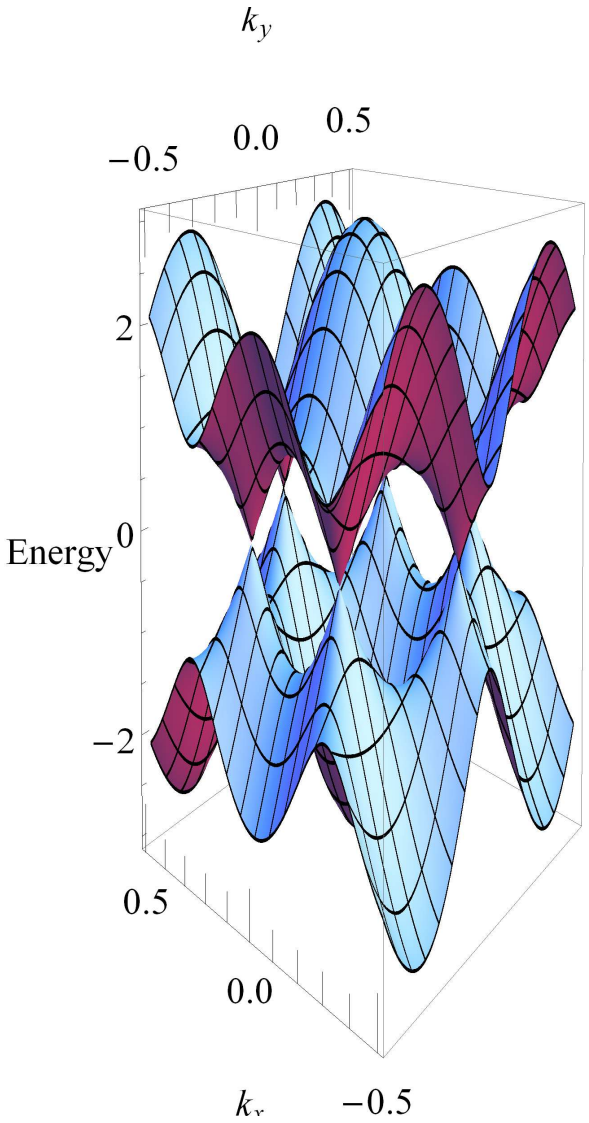

Figure 2.4: 3D plot of graphene spectrum; energy is plotted against wave numbers k_x and k_y, x and y components of k. The spectrum is gapless at the corners of the first Brillouin zone as the conduction and valence bands touch.

The energy $|E - E_0|$ vanishes as k_x and k_y take the following values,

$$\begin{aligned} k_x = \pm\frac{1}{\sqrt{3}a} \;;\; k_y = \pm\frac{1}{3a} \;\text{ or} \\ k_x = 0 \quad ;\; k_y = \pm\frac{2}{3a} \end{aligned} \tag{2.18}$$

The values in Eq. 2.18 are the x and y components of the wave vectors to the corners of the Brillouin zone, see Fig.2.3. The vanishing of the energy at these points means that the spectrum is gapless, i.e., the energy gap between the conduction and valence bands

is zero. To study the behavior of the spectrum very close to the Brillouin zone corners, called valleys of electronic spectrum, we expand Eq. 2.17 in terms of one of the Brillouin zone corner points, say $\mathbf{K}$, and small vector $\mathbf{q}$. Let $\mathbf{k} = \mathbf{K} + \mathbf{q}$, where $|\mathbf{q}|$ is very small. Therefore,

$$\begin{aligned}
\cos(\pi\, k_y a) &= \cos(\pi\,(K_y + q_y)a) = \cos(\pi\, K_y a)\cos(\pi\, q_y a) - \sin(\pi\, K_y a)\sin(\pi\, q_y a) \\
&= \frac{1}{2}\left(1 - \frac{(\pi\, q_y a)^2}{2!}\right) - \frac{\sqrt{3}}{2}(\pi\, q_y a) \\
\cos(\sqrt{3}\pi k_x a) &= \cos(\sqrt{3}\pi(K_x + q_x)a) \\
&= \cos(\sqrt{3}\pi\, K_x a)\cos(\sqrt{3}\pi\, q_x a) - \sin(\sqrt{3}\pi\, K_x a)\sin(\sqrt{3}\pi\, q_x a) \\
&= -1 + \frac{(\sqrt{3}\pi\, q_y a)^2}{2!}
\end{aligned}$$

where $K_x = \frac{1}{\sqrt{3}a}$, $K_y = \frac{1}{3a}$, see Eq. 2.18, and the trigonometric functions were approximated by taking their Taylor expansion $\cos(x) \approx 1 - x^2/2!$ and $\sin(x) \approx x$. This approximation is justified because $|\mathbf{q}|$ is taken to be very small; $|\mathbf{q}| \ll 1 \Rightarrow q_x a, q_y a \ll 1$. Substituting the above expressions for $\cos(\sqrt{3}\pi k_x a)$ and $\cos(\pi\, k_y a)$ into Eq. 2.17, we obtain,

$$E - E_0 = \pm\sqrt{3}\pi\gamma_0 a\sqrt{q_x^2 + q_y^2} \tag{2.19}$$

Therefore, we can write the electron spectrum in graphene as,

$$\boxed{\epsilon(\mathbf{q}) = E - E_0 = \pm\sqrt{3}\pi\gamma_0 a|\mathbf{q}| = \pm v_F \hbar q} \tag{2.20}$$

where $v_F = \sqrt{3}\pi a\gamma_0/\hbar$ is the Fermi velocity and $\hbar\, q$ is the electron momentum $|\mathbf{p}|$. By inserting the value of γ_0, ranging from -2.7 to -3.1 eV, into the expression for Fermi velocity we get $v_F \approx 1 \times 10^6 m/s$. This value for the Fermi velocity is exceptionally large and shows that electrons under the effect of the honeycomb potential of carbon atoms behave as if they were relativistic massless fermions in free space; in other words, the dispersion relation gives rise to phenomena as if Dirac fermions occupy the energy bands. It is noteworthy to compare Eq. 2.20 with the energy of a photon, $E = p\, c$; both are linear in momentum with Fermi velocity replacing the speed of light in graphene's case.

We could have arrived at the same dispersion relation, Eq. 2.20, if we solved the secular equation for the effective Hamiltonian,

$$H = \begin{pmatrix} H_{11}^{'} - E_0 & H_{12}^{'} \\ H_{21}^{'} & H_{22}^{'} - E_0 \end{pmatrix} \approx \begin{pmatrix} 0 & H_{12}^{'} \\ H_{12}^{'*} & 0 \end{pmatrix} = \begin{pmatrix} 0 & \hbar v_F(q_x + i\, q_y) \\ \hbar v_F(q_x - i\, q_y) & 0 \end{pmatrix} \tag{2.21}$$

where $H_{ij}^{'} = H_{ij}/N$. This matrix has the form of Dirac Hamiltonian for relativistic particles.

2.2 Band Structure of Bilayer Graphene

In this section we derive the spectrum of bilayer graphene which is composed of two AB stacked graphene layers. The wave function in bilayer graphene is:

$$\Psi(\mathbf{r}) = A\psi_1 + B\psi_2 + C\psi_3 + D\psi_4 = A\sum_A e^{2\pi i\mathbf{k}.\mathbf{r}_A}\chi\left(\mathbf{r}-\mathbf{r}_A\right) + B\sum_B e^{2\pi i\mathbf{k}.\mathbf{r}_B}\chi\left(\mathbf{r}-\mathbf{r}_B\right)$$
$$+C\sum_{\tilde{A}} e^{2\pi i\mathbf{k}.\mathbf{r}_{\tilde{A}}}\chi\left(\mathbf{r}-\mathbf{r}_{\tilde{A}}\right) + D\sum_{\tilde{B}} e^{2\pi i\mathbf{k}.\mathbf{r}_{\tilde{B}}}\chi\left(\mathbf{r}-\mathbf{r}_{\tilde{B}}\right)$$

where $\chi(\mathbf{r})$ is the wave function of the $2p_z$ electron in hydrogen atom. The wave function is normalized, i.e., $A^2+B^2+C^2+D^2=1$. ψ_1 and ψ_2 are the wave functions of an electron due to the periodic potential of lattice points $\mathbf{A}$ and $\mathbf{B}$ in the first layer of bilayer graphene, and ψ_3 and ψ_4 are the wave functions of an electron due to the periodic potential of lattice points $\tilde{\mathbf{A}}$ and $\tilde{\mathbf{B}}$ in the second layer. Thus, the wave function in bilayer graphene is the summation of all $2p_z$ orbitals, multiplied by a phase factor, due to all carbon atoms in the two layers.

Following the same procedure, Ψ is substituted into the the Schrödinger equation, multiplied by $\psi^*_{1,2,3,4}$ and integrated over volume to get the following four equations.

$$A\,H_{11} + B\,H_{12} + C\,H_{13} + C\,H_{14} = A\,E\,S \tag{2.22}$$

$$A\,H_{21} + B\,H_{22} + C\,H_{23} + D\,H_{24} = B\,E\,S \tag{2.23}$$

$$A\,H_{31} + B\,H_{32} + C\,H_{33} + D\,H_{34} = C\,E\,S \tag{2.24}$$

$$A\,H_{41} + B\,H_{42} + C\,H_{43} + D\,H_{44} = D\,E\,S \tag{2.25}$$

where $H_{i\,j} = H^*_{ji} = \int d\tau\,\psi^*_i\,\hat{H}\psi_j$, $S = \int d\tau\,\psi^*_i\,\psi_i = N$, $i = 1,2,3,4$ and $\int d\tau\,\chi^*\left(\mathbf{r}\right)\hat{H}\chi\left(\mathbf{r}\right) = E^{'}_0$ is the energy of an electron in the $2p_z$ orbital under the effect of the new Hamiltonian. Because we are interested in the energy difference $E - E^{'}_0$, the Schrödinger equation can be written as,

$$\begin{pmatrix} H^{'}_{11}-E^{'}_0 & H^{'}_{12} & H^{'}_{13} & H^{'}_{14} \\ H^{'}_{21} & H^{'}_{22}-E^{'}_0 & H^{'}_{23} & H^{'}_{24} \\ H^{'}_{31} & H^{'}_{32} & H^{'}_{33}-E^{'}_0 & H^{'}_{34} \\ H^{'}_{41} & H^{'}_{42} & H^{'}_{43} & H^{'}_{44}-E^{'}_0 \end{pmatrix} \begin{pmatrix} A \\ B \\ C \\ D \end{pmatrix} = \epsilon \begin{pmatrix} A \\ B \\ C \\ D \end{pmatrix} \tag{2.26}$$

where $H^{'}_{i\,j} = H_{i\,j}/N$ and $\epsilon = E - E_0$. By symmetry and from Eq. 2.16,

$$H_{11} = H_{22} = H_{33} = H_{44} = N\left[E^{'}_0 - 2\gamma^{'}_0\left(2\cos(\pi k_x\sqrt{3}a)\cos(\pi k_y a) + \cos(2\pi k_y a)\right)\right]$$

where $\gamma^{'}_0$ is the hopping energy between in-plane second nearest neighbor atoms, i.e., $\mathbf{A} \rightleftharpoons \mathbf{A}$, $\mathbf{B} \rightleftharpoons \mathbf{B}$, $\tilde{\mathbf{A}} \rightleftharpoons \tilde{\mathbf{A}}$ and $\tilde{\mathbf{B}} \rightleftharpoons \tilde{\mathbf{B}}$. Because the value of $\gamma^{'}_0$ is very small it will be ignored

in the following calculations. Thus, the diagonal of the Hamiltonian would be zero if the two layers were kept at zero potential. If however, the two layers were kept at different potentials, say upper layer at U and lower at $-U$, the diagonal would take the values $(U, U, -U, -U)$.

The four matrix elements: H_{12}, H_{21}, H_{34} and H_{43} are equivalent because they represent the probability of an electron hopping to nearest neighbor on the same layer, i.e., $\mathbf{A} \rightleftharpoons \mathbf{B}$ and $\tilde{\mathbf{A}} \rightleftharpoons \tilde{\mathbf{B}}$. The values of these terms were already calculated in Section 2.1; therefore, $H_{12} = H_{21}^* = H_{34}^* = H_{43} = v_F \hbar q$.

The matrix elements H_{13} and H_{31} are the probabilities that an electron hops from site $\mathbf{A}(\tilde{\mathbf{A}})$ on one layer to site $\tilde{\mathbf{A}}(\mathbf{A})$ on the second one. By using the same procedure, we obtain,

$$H_{13} = \int d\tau\, \psi_1^*\, \hat{H} \psi_3 = \sum_A \sum_{\tilde{A}} e^{2\pi i \mathbf{k}.(\mathbf{r}_{\tilde{A}} - \mathbf{r}_A)} \underbrace{\int d\tau\, \chi^* \left(\mathbf{r} - \mathbf{r}_A\right) \hat{H} \chi \left(\mathbf{r} - \mathbf{r}_{\tilde{A}}\right)}_{I} \tag{2.27}$$

where the term I is the energy needed for an electron to hop from one $2p_z$ orbital at site $\mathbf{A}(\tilde{\mathbf{A}})$ to another at site $\tilde{\mathbf{A}}(\mathbf{A})$. For tight binding approximation, only hopping to the nearest $\tilde{\mathbf{A}}(\mathbf{A})$ sites is taken into account which is the one directly above (below) it. Thus, for one atom at site $\mathbf{A}$ the displacement vector to the nearest $\tilde{\mathbf{A}}$ is $\mathbf{r}_{\tilde{A}} = \mathbf{r}_A \pm d\,\hat{\mathbf{z}}$ where $d = 3.35\ ^o\text{A}$ is the distance between graphene layers. By substituting these values for $\mathbf{r}_{\tilde{A}}$ at the nearest neighbors sites, H_{13} becomes,

$$H_{13} = \sum_A e^{2\pi i \mathbf{k}.(\mathbf{r}_A + d\,\hat{\mathbf{z}} - \mathbf{r}_A)} \underbrace{\int d\tau\, \chi^* \left(\mathbf{r} - \mathbf{r}_A\right) \hat{H} \chi \left(\mathbf{r} - \mathbf{r}_A - d\,\hat{\mathbf{z}}\right)}_{\gamma_1} = N e^{2\pi i k_z d} \gamma_1 \tag{2.28}$$

Therefore, the modulus of H_{13} is,

$$|H_{13}| = |H_{31}| = N\gamma_1 \tag{2.29}$$

Since the hopping energies from $\mathbf{A}$ $(\tilde{\mathbf{A}})$ to $\tilde{\mathbf{B}}(\mathbf{B})$ are in the order of 0.04 eV, we can neglect H_{14}, H_{23} and their conjugates. Also, because the hopping energy that connects $\mathbf{B}$ and $\tilde{\mathbf{B}}$, ≈ 0.3 eV, is smaller than the hopping energy between $\mathbf{A}$ and $\tilde{\mathbf{A}}$, H_{24} and its conjugate are ignored in the Hamiltonian. Thus after keeping only terms that represent hopping between in-plane nearest neighbors and between $\mathbf{A}$ and $\tilde{\mathbf{A}}$, the Hamiltonian for bilayer graphene kept at zero potential becomes,

$$H = \begin{pmatrix} 0 & H_{12}^{'} & H_{13}^{'} & 0 \\ H_{21}^{'} & 0 & 0 & 0 \\ H_{31}^{'} & 0 & 0 & H_{34}^{'} \\ 0 & 0 & H_{43}^{'} & 0 \end{pmatrix} = \begin{pmatrix} 0 & v_F \hbar q & \gamma_1 & 0 \\ v_F \hbar q^* & 0 & 0 & 0 \\ \gamma_1 & 0 & 0 & v_F \hbar q^* \\ 0 & 0 & v_F \hbar q & 0 \end{pmatrix} \tag{2.30}$$

where $q = q_x + iq_y$. If the bilayer was gated, a perpendicular electric field would break the symmetry between the layers resulting in one flake being at higher potential than the other one. Assuming a potential difference of $2U$, the Hamiltonian becomes,

$$H = \begin{pmatrix} U & v_F\hbar q & \gamma_1 & 0 \\ v_F\hbar q^* & U & 0 & 0 \\ \gamma_1 & 0 & -U & v_F\hbar q^* \\ 0 & 0 & v_F\hbar q & -U \end{pmatrix} \tag{2.31}$$

By solving the secular equation $\mathbf{H} - \epsilon(q)\mathbf{I}$, we get the dispersion relation,

$$\epsilon_{\pm}^2(q) = U^2 + v_F^2\hbar^2q^2 + \frac{\gamma_1^2}{2} \pm \sqrt{4U^2v_F^2\hbar^2q^2 + \gamma_1^2v_F^2\hbar^2q^2 + \frac{\gamma_1^4}{4}} \tag{2.32}$$

where the positive and negative signs correspond to two sets of bands. By taking

$$U \ll v_F\hbar q \ll \gamma_1 \tag{2.33}$$

and using the binomial series to expand the term under the square root we get,

$$\begin{aligned} &\sqrt{4U^2v_F^2\hbar^2q^2 + \gamma_1^2v_F^2\hbar^2q^2 + \frac{\gamma_1^4}{4}} = \frac{\gamma_1^2}{2}\sqrt{\frac{16U^2v_F^2\hbar^2q^2}{\gamma_1^4} + \frac{4v_F^2\hbar^2q^2}{\gamma_1^2} + 1} \\ &\approx \frac{\gamma_1^2}{2}\left[1 + \frac{1}{2}\frac{16U^2v_F^2\hbar^2q^2}{\gamma_1^4} + \frac{1}{2}\frac{4v_F^2\hbar^2q^2}{\gamma_1^2} - \frac{1}{8}\left(\frac{4v_F^2\hbar^2q^2}{\gamma_1^2}\right)^2 - \frac{1}{8}\left(\frac{1}{2}\frac{16U^2v_F^2\hbar^2q^2}{\gamma_1^4}\right)^2\right] \\ &\approx \frac{\gamma_1^2}{2} + \frac{4U^2v_F^2\hbar^2q^2}{\gamma_1^2} + v_F^2\hbar^2q^2 - \frac{(v_F\hbar q)^4}{\gamma_1^2} \end{aligned} \tag{2.34}$$

where we ignored the last term in the second line because it is very small, see Eq. 2.33. Insert Eq. 2.34 into Eq. 2.32 (with the minus sign) to get the dispersion relation for the valence and conduction bands,

$$\begin{aligned} \epsilon_-^2(q) &= U^2 - \frac{4U^2v_F^2\hbar^2q^2}{\gamma_1^2} + \frac{v_F^4\hbar^4q^4}{\gamma_1^2} \\ \Rightarrow \epsilon &= \pm\sqrt{U^2 - \frac{4U^2v_F^2\hbar^2q^2}{\gamma_1^2} + \frac{v_F^4\hbar^4q^4}{\gamma_1^2}} \end{aligned} \tag{2.35}$$

The second term in Eq. 2.35 is very small and can be neglected by taking $U \ll v_F\hbar q$. Therefore, throughout the coming calculations in band gapped bilayer graphene we take the dispersion relation to be,

$$\boxed{\epsilon(q) = \pm\sqrt{U^2 + \frac{v_F^4\hbar^4q^4}{\gamma_1^2}}} \tag{2.36}$$

The spectrum for Eq. 2.35 forms the valence and conduction bands, separated by a gap, that take the shape of a Mexican hat; that distinctive shape disappears gradually to a more parabolic form as we take U to be smaller and smaller.

For the gapless case, i.e., the two layers are grounded, we take $U = 0$ to get the energy,

$$\boxed{\epsilon(q) = \pm\frac{v_F^2\hbar^2 q^2}{\gamma_1} = \pm\frac{p^2}{2m}} \tag{2.37}$$

where $\gamma_1 = 0.4$ eV and m is the effective mass, defined as,

$$m = \hbar^2\left[\frac{d^2\epsilon}{dq^2}\right]^{-1} = \hbar^2\left[\frac{2v_F^2\hbar^2}{\gamma_1}\right]^{-1} \tag{2.38}$$

and has a value of $m = \gamma_1/(2v_F^2) \approx 0.05\, m_0$ (m_0 is the mass of the electron). The same expression for the effective mass, Eq. 2.38, is used for Eq. 2.36 because we assumed $U \ll v_F\hbar q$. The spectrum, Eq. 2.37 forms two parabolic bands that touch at $\epsilon = 0$.

CHAPTER 3

PLASMA OSCILLATIONS AND PLASMONS

Plasma oscillation are the vibrations of charged particles with certain frequency ω. A simple example is the longitudinal oscillation of electron gas in a neutral bulk of metallic material. To estimate the frequency of such oscillations, the metal is approximated, using Drude model, as an arrangement of fixed positive ions surrounded by Fermi gas of electrons that are treated as classical particles obeying Newton's laws.

We will derive bulk plasma frequency by following the same procedure presented in Ref. [2]. Let's consider a metallic slab under the effect of a uniform electric field; electrons move from equilibrium position to one side of the block until the induced electric field inside the material cancels the applied one. After turning off the field, electrons, under the effect of repulsive forces from one another and attraction to the positively charged region of the block, move to the equilibrium position to lower their potential energy. As their potential energy is converted into kinetic energy they gain momentum and overshoot to the other side of the block, due to their inertia, converting their kinetic energy into potential energy again and creating an electric field in the block. This process is repeated until some dissipative force dampens the system. The cycle of electrons moving back and forth and changing their kinetic and potential energy in the process is a manifestation of harmonic oscillation.

Under the effect of an external electric field the electron gas shifts a distance x from equilibrium. The system now has three regions, one neutral region in the middle and two charged regions on the sides of the slab. The two charged regions can be approximated as capacitor plates of thickness x with uniform electric field in between. We can write the electric field as,

$$E = 4\pi\sigma = 4\pi nex \tag{3.1}$$

where the surface charge density of these two regions, σ, is just the number density of electrons in the material, n, multiplied by the distance x, the width of the charged region

or equivalently the distance by which the electrons were displaced from the equilibrium position. The restoring force on an electron due to the electric field is,

$$F = -4\pi n e^2 x = m\frac{d^2x}{dt^2} \tag{3.2}$$

where m is the electron's mass. Eq. 3.2 is just the equation of motion of a simple harmonic oscillator, $d^2x/dt^2 = -\omega^2 x$, derived from Newton and Coulomb laws. Thus, the bulk plasma frequency is,

$$\omega_p = \sqrt{\frac{4\pi n e^2}{m}} \tag{3.3}$$

In this simple system the frequency is independent of the wavenumber indicating that the plasma oscillations are not propagating waves. In general cases however, plasma oscillations constitute propagating waves with frequencies that are proportional to a function in wavenumber. In studying plasma oscillations the objective is to find the dispersion relation, i.e., the relation between the frequency and wavenumber of the propagating oscillations.

A heuristic argument can be made to study the plasma oscillations in a two-dimensional system, a sheet of metal for example. In that case the charged regions would be two infinite charged wires instead of charged plates and consequently the electric field across the slab would depend on the distance between the regions. Unlike the uniform electric field in the previous example, $4\pi\sigma$, the distance dependence $\propto 1/r \sim 1/\lambda$ of the electric field in the 2D case indicates that frequency is dependent on the wave number and therefore, the plasma oscillations are propagating waves. In the one-dimensional case, a long wire, the wavenumber dependence would be even stronger because the charged regions would be two point charges and consequently the electric field would be proportional to the inverse distance squared. The three cases show that the dimensionality of the system affects the dispersion relation.

Quantization of plasma oscillations gives rise to plasmons, the collective excitations of charges. Quantization is in the sense that energies of oscillations, and consequently frequencies, are quantized. In other words, an electron interacting with a plasmon would lose energy to excite the plasmon in integral multiples of plasmon energy [2].

To obtain the dispersion relations for plasmons propagating in bilayer graphene, we used the hydrodynamic model instead of Drude's model. In the hydrodynamic scheme, the Pauli exclusion principle is taken into account and thus adds to the complexity of the problem. In addition to the time dependent self-consistent electric field of the system, the constraint that each state is occupied by only one electron creates a sort of force in the

sense that increasing the charge density requires more energy to excite the excess electrons to higher energy levels [7]. Thus incorporating density of states and energy spectrum of the bilayer complicates the problem considerably. In the following chapters, the device and the methods used to obtain the dispersion relation of plasmon waves are explained in great detail.

CHAPTER 4

THOMAS-FERMI METHOD

The Thomas-Fermi method is a semiclassical approach that simplifies the Schrödinger equation by replacing the wave function with the charge density as the principal quantity. It was introduced independently by Thomas and Fermi in 1927 and 1928. The method uses quantum mechanical principles like the uncertainty principle and Pauli exclusion principle whereas momentum is treated like a number rather than an operator as part of the classical approach. The method is applied under the assumption that the system is treated like gas of electrons under the effect of self-consistent electrostatic potential that changes very slowly over the wavelength of an electron. In this section we derive the Thomas-Fermi equation for bilayer graphene from Lenz energy functional by following the same procedure presented in Ref. [16].

The energy of a graphene strip is the summation of the kinetic energies of charge carriers, the potential energy under the effect of E_0 and the potential energy due to the induced charge distribution. Therefore, the ground-state energy as a functional of the charge density $n(x)$ can be written as,

$$E_{tot} = T + U_{ext} + U_{ind}$$

where T is the kinetic energy of charges, U_{ext} is the potential energy due to an external field and U_{ind} is the potential energy of induced charge density. The total kinetic energy is obtained by integrating the kinetic energy density over real space. Kinetic energy density is the kinetic energy of one electron $p^2/2m$ integrated over infinitesimal band of orbitals per unit momentum per unit area.

$$t = \pm \int_0^{p_F} \frac{p^2}{2m} \frac{dN}{A}$$

where $dN/dp = 2\,A\,p/(\pi\hbar^2)$ such that A is the area of the Fermi circle and N is the total number of states. Thus, we get,

$$t = \pm \frac{1}{m\,\pi\hbar^2} \int_0^{p_F} p^3 dp = \pm \frac{1}{4\,m\,\pi\hbar^2} p_F^4 = -\mathrm{sgn}(\rho_0) \frac{\hbar^2 \pi \rho_0^2(x)}{4\,m\,e^2} \tag{4.1}$$

where $\rho_0(x) = sgn(x)|e|n(x)$ and $n(x) = p_F^2/(\pi\hbar^2)$, Eq. A.2. Integrating Eq. 4.1 we obtain the total kinetic energy,

$$T = -\mathrm{sgn}(\rho_0)\int_{-d}^{d}\frac{\hbar^2\pi\rho_0^2(x)}{4\,m\,e^2}dx \tag{4.2}$$

The potential energy of all electrons and holes due to an external field E_0 is,

$$U_{ext} = -\int_{-d}^{d} E_0\,x\,\rho_0(x)dx \tag{4.3}$$

and the potential energy due to electron-electron interaction as a result of the induced charge density is,

$$U_{ind} = -\frac{1}{2}\int_{-d}^{d}\int_{0}^{d} 2\rho_0(x)\rho_0(x')\ln\frac{x+x'}{|x-x'|}dx\,dx' \tag{4.4}$$

where the factor of half is to compensate for double counting. By adding Eqs. 4.2, 4.3 and 4.4 we obtain the total energy,

$$\begin{aligned} E_{tot} &= -\mathrm{sgn}(\rho_0)\int_{-d}^{d}\frac{\hbar^2\pi\rho_0^2(x)}{4\,m\,e^2}dx - \int_{-d}^{d}E_0\,x\,\rho_0(x)dx - \int_{-d}^{d}\int_{0}^{d}\rho_0(x)\rho_0(x')\ln\frac{x+x'}{|x-x'|}dx\,dx' \\ &= -\int_{0}^{d}\frac{\hbar^2\pi\rho_0^2(x)}{2\,m\,e^2}dx - \int_{0}^{d}2E_0\,x\,\rho_0(x)dx - 2\int_{0}^{d}\int_{0}^{d}\rho_0(x)\rho_0(x')\ln\frac{x+x'}{|x-x'|}dx\,dx' \end{aligned}$$

To find the extremum value for the total energy $E_{tot} \geq 0$, we use the substitution $\rho_0(x) = sgn(x)|e|n(x)$ to obtain,

$$\int\left[-\frac{\hbar^2\pi\,e\,\rho_0(x)}{m\,e^2} - 2e\,E_0\,x - 4\,e\int_{0}^{d}\rho_0(x')\ln\frac{x+x'}{|x-x'|}dx'\right]\delta n(x)dx \geq 0$$

Because the variation $\delta n(x)$ is arbitrary, the term between parenthesis must be zero. Thus,

$$-\frac{\hbar^2\pi\,\rho_0(x)}{m\,e} - 2e\,E_0\,x - 4\,e\int_{0}^{d}\rho_0(x')\ln\frac{x+x'}{|x-x'|}dx' = 0$$

Divide by 2 and the electric charge e to obtain the Thomas-Fermi equation for gapless bilayer graphene,

$$\frac{\pi\hbar^2\rho_0(x)}{2me^2} + E_0\,x + 2\int_{0}^{d}\rho_0(x')\ln\frac{x+x'}{|x-x'|}dx' = 0 \tag{4.5}$$

CHAPTER 5

HYDRODYNAMIC EQUATIONS

In this chapter we derive the Boltzmann transport equation to obtain the hydrodynamics relation used in deriving the main integro-differential equation. Let's consider a system of particles where the position and momentum of each particle are known at all times. As the particles interact by elastically colliding with each other, their momenta and consequently the momentum distribution function change. The distribution function gives the fraction of particles in the system that have a certain momentum at a certain time. The equation that describes how the distribution function evolves in time depending on the nature of collisions and forces is called the Boltzmann transport equation. We derive the Boltzmann transport equation by following the same procedure presented in Ref. [8]. The distribution function that characterizes the system is then inserted into the transport equation to obtain the hydrodynamic equation.

let $f(\mathbf{r}, \mathbf{p}, t)$ be the distribution function of particles of momentum $\mathbf{p}$ at position $\mathbf{r}$. The number of particles that would be added to $f(\mathbf{r}, \mathbf{p}, t)$, i.e., would have momentum $\mathbf{p}$, due to collision in time dt is equal to,

$$\left[\int P(\mathbf{p}|\mathbf{p_0}) f(\mathbf{r}, \mathbf{p_0}, t) d\mathbf{p}_0\right] dt \tag{5.1}$$

where $P(\mathbf{p}|\mathbf{p_0})dt$ is the probability that a particle having a momentum $\mathbf{p_0}$ is scattered by collision to momentum $\mathbf{p}$ in time dt, and $f(\mathbf{r}, \mathbf{p_0}, t)$ is the number of particles moving with momentum $\mathbf{p_0}$. The number of particles subtracted from $f(\mathbf{r}, \mathbf{p}, t)$ due to collision in time dt is equal to,

$$\left[\int P(\mathbf{p_0}|\mathbf{p}) d\mathbf{p}_0\right] f(\mathbf{r}, \mathbf{p}, t) dt \tag{5.2}$$

where $P(\mathbf{p_0}|\mathbf{p})$ is the probability that a particle having a momentum $\mathbf{p}$ is scattered by collision to momentum $\mathbf{p_0}$ in time dt. The integrals in Eqs. 5.1 and 5.2 are taken over $\mathbf{p_0}$ to take into consideration the scattering of particles to or from momentum $\mathbf{p}$ for all possible values of $\mathbf{p_0}$. The number of particles with momentum $\mathbf{p}$ at position $\mathbf{r}$, i.e., $f(\mathbf{r}, \mathbf{p}, t)$, also

increases in time dt due to the free motion of particles with momentum $\mathbf{p}$ from position $\mathbf{r} - \mathbf{v}\,dt$ to $\mathbf{r}$. Therefore, the number of particles of momentum $\mathbf{p}$ at position $\mathbf{r}$ increases after time dt by,

$$f(\mathbf{r} - \frac{\mathbf{p}}{m}dt, \mathbf{p}, t) \tag{5.3}$$

If force $\mathbf{F}$ is applied, particles with momentum $\mathbf{p} - \mathbf{F}dt$ at an earlier time t will acquire momentum $\mathbf{p}$ at a later time $t + dt$ under the effect of $\mathbf{F}$. To account for this increase in the number of particles with momentum $\mathbf{p}$ we add to $f(\mathbf{r}, \mathbf{p}, t)$ the distribution function of particles with momentum $\mathbf{p} - \mathbf{F}dt$ at an earlier time t,

$$f(\mathbf{r}, \mathbf{p} - \mathbf{F}dt, t) \tag{5.4}$$

The distribution function at time $t+dt$ due to all contributions, Eqs. 5.1, 5.2, 5.3 and 5.4, is,

$$\begin{aligned} f(\mathbf{r}, \mathbf{p}, t + dt) = &\left[\int P(\mathbf{p}|\mathbf{p_0}) f(\mathbf{r}, \mathbf{p_0}, t) d\mathbf{p}_0\right] dt - \left[\int P(\mathbf{p_0}|\mathbf{p}) d\mathbf{p}_0\right] f(\mathbf{r}, \mathbf{p}, t) dt \\ &+ f(\mathbf{r} - \frac{\mathbf{p}}{m}dt, \mathbf{p}, t) + f(\mathbf{r}, \mathbf{p} - \mathbf{F}dt, t) \end{aligned} \tag{5.5}$$

By expanding $f(\mathbf{r}, \mathbf{p}, t + dt)$, $f(\mathbf{r} - \frac{\mathbf{p}}{m}dt, \mathbf{p}, t)$ and $f(\mathbf{r}, \mathbf{p} - \mathbf{F}dt, t)$ using Taylor series,

$$\begin{aligned} f(\mathbf{r}, \mathbf{p}, t + dt) &= f(\mathbf{r}, \mathbf{p}, t) + \frac{\partial f}{\partial t}dt + ... \\ f(\mathbf{r} - \frac{\mathbf{p}}{m}dt, \mathbf{p}, t) &= f(\mathbf{r}, \mathbf{p}, t) - (\nabla f) \cdot \frac{\mathbf{p}}{m}dt + ... \\ f(\mathbf{r}, \mathbf{p} - \mathbf{F}dt, t) &= f(\mathbf{r}, \mathbf{p}, t) - \frac{\partial f}{\partial \mathbf{p}} \cdot \mathbf{F}dt + ... \end{aligned}$$

we get the Boltzmann transport equation,

$$\frac{\partial f_{\mathbf{p}}}{\partial t} + \left(\frac{\mathbf{p}}{m}.\nabla\right) f_{\mathbf{p}} + \mathbf{F} \cdot \frac{\partial f_{\mathbf{p}}}{\partial \mathbf{p}} \propto \int P(\mathbf{p}|\mathbf{p_0}) f(\mathbf{r}, \mathbf{p_0}, t) d\mathbf{p}_0 - \left[\int P(\mathbf{p_0}|\mathbf{p}) d\mathbf{p}_0\right] f(\mathbf{r}, \mathbf{p}, t)$$

where the right hand side is the collision integral $I[f_{\mathbf{p}}]$, i.e., "the rate of change of the distribution function by virtue of collisions." [13]. Multiply the previous equation by $(e\,\mathbf{v})$ and sum over all values of momentum $\mathbf{p}$,

$$e\sum_{\mathbf{p}} \mathbf{v} \frac{\partial f_{\mathbf{p}}}{\partial t} + e\sum_{\mathbf{p}} \mathbf{v}\,(\mathbf{v}.\nabla)\, f_{\mathbf{p}} + e^2 \sum_{\mathbf{p}} \mathbf{v} \left(\mathbf{E} \cdot \frac{\partial f_{\mathbf{p}}}{\partial \mathbf{p}}\right) \propto e\sum_{\mathbf{p}} \mathbf{v}\, I[f_{\mathbf{p}}]$$

where we have used the simple relations $\mathbf{p}/m = \mathbf{v}$ and $\mathbf{F} = e\,\mathbf{E}$. Because we assume that the plasmon frequencies are much greater than the collision frequency, we can take the R.H.S to be zero,

$$\frac{\partial \mathbf{J}}{\partial t} + e\sum_{\mathbf{p}} \mathbf{v}\,(\mathbf{v}.\nabla)\, f_{\mathbf{p}} + e^2 \sum_{\mathbf{p}} \mathbf{v} \left(\mathbf{E} \cdot \frac{\partial f_{\mathbf{p}}}{\partial \mathbf{p}}\right) = 0 \tag{5.6}$$

where $e\sum_{\mathbf{p}} \mathbf{v}\, f_{\mathbf{p}} = \mathbf{J}$ is the current density.

The distribution function of fermions in a system at temperature $T = 0$ K free form the influence of any force is just the Heaviside step function,

$$\Theta(\mu(\mathbf{r},t) - \epsilon_p) \tag{5.7}$$

However, because our system, a bilayer graphene flake, is under the effect of electric field $\mathbf{E}$ for time τ, the $\mathbf{k}$ vector of each orbital increases by $e\,\mathbf{E}\tau/\hbar$. This leads to the shift of the Fermi circle, see Fig. A.1, that encloses the occupied orbitals by $\delta\mathbf{k}$. Assuming the change in the wavevector/momentum is small, we expand the distribution function using Taylor series,

$$\begin{aligned} f(\mathbf{p}+d\mathbf{p},\mathbf{r},t) &= f(\mathbf{p},\mathbf{r},t) + \frac{\partial f}{\partial \mathbf{p}}\cdot d\mathbf{p} + ... \\ &= \Theta(\mu(\mathbf{r},t)-\epsilon_p) + \frac{\partial}{\partial \mathbf{p}}\Theta(\mu(\mathbf{r},t)-\epsilon_p)\cdot d\mathbf{p} \\ &= \Theta(\mu(\mathbf{r},t)-\epsilon_p) + \frac{\partial}{\partial \mu}\Theta(\mu(\mathbf{r},t)-\epsilon_p)\frac{d\mu}{d\mathbf{p}}\cdot d\mathbf{p} \end{aligned}$$

Using the relations $d\mu/d\mathbf{p} = \mathbf{v}$, $d\mathbf{p} = e\,\mathbf{E}\,\tau$ and $d\Theta(x)/dx = \delta(x)$ we obtain,

$$f(\mathbf{p}+d\mathbf{p},\mathbf{r},t) = \Theta(\mu(\mathbf{r},t)-\epsilon_p) + \delta(\mu(\mathbf{r},t)-\epsilon_p)\mathbf{v}\cdot\mathbf{E}\,e\,\tau$$

Substitute for the electric field by using the relation $\mathbf{J} = n\,\mathbf{E}\,e^2\,\tau/m$, where n is the charge density and m is the mass of the electron,

$$\begin{aligned} f(\mathbf{p}+d\mathbf{p},\mathbf{r},t) &= \Theta(\mu(\mathbf{r},t)-\epsilon_p) + \delta(\mu(\mathbf{r},t)-\epsilon_p)\frac{m}{n\,e}\mathbf{v}\cdot\mathbf{J} \\ &= \Theta(\mu(\mathbf{r},t)-\epsilon_p) + \delta(\mu(\mathbf{r},t)-\epsilon_p)\,\frac{p_F}{v_F}\,\frac{\pi\hbar^2}{p_F^2\,e}\mathbf{v}\cdot\mathbf{J} \\ &= \Theta(\mu(\mathbf{r},t)-\epsilon_p) + \delta(\mu(\mathbf{r},t)-\epsilon_p)\frac{v_F\pi\hbar^2}{v_F^2\,p_F\,e}\mathbf{v}\cdot\mathbf{J} \\ &= \Theta(\mu(\mathbf{r},t)-\epsilon_p) + 2\frac{\mathbf{v}\cdot\mathbf{J}(\mathbf{r},t)}{ev_F^2\nu(\mu)}\delta(\mu(\mathbf{r},t)-\epsilon_p) \end{aligned}$$

where in the second line we have inserted $n = p_F^2/(\pi\hbar^2)$, see Eq. A.2, and $m = p_F/v_F$. In the third line we multiplied the numerator and denominator by v_F and in the fourth line we used the relation $v_F/p_F = 2/(\pi\,\hbar^2\,\nu(\mu))$, see Eq. A.4. Thus, the distribution function is nothing but the Heaviside step function plus a second term that accounts for the displacement of the whole Fermi circle under the influence of force $\mathbf{F}$.

$$f_{\mathbf{p}}(\mathbf{r},t) = \Theta(\mu(\mathbf{r},t)-\epsilon_p) + 2\frac{\mathbf{v}\cdot\mathbf{J}(\mathbf{r},t)}{ev_F^2\nu(\mu)}\delta(\mu(\mathbf{r},t)-\epsilon_p) \tag{5.8}$$

By inserting Eq. 5.8 into Eq. 5.6 we obtain the hydrodynamic equation,

$$\boxed{\frac{\partial \mathbf{J}}{\partial t} = \frac{1}{2} e v_F^2 \nu(\mu)(e\mathbf{E} - \nabla\mu).} \tag{5.9}$$

where $v_F = d\mu/dp_F$ is the Fermi velocity and $\nu(\mu) = 2p_F/\pi\hbar^2 v_F$ is the density of states.

CHAPTER 6

GAPLESS BILAYER GRAPHENE

6.1 Introduction

In this chapter we compute the dispersion relations, frequencies as functions of wave number, for plasmons excited in grounded bilayer graphene under the effect of applied in-plane electric field $\mathbf{E_0}$. Frequencies of plasmon excitations are calculated in the two cases where the plasmon wavelength λ is much smaller or much greater than the dimensions of the flakes.

We considered two graphene sheets at the same potential with width $2d$ in the x direction and length that extends over the y-axis to infinity, see Fig. 6.1 (a). In-plane electric field $\mathbf{E_0}$ is applied parallel to the x-axis to induce charge density ρ_0 across the width of the flakes such that half of the flake is positively charged and the other half is negatively charged. This generation of charges is facilitated by the absence of a band gap between the valence and conduction bands of bilayer graphene. The equilibrium charge density $\rho_0(x)$ has some general characteristics; it is an odd function of x where the line bisecting the flake's width has zero charge, i.e., $\rho_0(0) = 0$, and the absolute value $|\rho_0|$ increases as we move towards the edges. The equilibrium charge density as a function of x is determined by solving the Thomas-Fermi equation.

Fluctuations of the equilibrium charge density ρ_0 establish propagating oscillations that constitute plasmons. The applied electric field $\mathbf{E_0}$ introduces non-uniformity in the charge distribution along the x-axis and consequently plasmon waves are enforced to propagate in the y direction. Thus, the direction of the applied electric field determines the direction of plasmon propagation. The effect of the magnitude of $\mathbf{E_0}$ on plasmon frequencies would be derived in this chapter. Higher charge density $|\rho_0|$ at the edges means that the average distance between induced charges is smaller close to the edges than it is to the middle of the flake; consequently it is harder for electrons or holes at the edges to move freely to generate fluctuations that constitute plasmon excitations on a larger scale. Therefore, plasmons tend

to decay on the outer edges of the bilayer flake. Such knowledge of the behavior of plasmons based solely on physical grounds helped in guessing the solution to the integro-differential equation set up from hydrodynamic equations.

The problem is approached semiclassically by using the hydrodynamic model that treated charges as liquid of fermions. The enforcement of the Pauli exclusion principle through the calculation of density of states, and the computation of energy bands of bilayer graphene from the Schrödinger equation constitute the quantum mechanical portion of the method. The classical part of the model lies in the treatment of electrons and holes as fluid of charges by applying electrostatic and hydrodynamic equations. Thus, the classical approximation is applicable to the device if the charge density is high enough to allow a description of charges as continuous liquid, i.e., the distance between adjacent charges is much smaller than the width of the flake and wavelength of plasmons. The main parameter that affects the charge density is the applied electric field E_0; stronger E_0 means smaller characteristic length, the distance between adjacent charges, and consequently greater charge accumulation on the flake. As a result, some constraints must be imposed on E_0 for our model and subsequent calculations to be valid. Let L_E be the characteristic length of the electric field; the relation between E_0 and L_E is obtained by realizing that the bilayer flake achieves electrostatic equilibrium when repulsion between adjacent induced charges cancels the force due to E_0, i.e.,

$$E_0 \approx \frac{e}{L_E^2} \tag{6.1}$$

Therefore, by imposing the condition that the characteristic length is much smaller than the flake's width to allow modeling of induced charges as continuous fluid, i.e., $L_E \ll d$ we obtain [6],

$$\sqrt{\frac{e}{E_0}} \ll d \tag{6.2}$$

where $2d$ is the width of the flake. For the quantum effects not to affect the classical description of plasmon waves, the wavelength of oscillations must be much greater than the Fermi wavelength λ_F of the induced charges. Since $\lambda_F \sim 1/k_F$ and $k_F^2 \sim \rho_0/e$, see Eq. A.2, we obtain,

$$\lambda_F \sim \frac{1}{k_F} \sim \sqrt{\frac{e}{\rho_0}} \sim L_E \sim \sqrt{\frac{e}{E_0}} \tag{6.3}$$

where we have used $\rho_0/e \sim 1/L_E^2$, i.e., the number density of charge carriers is of the order of the reciprocal of the characteristic length squared. By applying the condition $\lambda \gg \lambda_F$, we get the following constraint on E_0,

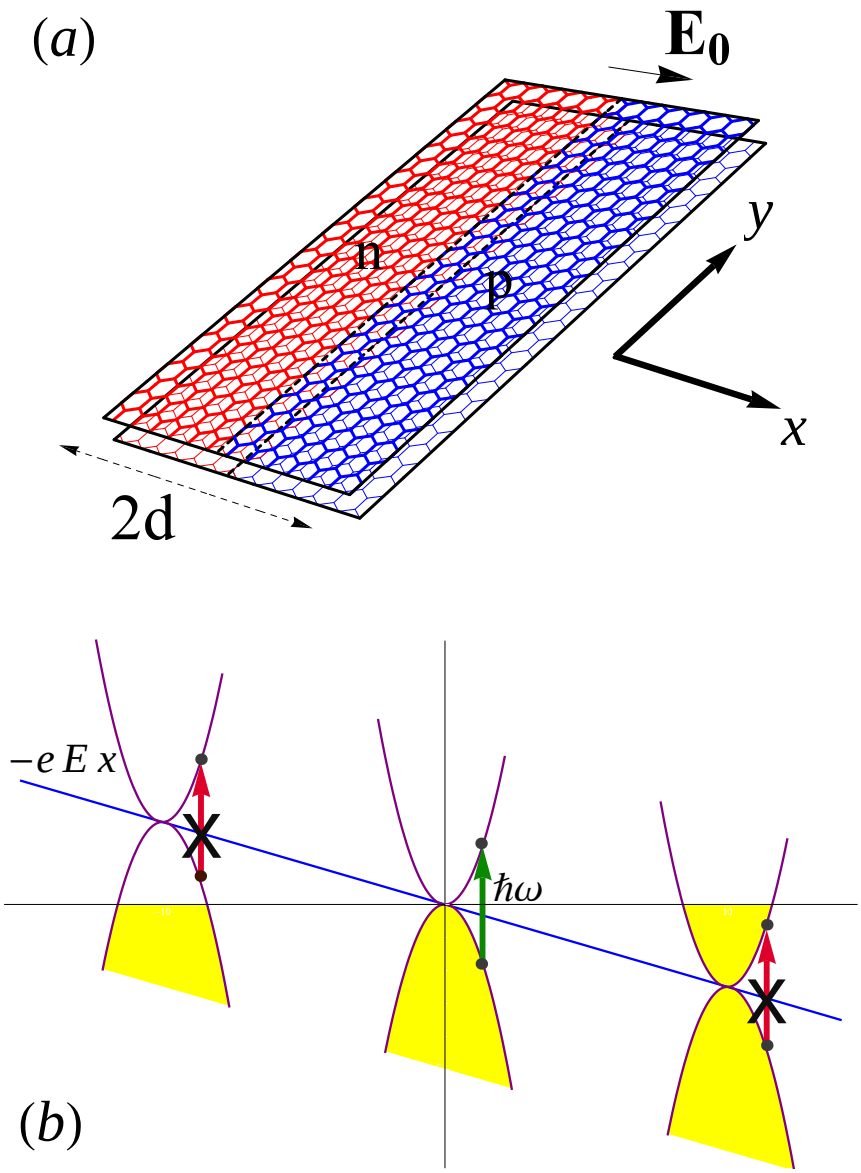

Figure 6.1: Sketch of bilayer graphene and its electronic spectrum a) Bilayer graphene flake of width $2d$ is placed in electric field that induces charge density ρ_0. The red region shows the negatively charged (denoted by n) half-width of the flake and the blue region shows the positively charged (denoted by p) other half of the flake. Fluctuations over ρ_0 constitute guided plasmons that propagate along the y-axis. b) Schematic picture of the electron band structure superimposed on the electrostatic potential due to applied field: in equilibrium the sum of the electrostatic potential and kinetic energy of electrons (at the Fermi level) is constant. Vertical arrows indicate electromagnetic waves absorption of a given frequency: while possible near the center of the flake (green arrow), such transitions are forbidden (red arrows) when both initial and final states are empty or occupied.

$$\sqrt{\frac{e}{E_0}} \ll \lambda,\, d \quad \text{(Gaussian Units)} \tag{6.4}$$

The total charge density on the flake is,

$$\rho_0(x) + \delta\rho(\mathbf{r}, t) = \rho(\mathbf{r}, t) \tag{6.5}$$

where $\rho_0(x)$ is the equilibrium charge density and $\delta\rho(\mathbf{r}, t)$ is the change or fluctuations of $\rho_0(x)$ that constitute plasmons. Throughout this work the spacing between the two layers of graphene is taken to be negligible and thus was ignored.

6.2 The General Integro-Differential Equation

In this section, we derive the general integro-differential equation in $\delta\rho(x)$ for general plasmon wavelength λ. We start with the Thomas-Fermi equation, derived in Chapter 4, to obtain the equilibrium charge density $\rho_0(x)$ induced under the effect of electric field E_0. To calculate the change in charge density, i.e., plasmon amplitude, we use three main equations that represent the dynamics of the total charge density $\rho(x)$ to obtain an equation in one variable $\delta\rho(x)$.

The Thomas-Fermi integral equation states that for the device to be in equilibrium the electrochemical potential of charge carriers must be constant across the flakes, i.e., charge carriers at different locations have different values for electric and chemical potential that must add up to the same value for all values of x. The Thomas-Fermi integral equation in $\rho_0(x)$ can be written as,

$$\boxed{E_0 x + 2\int_0^d dx' \rho_0(x') \ln\frac{x + x'}{|x - x'|} + \frac{\pi\hbar^2\rho_0(x)}{2me^2} = 0} \tag{6.6}$$

where the first term is the potential due to the applied electric field $\mathbf{E}_0$ and the second term is the potential due to the induced charges. The third term is the chemical potential, see Eqs A.2 and 2.37; at $T = 0$ the chemical potential is the same as the Fermi energy, $\mu = \epsilon_F$, therefore,

$$\mu = \frac{p_F^2}{2m} = \frac{\pi\,\hbar^2 n(x)}{2m} = -\frac{\pi\,\hbar^2\rho_0(x)}{2\,m\,|e|}$$

where the equilibrium charge density is just the number density of charge carriers multiplied by the charge of the electron, i.e., $\rho_0(x) = sgn(x)|e|\,n(x)$. The coefficient of the last term,

Bohr radius, is very small, $\hbar^2/m\,e^2 \approx 10.6\ {}^0\text{A}$ and thus, can be ignored to simplify Eq. 6.6. The exact solution [15], see Fig. 6.2, to the remaining equation is,

$$\rho_0(x) = \frac{E_0 x}{\sqrt{d^2 - x^2}} \tag{6.7}$$

Having calculated the equilibrium charge density, the objective now is to compute $\delta\rho$ and frequencies of plasmon modes. As mentioned earlier, plasmons oscillations take place due to fluctuations of charge density, and thus are the result of complicated dynamics and interactions between charges, electric field and current density. The dynamics responsible for plasmon formation can be pictured as a closed loop where the applied electric field sets charge carriers in motion producing a current that changes the charge distribution across the flake that in turn modifies the effective electric field which starts the cycle again by generating a current through the flake to modify the charge density [5]. This closed loop can be represented through three equations that when combined together we obtain a self-consistent equation in charge density fluctuations.

Eq. 5.9, derived in Chapter 5, represents the effect of the electric field on charge carriers by inducing flow of current,

$$\dot{\mathbf{J}}(\mathbf{r}, t) = \frac{e\, v_F^2 \nu(\mu)}{2}(e\mathbf{E} - \nabla\mu) \tag{6.8}$$

where $v_F = d\mu/dp_F$ is the Fermi velocity and $\nu(\mu) = 2p_F/(\pi\hbar^2 v_F)$ is the density of states. Consequently, the flow of current changes the charge density through the continuity equation,

$$\dot{\rho}(\mathbf{r}, t) + \nabla \cdot \mathbf{J}(\mathbf{r}, t) = 0. \tag{6.9}$$

and the induced charge density ρ modifies the total electric field through Coulomb law,

$$\mathbf{E}(\mathbf{r}, t) = \mathbf{E}_0 - \nabla \int d^2 r' \frac{\rho(\mathbf{r}', t)}{|\mathbf{r} - \mathbf{r}'|} \tag{6.10}$$

To obtain a general equation in $\delta\rho$, we insert Eq. 6.8 and Eq. 6.10 into Eq. 6.9. First, we simplify Eq. 6.8 by noticing that the term $e\, v_F^2 \nu(\mu)/2$ depends on the spectrum of the bilayer graphene, and thus can be simplified to,

$$\frac{e\, v_F^2 \nu(\mu)}{2} = \frac{e v_F\, p_F}{\pi\hbar^2} = \frac{e p_F^2}{\pi\hbar^2 m} = \frac{|\rho|}{m}$$

where the Fermi velocity can be written as the derivative of the chemical potential with respect to momentum,

$$v_F = \frac{d\mu}{dp_F} = \frac{d\mu}{d\rho}\frac{d\rho}{dp_F} = \frac{\hbar^2\pi}{2me} \times \frac{2ep_F}{\pi\hbar^2}$$

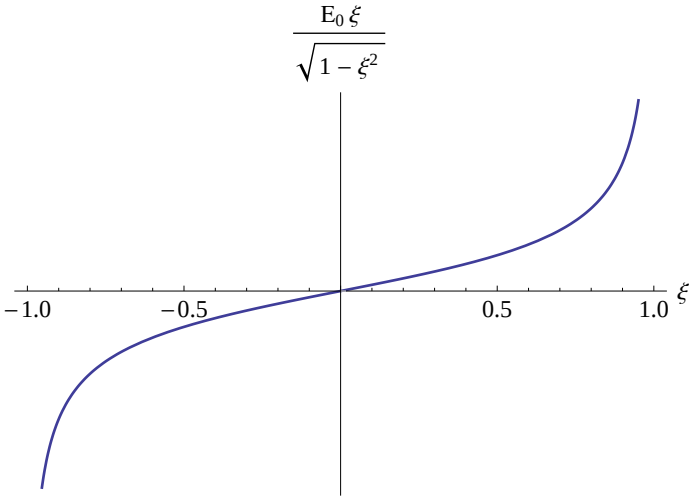

Figure 6.2: The equilibrium charge density $\rho_0(x)$ in terms of dimensionless variable x/d.

and

$$p_F^2 = \frac{\pi\hbar^2|\rho|}{e}$$

Because the charge density has the same time dependence as a plane wave, $\dot{\rho}(\mathbf{r},t) = -i\omega\delta\rho(x)e^{iqy-iwt}$, the continuity equation becomes,

$$-i\omega\delta\rho(x)e^{iqy-iwt} + \frac{i}{\omega}\nabla_r \cdot \dot{\mathbf{J}}(\mathbf{r},t) = 0 \tag{6.11}$$

Substitute Eq. 6.8 into Eq. 6.11 to get,

$$-i\omega\delta\rho(x)e^{iqy-iwt} + \frac{i}{\omega m}\nabla_r \cdot |\rho| \left[e\mathbf{E}_0 - e\nabla_r \int d^2r' \frac{\rho(\mathbf{r}',t)}{|\mathbf{r}-\mathbf{r}'|} - \nabla\mu \right] = 0 \tag{6.12}$$

By substituting for the total charge density as the sum of equilibrium charge distribution and charge fluctuations, $\rho = \rho_0 + \delta\rho$, into Eq. 6.12, we get,

$$\begin{aligned} -i\omega\delta\rho(x)e^{iqy-iwt} + \frac{i}{\omega m}\nabla_r \cdot |\rho_0|\nabla_r \left[eE_0x - e\int d^2r' \frac{\rho_0(\mathbf{r}',t)}{|\mathbf{r}-\mathbf{r}'|} - \mu \right] \\ -\frac{ie}{\omega m}\nabla_r \cdot \rho_0\nabla_r \int d^2r' \frac{\delta\rho(\mathbf{r}',t)}{|\mathbf{r}-\mathbf{r}'|} = 0 \end{aligned}$$

The term $\left[eE_0x - e\int d^2r'\rho_0(\mathbf{r}',t)/|\mathbf{r}-\mathbf{r}'| - \mu\right]$ vanishes by Thomas-Fermi relation. Thus, the integral equation after multiplying by $\omega/(ie^{-i\omega t})$ becomes,

$$\omega^2\delta\rho(x)e^{iqy} + \frac{e}{m}\nabla_r \cdot |\rho_0(x)|\nabla_r \int d^2r' \frac{\delta\rho(x')e^{iqy'}}{|\mathbf{r}-\mathbf{r}'|} = 0 \tag{6.13}$$

In the following steps, the gradient and divergence operators are expanded to reach a simplified form of the equation,

$$\begin{aligned}
&\omega^2\delta\rho(x)e^{iqy} + \frac{e}{m}(\frac{\partial}{\partial x}\mathbf{i}+\frac{\partial}{\partial y}\mathbf{j}).\left[|\rho_0(x)|(\frac{\partial}{\partial x}\mathbf{i}+\frac{\partial}{\partial y}\mathbf{j})\int_{-d}^{d}dx'\int_{-\infty}^{\infty}dy'\frac{\delta\rho(x')e^{iqy'}}{\sqrt{(x-x')^2+(y-y')^2}}\right] \\
&\qquad = 0 \\
&\omega^2\delta\rho(x)e^{iqy} + \frac{e}{m}\frac{\partial}{\partial x}\mathbf{i}.\left[|\rho_0(x)|(\frac{\partial}{\partial x}\mathbf{i}+\frac{\partial}{\partial y}\mathbf{j})\int_{-d}^{d}dx'\int_{-\infty}^{\infty}dy'\frac{\delta\rho(x')e^{iqy'}}{\sqrt{(x-x')^2+(y-y')^2}}\right] \\
&\qquad + \frac{e}{m}\frac{\partial}{\partial y}\mathbf{j}.\left[|\rho_0(x)|(\frac{\partial}{\partial x}\mathbf{i}+\frac{\partial}{\partial y}\mathbf{j})\int_{-d}^{d}dx'\int_{-\infty}^{\infty}dy'\frac{\delta\rho(x')e^{iqy'}}{\sqrt{(x-x')^2+(y-y')^2}}\right] = 0 \\
&\omega^2\delta\rho(x)e^{iqy} + \frac{e}{m}\frac{\partial}{\partial x}\left[|\rho_0(x)|\frac{\partial}{\partial x}\int_{-d}^{d}dx'\int_{-\infty}^{\infty}dy'\frac{\delta\rho(x')e^{iqy'}}{\sqrt{(x-x')^2+(y-y')^2}}\right] \\
&\qquad + \frac{e}{m}|\rho_0(x)|\frac{\partial^2}{\partial y^2}\int_{-d}^{d}dx'\int_{-\infty}^{\infty}dy'\frac{\delta\rho(x')e^{iqy'}}{\sqrt{(x-x')^2+(y-y')^2}} = 0
\end{aligned} \tag{6.14}$$

By substituting $\int_{-\infty}^{\infty}dy'e^{iqy'}/\sqrt{(x-x')^2+(y-y')^2} = 2e^{iqy}K_0(q|x-x'|)$, see Appendix B.1, the integral equation becomes,

$$\begin{aligned}
\omega^2\delta\rho(x)e^{iqy} \quad &+ \quad \frac{2e}{m}\frac{\partial}{\partial x}\left[|\rho_0(x)|\frac{\partial}{\partial x}\int_{-d}^{d}dx'\delta\rho(x')2K_0(q|x-x'|)e^{iqy}\right] \\
&+ \quad \frac{2e}{m}|\rho_0(x)|\frac{\partial^2}{\partial y^2}\int_{-d}^{d}dx'\delta\rho(x')2K_0(q|x-x'|)e^{iqy} = 0
\end{aligned}$$

After differentiating the third term and dividing throughout by e^{iqy}, we get the final form of the general integro-differential equation,

$$\boxed{\omega^2\delta\rho(x) + \frac{2e}{m}\left[\frac{d}{dx}|\rho_0(x)|\frac{d}{dx} - q^2|\rho_0(x)|\right]\int_{-d}^{d}dx'\delta\rho(x')K_0(q|x-x'|) = 0} \tag{6.15}$$

6.3 First Case in the Limit of Short Wavelength $\lambda \ll d$

To simplify Eq. 6.15, we approximated the charge density at equilibrium $\rho_0(x)$ and extended the limits of the integro-differential equation to infinity. In the limit of small wavelength, plasmon decays fast along the width of the flake and vanishes at distance $x \sim \lambda$ from the p-n junction and thus, automatically satisfies the boundary condition of vanishing currents at flake edge. In this limit $x \ll d$, where charge fluctuations are non vanishing, the charge density at equilibrium can be simplified to,

$$\rho_0(x) = \frac{E_0 x}{d\sqrt{1 - \underbrace{\frac{x^2}{d^2}}_{\approx 0}}} \approx \frac{E_0 x}{d} \tag{6.16}$$

Substituting Eq. 6.16 into Eq. 6.15 and extending the limits to infinity we get,

$$\omega^2 \delta\rho(x) + \frac{2eE_0}{m\,d}\left[\frac{d}{dx}|x|\frac{d}{dx} - q^2|x|\right]\int_{-\infty}^{\infty} dx'\delta\rho(x')K_0(q|x-x'|) = 0 \tag{6.17}$$

let $qx' = \xi'$, $qx = \xi \Rightarrow qdx' = d\xi'$ and $qdx = d\xi$ to write Eq. 6.17 in the dimensionless variable ξ,

$$\omega^2 \delta\rho(\xi) + \frac{2eE_0}{m\,d}\left[\frac{d}{d\xi}|\xi|\frac{d}{d\xi} - |\xi|\right]\int_{-\infty}^{\infty} d\xi'\delta\rho(\xi')K_0(|\xi-\xi'|) = 0 \tag{6.18}$$

Since the MacDonald function of order zero satisfies the following modified Bessel's differential equation,

$$\left(\frac{d}{d\xi}\xi\frac{d}{d\xi} - \xi\right)K_0(\xi) = 0$$

the second term in Eq. 6.18 can be simplified as follows.

$$\begin{aligned}
&\left(\frac{d}{d\xi}|\xi|\frac{d}{d\xi} - |\xi|\right)K_0(|\xi-\xi'|) = \left[|\xi|\frac{d^2}{d\xi^2} + sgn\xi\frac{d}{d\xi} - |\xi|\right]K_0(|\xi-\xi'|)\\
&= sgn(\xi)\left[\xi\frac{d^2}{d\xi^2} + \frac{d}{d\xi} - \xi\right]K_0(|\xi-\xi'|) = sgn(\xi)\left[\frac{d}{d\xi}\xi\frac{d}{d\xi} - \xi\right]K_0(|\xi-\xi'|)\\
&= \underbrace{sgn(\xi)\left[\frac{d}{d\xi}(\xi-\xi')\frac{d}{d\xi} - (\xi-\xi')\right]K_0(|\xi-\xi'|)}_{0} + sgn(\xi)\xi'\left(\frac{d^2}{d\xi^2} - 1\right)K_0(|\xi-\xi'|)
\end{aligned}$$

Therefore, Eq. 6.18 becomes,

$$\omega^2\delta\rho(\xi) + \frac{2eE_0}{m\,d}sgn(\xi)\int_{-\infty}^{\infty} d\xi'\delta\rho(\xi')\xi'\left(\frac{d^2}{d\xi^2} - 1\right)K_0(|\xi-\xi'|) = 0 \tag{6.19}$$

In the following steps, we use the inverse Fourier transform of the MacDonald function, $K_0(|\xi-\xi'|) = \int_{-\infty}^{\infty} dk e^{ik(\xi-\xi')}/2\sqrt{1+k^2}$, to simplify the second term of Eq. 6.19 to,

$$\begin{aligned}
\int_{-\infty}^{\infty} d\xi'\delta\rho(\xi')\xi'\left(\frac{d^2}{d\xi^2} - 1\right)K_0(|\xi-\xi'|) &= \int_{-\infty}^{\infty} d\xi'\delta\rho(\xi')\xi'\left(\frac{d^2}{d\xi^2} - 1\right)\int_{-\infty}^{\infty}\frac{dk}{2}\frac{e^{ik(\xi-\xi')}}{\sqrt{1+k^2}}\\
&= \int_{-\infty}^{\infty} d\xi'\frac{dk}{2}\delta\rho(\xi')\xi'\left(\frac{d^2}{d\xi^2} - 1\right)\frac{e^{ik(\xi-\xi')}}{\sqrt{1+k^2}}\\
&= -\int_{-\infty}^{\infty} d\xi' dk\delta\rho(\xi')\xi'\frac{e^{ik(\xi-\xi')}(1+k^2)}{\sqrt{1+k^2}}
\end{aligned}$$

and arrive at the following simplified form of Eq. 6.19,

$$\omega^2\delta\rho(\xi) - \frac{eE_0}{m\,d}sgn(\xi)\int_{-\infty}^{\infty} d\xi' dk \delta\rho(\xi')\xi' e^{ik(\xi-\xi')}\sqrt{1+k^2} = 0$$

By substituting $\delta\rho(\xi') = \int_{-\infty}^{\infty} dk'/\sqrt{2\pi}e^{ik'\xi'}\delta\tilde{\rho}(k')$, we get the integral equation,

$$\omega^2\delta\rho(\xi) - \frac{eE_0}{m\,d}sgn(\xi)\int_{-\infty}^{\infty}\frac{dkdk'}{\sqrt{2\pi}}\delta\tilde{\rho}(k')e^{ik\xi}\sqrt{1+k^2}\int_{-\infty}^{\infty} d\xi'\xi' e^{i(k'-k)\xi'} = 0 \tag{6.20}$$

Insert the solution of the integral $\int_{-\infty}^{\infty} d\xi'\xi' e^{i(k'-k)\xi'} = -2\pi i\frac{\partial}{\partial k'}\delta(k'-k)$, see Appendix B.2, into Eq. 6.20 to get,

$$\omega^2\delta\rho(\xi) + i\sqrt{2\pi}\frac{eE_0}{m\,d}sgn(\xi)\int_{-\infty}^{\infty} dk\, e^{ik\xi}\sqrt{1+k^2}\int_{-\infty}^{\infty} dk'\delta\tilde{\rho}(k')\frac{\partial}{\partial k'}\delta(k'-k) = 0$$

The second term is integrated by parts to obtain,

$$\omega^2\delta\rho(\xi) - i\sqrt{2\pi}\frac{eE_0}{m\,d}sgn(\xi)\int_{-\infty}^{\infty} dk\, e^{ik\xi}\sqrt{1+k^2}\frac{d}{dk}\tilde{\rho}(k) = 0 \tag{6.21}$$

Multiply Eq. 6.21 by $e^{-ik'\xi}$ and integrate over ξ,

$$\begin{aligned}
\omega^2\int_{-\infty}^{\infty} d\xi e^{-ik'\xi}\delta\rho(\xi) &= i\sqrt{2\pi}\frac{eE_0}{m\,d}\int_{-\infty}^{\infty} dk\,\sqrt{1+k^2}\frac{d}{dk}\tilde{\rho}(k)\int_{-\infty}^{\infty} d\xi sgn(\xi)e^{ik\xi-ik'\xi} \\
&= i\sqrt{2\pi}\frac{eE_0}{m\,d}\int_{-\infty}^{\infty} dk\,\sqrt{1+k^2}\frac{d}{dk}\tilde{\rho}(k)\left[-\int_{-\infty}^{0} d\xi e^{i(k-k')\xi}\right. \\
&\quad \left.+\int_{0}^{\infty} d\xi e^{i(k-k')\xi}\right] \\
&= i\sqrt{2\pi}\frac{eE_0}{m\,d}\int_{-\infty}^{\infty} dk\,\sqrt{1+k^2}\frac{d}{dk}\tilde{\rho}(k)\left[2i\int_{0}^{\infty} d\xi\sin[(k-k')\xi]\right]
\end{aligned} \tag{6.22}$$

By substituting $2i\int_0^{\infty} d\xi\sin[(k-k')\xi] = 2i/(k-k')$, see Appendix B.3, we get the integral equation reduced to the much simpler form,

$$\boxed{\omega^2\delta\tilde{\rho}(k') = -2\sqrt{2\pi}\frac{eE_0}{m\,d}P\int_{-\infty}^{\infty} dk\,\frac{\sqrt{1+k^2}\,\tilde{\rho}'(k)}{(k-k')}} \tag{6.23}$$

where the symbol P denotes principle value. The solution to this eigenvalue problem is presented in the next section with a detailed proof in Appendix C.

6.3.1 Fundamental Results

The eigenfunctions and eigenvalues that solve Eq. 6.23 are summarized in this section, and the proof of the validity of those eigensolutions is presented in Appendix C. Even and odd eigenfunctions that solve Eq. 6.23 are,

$$\delta\tilde{\rho}_\alpha^+(k) \propto \cos\left(\alpha \,\text{arcsinh}\; k\right) \tag{6.24}$$

$$\delta\tilde{\rho}_\alpha^-(k) \propto \sin\left(\alpha \,\text{arcsinh}\; k\right) \tag{6.25}$$

where the + and − superscripts are used to differentiate even from odd solutions. The corresponding even and odd eigenfrequencies are

$$\omega_+^2(\alpha) = \frac{(2\pi)^{3/2}\, e\, E_0}{m\, d}\frac{\alpha}{\tanh(\pi\,\alpha/2)} \tag{6.26}$$

$$\omega_-^2(\alpha) = \frac{(2\pi)^{3/2}\, e\, E_0}{m\, d}\alpha\tanh(\pi\,\alpha/2) \tag{6.27}$$

Because the eigenfrequencies squared are proportional to α, the constant α must be a positive real number. The fact that there are no other constraints on α, making it a continuous parameter, is surprising because this means that we have continuous spectrum for confined plasmon along the x-direction. Also, for $\alpha = 0$, the lowest even mode $\omega_{\alpha=0}^2$ reduces to $4\sqrt{2\pi}eE_0/(m\,d)$ while the lowest odd mode vanishes. Thus, even modes are gapped and have higher energies than odd modes. Plug Eq. 6.24 into Eq. 6.23 to obtain,

$$\begin{aligned}
&\omega_+^2\delta\tilde{\rho}_\alpha^+(q) = -2\sqrt{2\pi}\frac{eE_0}{m\,d}\,P\int_{-\infty}^{\infty} dk\,\frac{\sqrt{1+k^2}}{k-q}\frac{d}{dk}\cos\left(\alpha\,\text{arcsinh}\; k\right)\\
&\Rightarrow \frac{(2\pi)^{3/2}\, e\, E_0}{m\, d}\frac{\alpha}{\tanh(\pi\,\alpha/2)}\delta\tilde{\rho}_\alpha^+(q) = 2\sqrt{2\pi}\alpha\frac{eE_0}{m\,d}\,P\int_{-\infty}^{\infty} dk\frac{\sin\left(\alpha\,\text{arcsinh}\; k\right)}{k-q}\\
&\Rightarrow \frac{\pi}{\tanh(\pi\,\alpha/2)}\cos\left(\alpha\,\ln[q+\sqrt{1+q^2}]\right) = P\int_{-\infty}^{\infty} dk\frac{\sin\left(\alpha\,\text{arcsinh}\; k\right)}{k-q}\\
&\Rightarrow \cos\left(\alpha\,\ln[q+\sqrt{1+q^2}]\right) = \frac{\tanh(\pi\,\alpha/2)}{\pi}\,P\int_{-\infty}^{\infty} dk\frac{\sin\left(\alpha\,\text{arcsinh}\; k\right)}{k-q}
\end{aligned} \tag{6.28}$$

where in the second step we used Eq. 6.26 to substitute for ω_+^2. The last line shows that we can write Eq. 6.23 in the form of Hilbert transform,

$$H(x) = \frac{1}{\pi}P\int_{-\infty}^{\infty} dt\frac{g(t)}{t-x}$$

such that an even solution of certain α is the Hilbert transform of the odd solution of the same α. The coefficients of the eigenfunctions are chosen in such a way that we can cancel

the $\tanh(\pi\,\alpha/2)$ term in Eq. 6.28. Because the inverse Fourier transform of the Hilbert transform has the form,

$$\mathscr{F}^{-1}[H(x)] = i\,sgn(x)\mathscr{F}^{-1}[g(x)]$$

the odd solutions are multiplied by i to make them real functions in real space and the Hilbert transform equation is multiplied by $-i$ to keep the equality in Eq. 6.28. Thus, the final forms of the eigenfunctions are,

$$\delta\tilde{\rho}_\alpha^+(k) = \cosh(\pi\alpha/2)\cos\left(\alpha\,\mathrm{arcsinh}\;k\right) \tag{6.29}$$

$$\delta\tilde{\rho}_\alpha^-(k) = i\sinh(\pi\alpha/2)\sin\left(\alpha\,\mathrm{arcsinh}\;k\right) \tag{6.30}$$

The solutions are related by the Hilbert transform as follows,

$$\delta\tilde{\rho}_\alpha^+(q) = \frac{-i}{\pi}P\int_{-\infty}^{\infty} dk\frac{\delta\tilde{\rho}_\alpha^-(k)}{k-q}$$

and their inverse Fourier transforms satisfy the equation,

$$\delta\rho_\alpha^-(\xi) = sgn(\xi)\delta\rho_\alpha^+(\xi) \tag{6.31}$$

We applied the inverse Fourier transform to the solutions to obtain the plasmon charge distribution in real space, see Appendix C.3 for detailed calculations,

$$\delta\rho_\alpha^+(\xi) = \frac{\alpha\sinh(\pi\alpha)}{|\xi|\sqrt{2\pi}}K_{i\alpha}(|\xi|) \tag{6.32}$$

$$\delta\rho_\alpha^-(\xi) = \frac{\alpha\sinh(\pi\alpha)}{\xi\sqrt{2\pi}}K_{i\alpha}(|\xi|) \tag{6.33}$$

6.3.2 Analysis

To analyze the behavior of the solutions we start with studying the asymptotic behavior of the plasmon propagation at small and large distances form the p-n junction. Because even and odd solutions are related by Eq. 6.31, it is enough to study the behavior of even modes. For large $\xi \gg 1$, the asymptotic behavior of the MacDonald function is $K_{i\alpha}(\xi) \approx \sqrt{\frac{\pi}{2\xi}}e^{-\xi}$. Thus, Eq. 6.32 becomes,

$$\delta\rho_\alpha^+(\xi) \approx \frac{\alpha\sinh(\pi\alpha)e^{-\xi}}{2\xi^{3/2}} \tag{6.34}$$

The exponential term shows that plasmons decay very fast for large ξ, i.e., for large x, indicating that plasmons are localized in the x direction in the order of their wavelength $x \sim \lambda$.

In the limit of small $\xi \ll 1$, the eigenfunction simplifies to,

$$\delta\rho_\alpha^+(\xi) \approx -\frac{\alpha}{2\xi}\mathrm{Im}\frac{(\xi/2)^{i\alpha}}{\Gamma(1+i\alpha)} \tag{6.35}$$

where the term $\xi^{i\alpha}$ can be written as,

$$\xi^{i\alpha} = e^{\ln(\xi)^{i\alpha}} = e^{i\alpha\ln\xi} = \cos(\alpha\ln\xi) + i\sin(\alpha\ln\xi) \tag{6.36}$$

As ξ gets smaller, its logarithm gets more negative more rapidly and consequently the oscillations become faster. Thus, the eigenfunction becomes infinitely oscillatory with infinitely many nodes. Generally, localized oscillations are discrete such that eigenfunctions gain one more node as they go up the ladder of some discrete parameter, in our case the infinite oscillatory behavior at small x explains the continuous nature of the parameter α.

To analyze this result, we try to write the differential equation that is satisfied by the eigenfunctions in the form of Schrödinger equation. The differential equation satisfied by our solutions is,

$$\xi^2\delta\rho''(\xi) + 3\xi\,\delta\rho'(\xi) + (1-\xi^2+\alpha^2)\delta\rho(\xi) = 0 \tag{6.37}$$

let $\delta\rho(\xi) = g(\xi)f(\xi)$, thus, the differential equation becomes

$$\begin{aligned}\xi^2[g''(\xi)f(\xi) + g(\xi)f''(\xi) + 2g'(\xi)f'(\xi)] \quad &+ \quad 3\xi[g'(\xi)f(\xi) + g(\xi)f'(\xi)] \\ &+ \quad [1-\xi^2+\alpha^2]g(\xi)f(\xi) = 0\end{aligned}$$

Since the Schrödinger equation does not have a first derivative, we set the sum of terms that have first derivative of $f(\xi)$ to zero. Therefore,

$$2\xi^2 g'(\xi)f'(\xi) + 3\xi g(\xi)f'(\xi) = 0 \Rightarrow 2\xi^2 g'(\xi) + 3\xi g(\xi) = 0$$

Consequently the solutions to the functions $g(\xi)$ and $f(\xi)$ are,

$$g(\xi) = -\frac{2\xi}{3}g'(\xi) \Rightarrow g(\xi) = \xi^{-3/2}$$
$$f(\xi) = \sqrt{\xi}K_{i\alpha}(|\xi|)$$

By substituting $g(\xi)$ and $f(\xi)$ into the differential equation (Eq. 6.37) we obtain,

$$\xi^2\left[\frac{5}{2}\frac{3}{2}\xi^{-7/2}f(\xi) + \xi^{-3/2}f''(\xi)\right] + 3\xi\left[\frac{-3}{2}\xi^{-5/2}f(\xi)\right] + \left[1-\xi^2+\alpha^2\right]\xi^{-3/2}f(\xi) = 0$$

$$\frac{15}{4}\xi^{-3/2}f(\xi) + \xi^{1/2}f''(\xi) - \frac{9}{2}\xi^{-3/2}f(\xi) + [1-\xi^2+\alpha^2]\xi^{-3/2}f(\xi) = 0$$

$$\xi^{1/2}f''(\xi) + \left[\frac{15}{4}\xi^{-3/2} - \frac{9}{2}\xi^{-3/2} + \xi^{-3/2} - \xi^{1/2} + \alpha^2\xi^{-3/2}\right]f(\xi) = 0$$

$$f''(\xi) + \left[\frac{\frac{1}{4}+\alpha^2}{\xi^2} - 1\right]f(\xi) = 0$$

The above expression has the form of Schrödinger equation,

$$\psi''(x) + (\frac{2mE}{\hbar^2} - \frac{2mV}{\hbar^2})\psi(x) = 0$$

if we replace $\frac{2mE}{\hbar^2}$ by -1 and $-\frac{2mV}{\hbar^2}$ by $\frac{\frac{1}{4}+\alpha^2}{x^2}$. As a result, our solutions are similar to the eigenfunctions of a particle falling to the center in a 2D potential $-1/r^2$ [3]. The problem of continuous eigenvalues and infinite oscillations of eigenfunctions for small ξ might be resolved by using WKB approximation to quantize α. This approach, however, was complicated and a simpler way to quantize the eigenvalues was adopted.

The problem was resolved by realizing that the semiclassical approach here is applicable only to distances much larger than the Fermi wavelength, a condition initially assumed and stated. Very close to the p-n junction, however, the Fermi wavelength becomes large compared with the distance from the p-n junction. Thus, we defined a cutoff distance below which the semiclassical approach fails. Let's call this cutoff a and take it to be in the order of the Fermi wavelength $a \sim \lambda_F$. Since $\lambda_F = 2\pi/k_F$, where k_F is x dependent, the Fermi momentum is in the order of,

$$k_F \sim \sqrt{\rho_0 \pi / e} = \sqrt{\frac{E_0 x}{ed}}$$

where we have used Eq. A.2 and Eq. 6.16. Because we are interested in finding the Fermi wavelength at the cutoff, we take $x \sim a$. Thus, the cutoff distance is in the order of,

$$a \sim \sqrt{\frac{ed}{E_0 a}} \Rightarrow a^{3/2} \sim \sqrt{\frac{d}{L_E^2}} \Rightarrow a \sim l_E (d/l_E)^{1/3} \tag{6.38}$$

After estimating the cutoff distance, the challenge is to determine the quantization condition. From Eq. 6.36 we understand that the nodes increase logarithmically as we approach the p-n junction and thus the eigenfunctions can be regularized. Also, the behavior of the charge density accumulated at distances very close to the p-n junction affects the regularization scheme; physically we expect the charge density to decrease as we approach the p-n junction until it vanishes there. Hence, an infinite charge accumulation for example would pose major obstacle to the regularization procedure. To understand the behavior of charge accumulation at small ξ, we integrate Eq. 6.35 from zero to small value ϵ,

$$\int_0^\epsilon d\xi \delta\rho_\alpha^{(+)}(\xi) = A\cos(\alpha \ln(\xi/2) - \beta)$$

where β is the phase of the gamma function $\Gamma(1+i\alpha)$. The previous equation shows that the accumulated charge density has a constant finite amplitude and oscillates faster and faster

around zero as ξ approaches the p-n junction. Therefore, the average or the smoothed charge density $A\cos(\alpha\ln(\xi/2)-\beta)$ tends to vanish. Based on that analysis, we proposed the regularization condition,

$$K_{i\alpha}(qa)=0. \tag{6.39}$$

to quantize α and, consequently, plasmon spectrum. Therefore, the regularized eigenstate is,

$$\delta\rho_{\alpha}^{(+)}(\xi)\propto\begin{cases} K_{i\alpha}(\xi)/\xi, & \xi>qa \\ 0, & \xi\leq qa. \end{cases} \tag{6.40}$$

and the discrete values for $\alpha\ll 1$ can be approximated as follows,

$$\alpha_n=\frac{\pi n}{\ln\left(\dfrac{2e^{-\gamma}}{qa}\right)},\quad n=1,2,3,... \tag{6.41}$$

where $\gamma=0.58$ is the Euler's constant. The first three eigenfunctions $2\delta\rho_{\alpha_n}^{(+)}(\xi)/\cosh(\pi\alpha/2)$, $n=1,2$, and 3, are plotted in Fig. 6.3. The denominator is the total charge density accumulated along half the width of the flake that proved to be finite in spite of the singularity of the eigenfunctions,

$$\int_0^{\infty} d\xi\delta\rho_{\alpha}^{(+)}(\xi)=\frac{1}{2}\cosh\left(\frac{\pi\alpha}{2}\right).$$

In summary, in the limit of short wavelength, eigenfunctions and eigenvalues show peculiar behavior. Plasmon modes are continuous with even modes at higher energies than odd ones. This continuity could be explained by the infinite oscillatory behavior of the eigenfunctions at close distances to the p-n junction. That oscillatory behavior was regularized by imposing a cutoff at which no plasmon excitations exist. That regularization discretized the plasmon frequency.

6.4 Second Case: In the Limit of Long Wavelength $\lambda\gg d$

When the wavelength is in the order of or larger than the flake width, the electric field does not vanish at the edges of the flake. Therefore, a boundary condition has to be explicitly imposed so that no current moves across the flake's edge.

$$P\int_{-d}^{d} dx\,\frac{\delta\rho(x)}{x\pm d}=0 \tag{6.42}$$

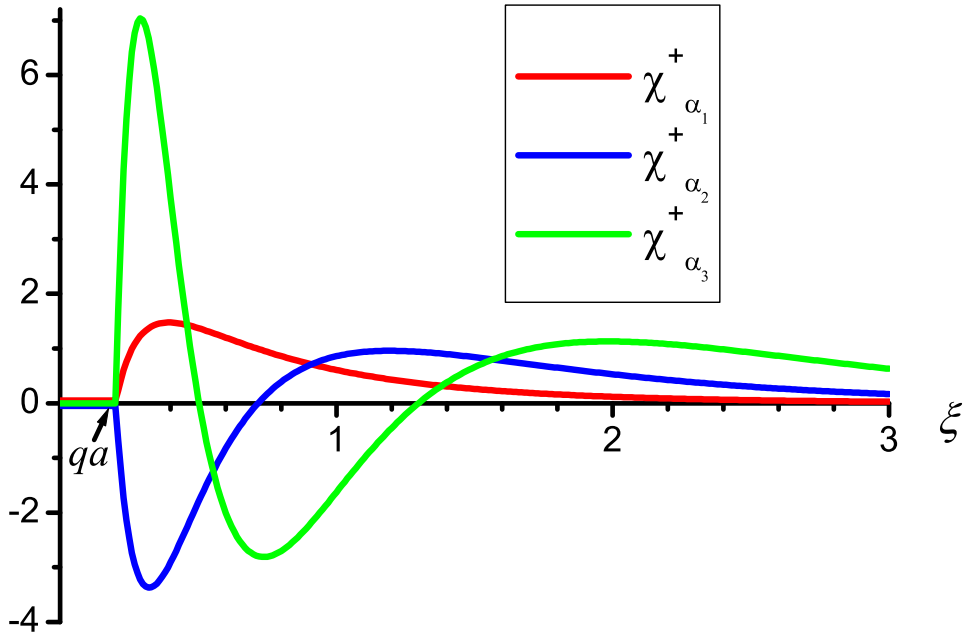

Figure 6.3: The normalized eigenfunctions $2\delta\rho^{(+)}_{\alpha_n}(\xi)/\cosh(\pi\alpha/2)$ are plotted, for the lowest three modes, $n = 1, 2$, and 3. The regularization parameter is $qa = 0.2$.

We start by trying to solve for the first even mode in the limit of small q by integrating both sides of Eq. 6.15,

$$\omega^2\delta\rho(x) + \frac{2e}{m}\left[\frac{d}{dx}|\rho_0(x)|\frac{d}{dx} - q^2|\rho_0(x)|\right]\int_{-d}^{d} dx'\delta\rho(x')K_0(q|x-x'|) = 0$$

to get,

$$\begin{aligned}
\int_{-d}^{d} dx\,\omega^2\delta\rho(x) &= -\frac{2e}{m}\int_{-d}^{d} dx\left[\frac{d}{dx}|\rho_0(x)|\frac{d}{dx} - q^2|\rho_0(x)|\right]\int_{-d}^{d} dx'\delta\rho(x')K_0(q|x-x'|) \\
&= -\frac{2e}{m}\int_{-d}^{d} dx\,\frac{d}{dx}\left(|\rho_0(x)|\frac{d}{dx}\int_{-d}^{d} dx'\delta\rho(x')K_0(q|x-x'|)\right) \\
&+ \frac{2e}{m}q^2\int_{-d}^{d} dx\,|\rho_0(x)|\int_{-d}^{d} dx'\delta\rho(x')K_0(q|x-x'|) \\
&= -\frac{2e}{m}\left[|\rho_0(x)|\underbrace{\frac{d}{dx}\int_{-d}^{d} dx'\delta\rho(x')K_0(q|x-x'|)}_{\approx J_x(\pm d)=0}\right]_{-d}^{d} \\
&+ \frac{2e}{m}q^2\int_{-d}^{d} dx\,|\rho_0(x)|\int_{-d}^{d} dx'\delta\rho(x')K_0(q|x-x'|) \qquad (6.43)
\end{aligned}$$

The first term in the last equality is zero due to the boundary condition, Eq 6.42. This can be shown by differentiating the integrand as follows,

$$\begin{aligned}\frac{d}{dx}\int_{-d}^{d} dx'\delta\rho(x')K_0(q|x-x'|) &= \int_{-d}^{d} dx'\delta\rho(x')\frac{d}{dx}K_0(q|x-x'|)\\ &= -q\,\mathrm{sgn}(x-x')\int_{-d}^{d} dx'\delta\rho(x')K_1(q|x-x'|)\\ &\approx -q\,\mathrm{sgn}(x-x')\int_{-d}^{d} dx'\frac{\delta\rho(x')}{q|x-x'|}\\ &= -\int_{-d}^{d} dx'\frac{\delta\rho(x')}{x-x'} \qquad (6.44)\end{aligned}$$

where we have used in the third line the asymptotic form of the the modified Bessel function $K_\alpha(x) \approx (\Gamma(\alpha)/2)\,(2/x)^\alpha$ for small arguments $0 < x \ll \sqrt{1+\alpha}$. After applying the integration limits on Eq. 6.44 we get,

$$\begin{aligned}\left[\frac{d}{dx}\int_{-d}^{d} dx'\delta\rho(x')K_0(q|x-x'|)\right]_{-d}^{d} &= \left[\int_{-d}^{d} dx'\frac{\delta\rho(x')}{x'-x}\right]_{-d}^{d}\\ &= P\int_{-d}^{d} dx'\frac{\delta\rho(x')}{x'-d} - P\int_{-d}^{d} dx'\frac{\delta\rho(x')}{x'+d} = 0\end{aligned}$$

The integrals of the last line must vanish due to the imposed boundary condition. Because $q = 2\pi/\lambda$ and $d \ll \lambda$, the dimensionless quantity $qd = 2\pi d/\lambda$ is a very small constant. Consequently $q|x-x'|$ is small for all values of $|x-x'|$ allowing the approximation of the MacDonald function to a logarithm,

$$\begin{aligned}K_0(q|x-x'|) \approx -\ln(q|x-x'|) - \gamma &= -\ln(\frac{d\,q|x-x'|}{d}) - \gamma\\ &= -\ln(\frac{|x-x'|}{d}) - \ln(d\,q) - \gamma\end{aligned}$$

where γ is Euler's constant. After replacing the MacDonald function with the logarithm Eq. 6.43 simplifies to,

$$\int_{-d}^{d} dx\,\omega^2\delta\rho(x) = \frac{2e}{m}q^2\int_{-d}^{d} dx\,|\rho_0(x)|\int_{-d}^{d} dx'\delta\rho(x')\left[-\ln(\frac{|x-x'|}{d}) - \ln(d\,q) - \gamma\right]$$

Substitute for $\rho_0(x)$, Eq. 6.7, to get,

$$\begin{aligned}&\int_{-d}^{d} dx\,\omega^2\delta\rho(x) = \frac{2e}{m}q^2\int_{-d}^{d} dx'\delta\rho(x')\int_{-d}^{d} dx\,\frac{E_0|x|}{\sqrt{d^2-x^2}}\left[-\ln(\frac{|x-x'|}{d}) - \ln(d\,q) - \gamma\right]\\ &= \frac{-2eE_0}{m}q^2\int_{-d}^{d} dx'\delta\rho(x')\left[\int_{-d}^{d} dx\,\frac{|x|}{\sqrt{d^2-x^2}}\ln(\frac{|x-x'|}{d}) + \int_{-d}^{d} dx\,\frac{|x|}{\sqrt{d^2-x^2}}\left[\ln(d\,q)+\gamma\right]\right]\\ &= \frac{-2eE_0}{m}q^2\int_{-d}^{d} dx'\delta\rho(x')\left[\int_{-d}^{d} dx\,\frac{|x|}{\sqrt{d^2-x^2}}\ln(\frac{|x-x'|}{d}) + 2d\left[\ln(d\,q)+\gamma\right]\right] \qquad (6.45)\end{aligned}$$

Because $qd \ll 1$ and consequently $|\ln(qd)| \gg 1$, we can ignore the other terms between brackets in the last line of Eq. 6.45,

$$\begin{aligned}\int_{-d}^{d} dx\, \omega^2 \delta\rho(x) &= \frac{-2eE_0}{m} q^2 \int_{-d}^{d} dx' \delta\rho(x') 2d\,[\ln(d\,q)] \\ &= \frac{-4\,d\,e\,E_0\,q^2}{m} \ln(d\,q) \int_{-d}^{d} dx' \delta\rho(x')\end{aligned}$$

As a result, we arrive at the approximate form of the first even eigenfrequency ω^2,

$$\boxed{\omega_{1+}^2 \approx \frac{4eE_0}{m} q^2 d\, \ln\left(\frac{1}{d\,q}\right)} \tag{6.46}$$

where $n\pm$ represents even/odd mode with $n-1$ nodes across the half width of the flake. From Eq. 6.46, it is clear that $\omega_{1+}(q=0) = 0$ because q^2 goes to zero faster than the logarithm goes to infinity. Thus, we can conclude that the lowest even mode is gapless and even. This finding contradicts the result we found in the previous section where the lowest mode in the limit of short wavelength was odd. This mode order reversal is surprising and interesting, it is discussed in detail in Section 6.5.

Another interesting behavior we have noticed is the absence of the first odd mode in the limit of $q \to 0$. In that limit, Eq. 6.15 can be approximated as,

$$\omega^2(q=0)\delta\rho(x) + \frac{2e}{m}\frac{d}{dx}\left[|\rho_0(x)|\frac{d}{dx}\int_{-d}^{d} dx' \delta\rho(x') K_0(q|x-x'|)\right] = 0$$

The differentiation operator inside the bracket is moved inside the integral to operate on the MacDonald function to get,

$$\omega^2(0)\delta\rho(x) = -\frac{2e}{m}\frac{d}{dx}\left[|\rho_0(x)| \int_{-d}^{d} dx' \frac{\delta\rho(x')}{x'-x}\right]$$

where the relation $\frac{d}{dx}K_0(q|x-x'|) = -q\,\mathrm{sgn}(x-x')K_1(q|x-x'|)$, and the asymptotic form of $K_1(q|x-x'|) \approx 1/(q|x-x'|)$ were used. Substituting for $\rho_0(x) = E_0 x/(d^2-x^2)^{1/2}$, Eq. 6.7, and changing variables $x/d \to \zeta$, we get,

$$\omega^2(0)\delta\rho(\zeta) = -\frac{2eE_0}{m\,d}\frac{d}{d\zeta}\left[\frac{|\zeta|}{\sqrt{1-\zeta^2}} \int_{-1}^{1} d\zeta' \frac{\delta\rho(\zeta')}{\zeta'-\zeta}\right] \tag{6.47}$$

In the case of gapless mode, i.e., $\omega(q=0) = 0$, the L.H.S of Eq. 6.47 vanishes and thus the term between brackets should be a finite constant at any ζ. The term $|\zeta|/(1-\zeta^2)^{1/2}$,

however, diverges at $\zeta = 1$ and consequently, the integral $\int_{-1}^{1} d\zeta' \delta\rho(\zeta')/(\zeta' - \zeta)$ has to vanish to make the term between brackets finite. Thus, the solution [14] to Eq. 6.47 is,

$$\delta\rho(\zeta) = \frac{1}{\sqrt{1-\zeta^2}} \tag{6.48}$$

with eigenvalue $\omega_1(q = 0) = 0$. Again, the lowest mode is even in contradiction to the short wavelength case.

The first odd mode in the limit $q \to 0$ is assumed to be the mode where there are no nodes across the flake's half width, i.e., a net charge is accumulated between the p-n junction and one edge of the flake at $\zeta = \pm 1$. To calculate the net accumulated charge, we integrate Eq. 6.47 over the flake's half-width to get,

$$\begin{aligned}
\omega^2(0) \int_0^1 d\zeta \delta\rho(\zeta) &= -\frac{2eE_0}{m\,d} \int_0^1 d\zeta \frac{d}{d\zeta} \left[\frac{|\zeta|}{\sqrt{1-\zeta^2}} \int_{-1}^{1} d\zeta' \frac{\delta\rho(\zeta')}{\zeta' - \zeta} \right] \\
&= -\frac{2eE_0}{m\,d} \frac{|\zeta|}{\sqrt{1-\zeta^2}} \int_{-1}^{1} d\zeta' \frac{\delta\rho(\zeta')}{\zeta' - \zeta} \Bigg|_{\zeta\to 0}^{\zeta\to 1} \\
&= \frac{2eE_0}{m\,d} \left[\frac{|\zeta|}{\sqrt{1-\zeta^2}} \int_{-1}^{1} d\zeta' \frac{\delta\rho(\zeta')}{\zeta' - \zeta} \Bigg|_{\zeta\to 0} - \frac{|\zeta|}{\sqrt{1-\zeta^2}} \int_{-1}^{1} d\zeta' \frac{\delta\rho(\zeta')}{\zeta' - \zeta} \Bigg|_{\zeta\to 1} \right]
\end{aligned} \tag{6.49}$$

The terms between brackets in Eq. 6.47 and Eq. 6.49 are proportional to the current in the x direction; this can be seen by going through the calculations that led to Eq. 6.15. Due to the boundary condition, Eq. 6.42, the second term in the last line has to vanish at the boundary, at $\zeta = 1$, i.e.,

$$J_x(\zeta = 1) \propto \frac{|\zeta|}{\sqrt{1-\zeta^2}} \int_{-1}^{1} d\zeta' \frac{\delta\rho(\zeta')}{\zeta' - \zeta} \Bigg|_{\zeta\to 1} = 0$$

Therefore, we arrive at the equation,

$$\frac{\omega^2(0) m\,d}{2eE_0} \int_0^1 d\zeta \delta\rho(\zeta) = \lim_{\zeta\to 0} \frac{|\zeta|}{\sqrt{1-\zeta^2}} \int_{-1}^{1} d\zeta' \frac{\delta\rho(\zeta')}{\zeta' - \zeta} \tag{6.50}$$

If the first odd mode is nodeless across the flake's half width, then the L.H.S. of Eq. 6.50 should be nonvanishing, i.e., charge accumulation takes place $\int_0^1 d\zeta \delta\rho(\zeta) \neq 0$. Consequently, the R.H.S., which is proportional to the current, should also be different from zero; in other words, we would have a current passing at $\zeta = 0$, i.e., across the p-n junction. The

equilibrium charge density $\rho_0(x=0)$ is zero at the p-n junction and thus, a nonvanishing current there means that the induced electric field should be infinite,

$$E \propto \int_{-1}^{1} d\zeta' \frac{\delta\rho(\zeta')}{\zeta' - \zeta} \sim \frac{1}{\zeta}$$

This can also be understood mathematically because the term $|\zeta|/\sqrt{1-\zeta^2}$ in Eq. 6.50 is zero at $\zeta = 0$ and thus the term $\int_{-1}^{1} d\zeta' \delta\rho(\zeta')/(\zeta' - \zeta)$ must be infinite to get finite current. A singular induced electric field can only be produced by a delta function plasmon profile, i.e., $\delta\rho(\zeta) \propto \delta(\zeta)$. This condition however contradicts the assumption that $\delta\rho(\zeta)$ is an odd function. Consequently, we have to deduce that the accumulated charge across the flake's half width is zero,

$$\int_{0}^{1} d\zeta \delta\rho(\zeta) = 0$$

and thus the lowest odd eigenstate must have at least one node between the p-n junction and the edges, i.e., in the limit $q \to 0$, the lowest odd eigenfrequency is ω_{2-}.

6.5 Mode Order Reversal at Intermediate Wavelengths, $q \sim 1/d$

Results (6.26), (6.27) and (6.46) have shown surprising reversal in the sequence of even and odd frequencies in different wavelength ranges. For long wavelengths, domain (a) in Fig. 6.4, even eigenfrequencies start with the gapless mode ω_0. However, in the limit of intermediate and short wavelengths, domains (b) and (c), odd eigenmodes start at lower frequencies than even ones implying that there exists an interesting mechanism by which this reversal of order takes place. This mechanism is explained through the physical picture illustrated in Fig. 6.5.

In the case of long wavelength $\lambda \gg 2d$, Fig. 6.5 (a), the first even mode (1+) has the lowest frequency due to the distribution of same sign charges for long distances across the width and length of the flake. Such distribution leads to the absence of transverse electric field and presence of weak longitudinal field E that exerts a restoring force on charge carriers. The motion of charges could be approximated as harmonic oscillations where the frequency is related to the force and consequently to the electric field through the relation $\omega^2 = F_{\text{rest}}/(m\Delta x)$. The first odd mode (1−) in long wavelength limit is prohibited for the reasons explained earlier and thus, no sketch of that mode is present in Fig. 6.5. In the case of higher order even modes, see mode (2+) in Fiq. 6.5, the pattern of positive and negative charges generates stronger transverse electric field E than in odd modes and consequently

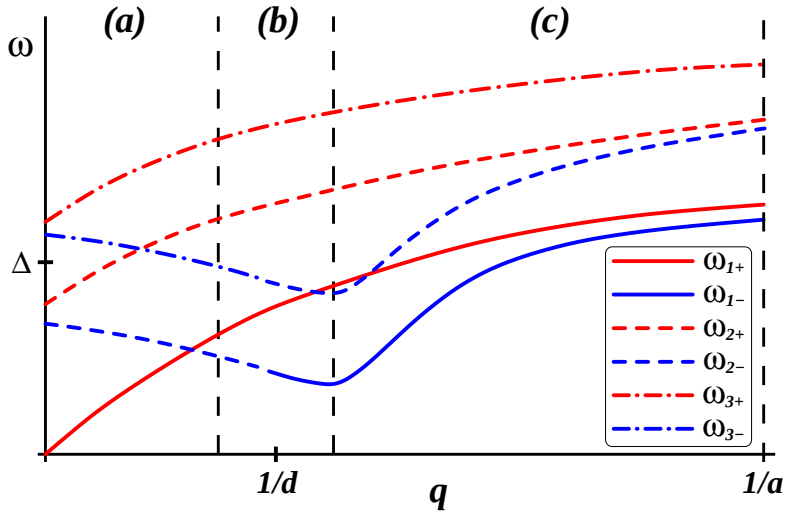

Figure 6.4: The sketch of even plasmon (red) and odd plasmon (blue) frequencies for $n = 1$ (solid lines) and $n = 2$ (dashed lines). The three regions, $q \ll 1/d$, $q \sim 1/d$, and $1/d \ll q < 1/a$ are denoted by (a), (b), and (c), respectively.

produces greater restoring force and frequency. For intermediate wavelengths $\lambda \sim 1/d$, i.e., in domain (b) in Fig. 6.5, the flake has positively charged regions and negatively charged ones that follow a checkerboard pattern such that each group of four charges forms two dipoles in the symmetric case and a quadrupole in the asymmetric case. Consequently the longitudinal electric field is larger in the even modes than that of the odd solutions producing greater frequencies in the former case, and as a result, reversing the pattern observed in the long wavelength range.

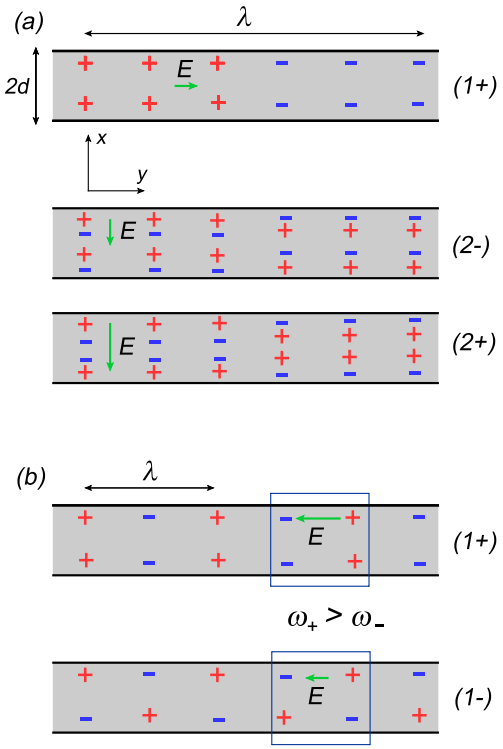

Figure 6.5: A physical picture of symmetric (denoted by S) and asymmetric (AS) plasmon modes for long and intermediate wavelengths. (a) In the limit of $q \to 0$ the first odd mode $(1-)$ is forbidden due to the difficulty of establishing current through the p-n junction. Thus, the first even mode $(1+)$ in the long wavelength range has the lowest frequency. It is shown in the uppermost sketch of $(1+)$ mode that the distribution of same sign charges along the flake's width generates a weak longitudinal electric field that is inversely proportional to λ^2; consequently the electric field vanishes in the limit of infinite wavelength, i.e., $q \to 0$ which implies that the first even mode is gapless. The second and third sketches show that the transverse electric field is greater in the $(2+)$ mode than in the $(2-)$ mode leading to stronger force and greater frequencies in even solutions than odd ones. (b) For intermediate wavelength $\lambda \sim d$, domain (b) in Fig. 6.4, odd eigenfrequencies start to decrease relative to even ones due to weaker longitudinal electric field in asymmetric modes. This could be explained by picturing the flake as checkerboard pattern of charge distribution where each group of four charges constitute either a double dipole in even modes or a quadrupole in odd ones.

CHAPTER 7

GATED BILAYER GRAPHENE

Gapless bilayer graphene has the disadvantage that it acts like a metal due to the gapless nature of its band structure. By opening a band gap, bilayer graphene can act like a semiconductor making it more adaptable to electronic applications. A band gap is opened in bilayer graphene by breaking the symmetry between the two layers through either chemically doping one of the layers or applying a perpendicular electric field. The second approach is preferred because the size of the band gap can be controlled by tuning the electric field using either a single gate, the case discussed in this work, or two gates.

A schematic diagram of the device is shown in Fig. 7.1 where the distance between the two layers, t, is assumed throughout the calculations to be much smaller than the distance between the bottom layer and the gate, i.e., $t \ll D$. The gate creates an electric field perpendicular to the layers' plane with magnitude $E = 4\pi en = 4\pi e(n_t + n_b)$ where e is the unit charge and n_t, n_b are the charge densities on the top and bottom layers. The electric field induces negative charge density, $-en_b$, on the bottom layer through hopping of electrons between the layers leaving an excess of positive charges on the top layer. The electric field between the layers is $E_m = E_g + E_{ind} = 4\pi e(n - n_b) = 4\pi en_t$ where E_g is the electric field from the gate and E_{ind} is the electric field due to induced charges on the bottom layer. There is positive charge density above the top layer and a negative density $-en_t$ just below. The potential difference between the gate and the bottom layer is $eV_g = eE_gD = 4\pi e^2nD$ and the potential difference between the layers is,

$$2U = eE_mt = 4\pi e^2n_tt \tag{7.1}$$

where the top layer is at potential U and the bottom layer at $-U$. Fig. 7.2 shows the potential energy due to the in-plane electric field E_0 superimposed on the band structure of the gated bilayer graphene. The band gap puts a threshold on the in-plane electric field E_0 below which no separation of charges happens leading to zero charge density and

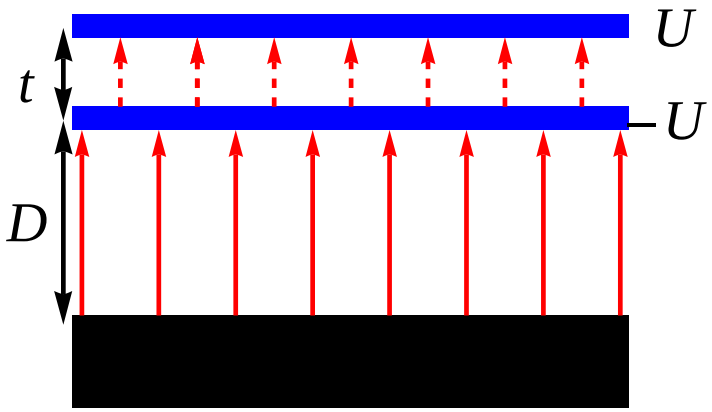

Figure 7.1: Schematic of n-type gated bilayer graphene. The two layers of graphene are represented by two blue slabs and the gate by a thicker black slab. The distance between the two layers is t and between the bottom layer and the gate is D. Since this is an n-type gating, field lines represented by arrows point upward. Positive charge density (holes) at the gate is denoted by $e(n_t + n_b)$ and it induces charge densities $-en_b$ on the bottom layer and $-en_t$ on the top layers . The potential difference between the two layers is $2U = 4\pi e^2 n_t t$

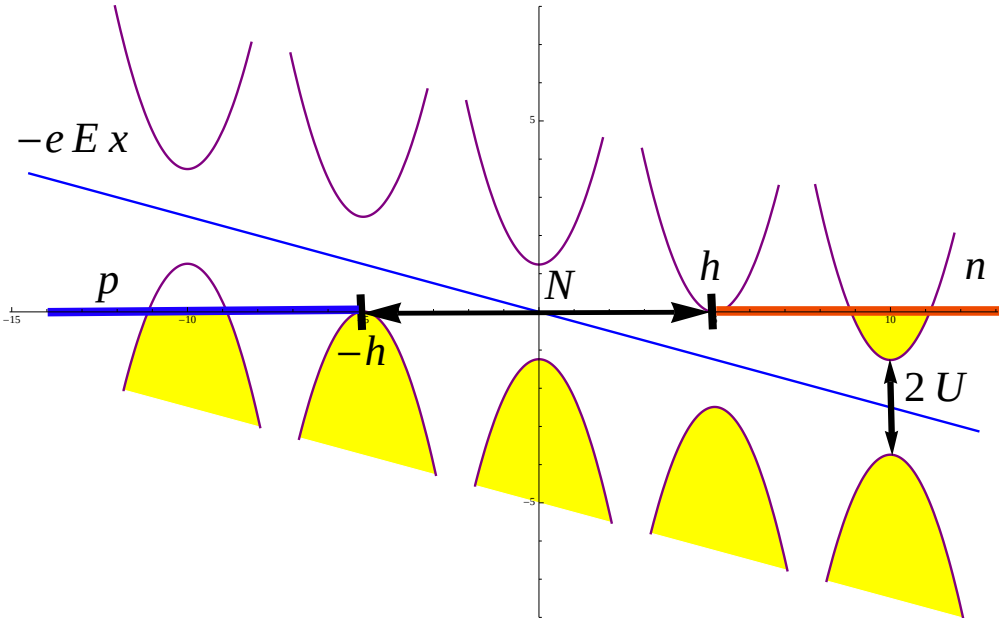

Figure 7.2: Electron band structure across the bilayer with an energy gap of $2U$. The positively charged p-region, denoted by blue line, and the negatively charged n-region, denoted by red line, are separated by a neutral (N) strip (black line) of width $2h = 2U/eE_0$ determined by the band gap and the slope of the potential due to the in-plane applied electric field E_0.

consequently absence of plasmons. A very large band gap would not allow the conduction band in the low potential region or the valence band in the high potential region to intersect the Fermi level. In other words, electrons would not have enough energy to flow from the valence band to the conduction band. Thus, the applied electric field must satisfy the condition, $E_0 \geq U/ed$. Because there is some region on the flake where U is too high, i.e., $U > |eE_0x|$, a neutral strip spreads over a width of $2h = 2U/eE_0$ separating the p- and n-regions.

Similar to the gapless case, we start with the condition that the electrochemical potential must be constant across the flake, i.e.,

$$\frac{\mu(x)}{e} + \phi(x) = 0 \tag{7.2}$$

where $\mu(x)$ is the chemical potential, $\phi(x) = -E_0\,x - 2\int_0^d dx'\rho_0(x')\ln(x + x'/|x - x'|)$ is the potential of the flake due to the applied in-plane field E_0 and the induced equilibrium charged density ρ_0. At temperature $T = 0$ K the chemical potential is equal to the Fermi energy $\mu = \epsilon_F$. The Fermi energy of bilayer graphene with a band gap, derived in Chapter 2, is

$$\epsilon_F(p) = \pm\sqrt{U^2 + (\frac{p_F^2}{2m})^2}$$

where $p_F^2 = \pi\hbar^2 n(x)$, see Eq. A.2, and $\rho_0(x) = sgn(x)|e|\,n(x)$. Therefore, the chemical potential is,

$$\mu(x) = -sgn(\rho_0)\sqrt{U^2 + \left(\frac{\rho_0(x)\pi\hbar^2}{2me}\right)^2} \tag{7.3}$$

To derive the equilibrium charge density, ρ_0, we insert Eq. 7.3 into the Thomas-Fermi equation, Eq. 7.2, to get,

$$E_0x + \mathrm{sgn}(x)\sqrt{\left(\frac{\pi a_B\rho_0(x)}{2}\right)^2 + \frac{U^2}{e^2}} + 2\int_0^d dx'\rho_0(x')\ln\frac{x + x'}{|x - x'|} = 0$$

The coefficient of the first term under the square root, Bohr radius $a_B = \hbar^2/(m\,e^2)$, is very small $\approx 10.6\,{}^0$A, and thus the term, $\pi a_B\rho_0(x)/2$, can be ignored to simplify the Thomas-Fermi equation to,

$$E_0x + \mathrm{sgn}(x)\frac{U}{e} + 2\int_0^d dx'\rho_0(x')\ln\frac{x + x'}{|x - x'|} = 0 \tag{7.4}$$

Eq. 7.4 was solved in Ref. [15] using conformal mapping to get,

$$\rho_0(x) = \mathrm{sgn}(x)E_0\sqrt{\frac{x^2 - h^2}{d^2 - x^2}}\,\Theta(|x| - h) \tag{7.5}$$

where h is half the length of the neutral strip. The integral equation in $\delta\rho$ is derived using three main equations, the continuity equation, Coloumb law and the hydrodynamic equation, Eq. 5.9,

$$\dot{\rho}(\mathbf{r},t) + \nabla \cdot \mathbf{J}(\mathbf{r},t) = 0 \tag{7.6}$$

$$\mathbf{E}(\mathbf{r},t) = \mathbf{E}_0 - \nabla \int d^2r' \rho(\mathbf{r}',t) \left[\frac{1}{|\mathbf{r}-\mathbf{r}'|} - \frac{1}{\sqrt{(\mathbf{r}-\mathbf{r}')^2 + 4D^2}} \right] \tag{7.7}$$

$$\dot{\mathbf{J}}(\mathbf{r},t) = \frac{e\, v_F^2 \nu(\mu)}{2} (e\mathbf{E} - \nabla\mu) \tag{7.8}$$

where the last term in Eq. 7.7 is added due to the effect of image charges at a distance $2D$ from the bilayer. The term $e\, v_F^2\nu(\mu)/2$ in Eq. 7.8 should be written entirely in terms of ρ and U, therefore,

$$e\, v_F^2\nu(\mu)/2 = \frac{e v_F\, p_F}{\pi\hbar^2} = \frac{e}{\pi\hbar^2} \times \frac{\left(\frac{\hbar^2\pi}{2me}\right)^2 \rho}{\sqrt{U^2 + \left(\frac{\hbar^2\pi\rho}{2me}\right)^2}} \times \frac{2ep_F}{\pi\hbar^2} \times p_F = \frac{\hbar^2\pi}{2m^2e} \frac{\rho^2}{\sqrt{U^2 + \left(\frac{\hbar^2\pi\rho}{2me}\right)^2}}, \tag{7.9}$$

where we have made the substitutions for the density of states $\nu(\mu) = 2p_F/\pi\hbar^2 v_F$, Fermi momentum $p_F^2 = \pi\hbar^2|\rho|/e$; since $\rho = \mathrm{sgn}(x) e\, n(x) = \mathrm{sgn}(x) e p_F^2/(\pi\hbar^2)$, and Fermi velocity,

$$v_F = \frac{d\mu}{dp_F} = \frac{d\mu}{d\rho}\frac{d\rho}{dp_F} = \frac{\left(\frac{\hbar^2\pi}{2me}\right)^2 \rho}{\sqrt{U^2 + \left(\frac{\hbar^2\pi\rho}{2me}\right)^2}} \times \frac{2ep_F}{\pi\hbar^2}$$

To simplify Eq. 7.9 we consider only the case where the width of the neutral strip is much greater than the Bohr radius, $h \gg a_B \Rightarrow \hbar^2\pi\rho/(2me) \ll U$, since $2h = 2U/eE_0$. Therefore, we can replace $e\, v_F^2\nu(\mu)/2$ with $\hbar^2\pi\rho^2/(2m^2eU)$ in Eq. 7.8 to get the much simplified form of the derivative of the current density,

$$\dot{\mathbf{J}}(\mathbf{r},t) = \frac{\hbar^2\pi}{2m^2e}\frac{\rho^2}{U}(e\mathbf{E} - \nabla\mu)$$

By following the same procedure as in Section 5.2, see Eq. 6.13, we get

$$-i\omega\delta\rho(x)e^{iqy-iwt} - \frac{i}{\omega}\frac{\hbar^2\pi}{2m^2U}\nabla_r \cdot \rho_0^2(x) \times \left[\nabla \int d^2r' \delta\rho(\mathbf{r}',t) \left[\frac{1}{|\mathbf{r}-\mathbf{r}'|} - \frac{1}{\sqrt{(\mathbf{r}-\mathbf{r}')^2 + 4D^2}} \right]\right] = 0$$

where we have inserted Eq. 7.7 and Eq. 7.8 into Eq. 7.6. Realizing that charge fluctuations are propagating waves, the time dependent part is separated by writing $\delta\rho(\mathbf{r}',t) = \delta\rho(x')e^{i(qy'-\omega t)}$, hence, the the equation becomes,

$$-i\omega\delta\rho(x)e^{iqy-iwt} - \frac{i}{\omega}\frac{\hbar^2\pi}{2m^2U}\nabla_r\cdot\rho_0^2(x)\nabla\left[\int_{-d}^{d}dx'\int_{-\infty}^{\infty}dy'\frac{\delta\rho(x')e^{i(qy'-\omega t)}}{\sqrt{(x-x')^2+(y-y')^2}}\right.$$
$$\left.-\int_{-d}^{d}dx'\int_{-\infty}^{\infty}dy'\frac{\delta\rho(x')e^{i(qy'-\omega t)}}{\sqrt{(x-x')^2+(y-y')^2+4D^2}}\right]=0 \tag{7.10}$$

By substituting the integrals $\int_{-\infty}^{\infty}dy'e^{iqy'}/\sqrt{(x-x')^2+(y-y')^2} = 2e^{iqy}K_0(q|x-x'|)$ and $\int_{-\infty}^{\infty}dy'e^{iqy'}/\sqrt{(x-x')^2+(y-y')^2+4D^2} = 2e^{iqy}K_0(q\sqrt{(x-x')^2+4D^2})$, see Appendix B.4, and multiplying by $\omega/(ie^{-i\omega t})$, the integro-differential equation reduces to,

$$-\omega^2e^{iqy}\delta\rho(x) - \frac{\hbar^2\pi}{m^2U}\nabla_r\cdot\rho_0^2(x)\nabla\int_{-d}^{d}dx'\delta\rho(x')e^{iqy}\big[K_0(q|x-x'|)$$
$$-K_0(q\sqrt{(x-x')^2+4D^2})\big]=0 \tag{7.11}$$

Eq. 7.11 is simplified by expanding the divergence and gradient operators to obtain,

$$\omega^2e^{iqy}\delta\rho(x) = -\frac{\hbar^2\pi}{m^2U}(\frac{\partial}{\partial x}\mathbf{i}+\frac{\partial}{\partial y}\mathbf{j})\cdot\rho_0^2(x)$$
$$\times\left[(\frac{\partial}{\partial x}\mathbf{i}+\frac{\partial}{\partial y}\mathbf{j})\int_{-d}^{d}dx'\delta\rho(x')e^{iqy}\left[K_0(q|x-x'|)-K_0(q\sqrt{(x-x')^2+4D^2})\right]\right]$$
$$=-\frac{\hbar^2\pi}{m^2U}\frac{\partial}{\partial x}\rho_0^2(x)\left[\frac{\partial}{\partial x}\int_{-d}^{d}dx'\delta\rho(x')e^{iqy}\left[K_0(q|x-x'|)-K_0(q\sqrt{(x-x')^2+4D^2})\right]\right]$$
$$-\frac{\hbar^2\pi}{m^2U}\rho_0^2(x)\frac{\partial^2}{\partial y^2}\int_{-d}^{d}dx'\delta\rho(x')e^{iqy}\left[K_0(q|x-x'|)-K_0(q\sqrt{(x-x')^2+4D^2})\right]$$
$$=-\frac{\hbar^2\pi}{m^2U}\frac{\partial}{\partial x}\rho_0^2(x)\left[\frac{\partial}{\partial x}\int_{-d}^{d}dx'\delta\rho(x')e^{iqy}\left[K_0(q|x-x'|)-K_0(q\sqrt{(x-x')^2+4D^2})\right]\right]$$
$$+\frac{\hbar^2\pi}{m^2U}\rho_0^2(x)q^2\int_{-d}^{d}dx'\delta\rho(x')e^{iqy}\left[K_0(q|x-x'|)-K_0(q\sqrt{(x-x')^2+4D^2})\right]$$

Cancel e^{iqy} and rearrange,

$$\omega^2\delta\rho(x)+\frac{\hbar^2\pi}{m^2U}\left[\frac{d}{dx}\rho_0^2(x)\frac{d}{dx}-\rho_0^2(x)q^2\right]\int_{-d}^{d}dx'\delta\rho(x')$$
$$\times\left[K_0(q|x-x'|)-K_0(q\sqrt{(x-x')^2+4D^2})\right]=0 \tag{7.12}$$

Because Eq. 7.12 is too complicated to solve exactly, we consider three limiting cases: (a) short wavelength limit, $\lambda \ll D \ll h$, (b) intermediate wavelength limit, $D \ll \lambda \ll h$, and (c) long wavelength limit, $h \ll \lambda$.

7.1 Short Wavelength, $\lambda \ll D \ll h$

We consider the case where the wavelength of plasmons are much smaller than the width of the neutral strip, $\lambda \ll h$. In other words, the propagating plasmons on each side of the flake are almost decoupled and thus can be considered independent. By substituting Eq. 7.5 for $\rho_0(x)$ in Eq. 7.12, the integro-differential equation becomes,

$$\omega^2\delta\rho(x) + \frac{\hbar^2\pi}{m^2U}\left[\frac{d}{dx}E_0^2\frac{x^2-h^2}{d^2-x^2}\,\Theta(|x|-h)\frac{d}{dx} - q^2E_0^2\frac{x^2-h^2}{d^2-x^2}\,\Theta(|x|-h)\right] \times \int_{-d}^{d} dx'\delta\rho(x')\left[K_0(q|x-x'|) - K_0(q\sqrt{(x-x')^2+4D^2})\right] = 0$$

We use the theta function that represents the neutral strip to split the integration limits as follows,

$$\omega^2\delta\rho(x) + \frac{\hbar^2\pi}{m^2U}\left[\frac{d}{dx}E_0^2\frac{x^2-h^2}{d^2-x^2}\frac{d}{dx} - q^2E_0^2\frac{x^2-h^2}{d^2-x^2}\right] \times \left[\int_{-d}^{-h} dx'\delta\rho(x')\left(K_0(q|x-x'|) - K_0(q\sqrt{(x-x')^2+4D^2})\right) + \int_{h}^{d} dx'\delta\rho(x')\left(K_0(q|x-x'|) - K_0(q\sqrt{(x-x')^2+4D^2})\right)\right] = 0$$

For the first integral with integration limits $-d$ to $-h$, the variable of integration x' can replaced by $-x'$ to get,

$$\omega^2\delta\rho(x) + \frac{\hbar^2\pi}{m^2U}\left[\frac{d}{dx}E_0^2\frac{x^2-h^2}{d^2-x^2}\frac{d}{dx} - q^2E_0^2\frac{x^2-h^2}{d^2-x^2}\right] \times \left[\int_{h}^{d} dx'\delta\rho(x')\left(K_0(q|x-x'|) - K_0(q\sqrt{(x-x')^2+4D^2})\right) \pm \int_{h}^{d} dx'\delta\rho(x')\left(K_0(q|x+x'|) - K_0(q\sqrt{(x+x')^2+4D^2})\right)\right] = 0 \tag{7.13}$$

where the $\pm$ is due to the fact that $\delta\rho(-x) = \delta\rho(x)$ if even or $\delta\rho(-x) = -\delta\rho(x)$ if odd. By letting $x - h = \tilde{x}$, the term $(x^2-h^2)/(d^2-x^2)$ can be written as,

$$(x-h)(x+h)/(d^2-x^2) = \tilde{x}(\tilde{x}+2h)/(d^2-2\tilde{x}h-h^2-\tilde{x}^2) \tag{7.14}$$

By taking $d \gg h \gg \tilde{x}$ we obtain,

$$\frac{x^2-h^2}{d^2-x^2} \approx \frac{2h\tilde{x}}{d^2} \tag{7.15}$$

After replacing the integration variable x with $\tilde{x}$ and changing the integration limits from 0 to $d-h=l$, Eq. 7.13 can be written as,

$$\omega^2\delta\rho(x)+\frac{\hbar^2\pi}{m^2U}\frac{2hE_0^2}{d^2}\left[\frac{d}{d\tilde{x}}\tilde{x}\frac{d}{d\tilde{x}}-q^2\tilde{x}\right]\int_0^l d\tilde{x}'\delta\rho(\tilde{x}')\Big[K_0(q|\tilde{x}-\tilde{x}'|)$$
$$-K_0(q\sqrt{(\tilde{x}-\tilde{x}')^2+4D^2})\pm K_0(q|\tilde{x}+\tilde{x}'+2h|)\mp K_0(q\sqrt{(\tilde{x}+\tilde{x}'+2h)^2+4D^2})\Big]=0$$

The last two terms can be ignored because they never diverge and almost cancel each other. Because the wavelength is taken much smaller than the distance between the flakes and gate, D, the charges interact in a much smaller scale than the distance to image charges. Thus, the effect of the image charges can be ignored by eliminating the term $K_0(q\sqrt{(\tilde{x}-\tilde{x}')^2+4D^2})$ to reach the equation,

$$\omega^2\delta\rho(\tilde{x})+\frac{\hbar^2\pi}{m^2U}\frac{2hE_0^2}{d^2}\left[\frac{d}{d\tilde{x}}\tilde{x}\frac{d}{d\tilde{x}}-q^2\tilde{x}\right]\int_0^l d\tilde{x}'\delta\rho(\tilde{x}')K_0(q|\tilde{x}-\tilde{x}'|)=0 \tag{7.16}$$

Eq. 7.16 has a similar form to that of Eq. 6.18. In that case, see Chapter 6, the eigenfrequencies depended very weakly on q as $\omega^2\propto 1/\ln(1/q)$. Therefore, the spectrum for band gapped bilayer graphene in the limit of very short wavelength can be approximated as,

$$\omega^2\sim\frac{hE_0^2}{m^2d^2U} \tag{7.17}$$

where the spectrum is doubly degenerate due to the decoupling of plasmons modes on both sides of the flake.

7.2 Intermediate Wavelength, $D\ll\lambda\ll h$

Since the wavelength is still much smaller than the neutral strip h, $\rho_0(x)$ can be approximated as in Eq. 7.15. However, image charges cannot be ignored in that case because the wavelength is much greater than the bilayer-to-gate separation and consequently the charge density $\delta\rho(x)$ changes very slowly in comparison to the K_0 term. Therefore, we can replace,

$$K_0(q|x-x'|)-K_0(q\sqrt{(x-x')^2+4D^2})=\frac{1}{2}\int_{-\infty}^{\infty}\frac{dk}{\sqrt{q^2+k^2}}\left(1-e^{-2D\sqrt{q^2+k^2}}\right)e^{ik(x-x')}$$

with a delta function $2\pi D\delta(x-x')$ to simplify Eq. 7.12 to,

$$\omega^2\delta\rho(\tilde{x})+2\pi\frac{\hbar^2\pi}{m^2U}\frac{2hE_0^2}{d^2}\left[\frac{d}{d\tilde{x}}\tilde{x}\frac{d}{d\tilde{x}}-q^2\tilde{x}\right]\int_0^l d\tilde{x}'\delta\rho(\tilde{x}')D\delta(\tilde{x}-\tilde{x}')=0$$

where we have substituted $\rho_0^2 = 2hE_0^2\tilde{x}/d^2$. By letting $4\pi^2\hbar^2\, E_0^2 h\, D/(d^2m^2U) = C^2$ and dividing the equation by C^2, the integral equation converts into the following differential one,

$$\tilde{x}\frac{d^2}{d\tilde{x}^2}\delta\rho(\tilde{x}) + \frac{d}{d\tilde{x}}\delta\rho(\tilde{x}) + \left[\frac{\omega^2}{C^2} - q^2\tilde{x}\right]\delta\rho(\tilde{x}) = 0 \tag{7.18}$$

This equation has the form of the radial Schrödinger equation for a 2D hydrogen atom [20]:

$$\frac{d^2}{dr^2}R(r) + \frac{1}{r}\frac{d}{dr}R(r) + \left[\frac{2m_e}{\hbar^2}\left[E + \frac{Ze^2}{r}\right] - \frac{l^2}{r^2}\right]R(r) = 0$$

with the quantum number $l = 0$. Let's define $\tilde{x} = N\,C^2\,z/\omega^2$ and replace $\delta\rho(\tilde{x})$ by $\delta\rho(z) = e^{-z/2}G(z)$, then Eq. 7.18 becomes,

$$ze^{-z/2}G''(z) + (1-z)e^{-z/2}G'(z) + \left[N - 1/2 + \frac{z}{4} - q^2\left(\frac{NC^2}{w^2}\right)^2 z\right]e^{-z/2}G(z) = 0$$

By dividing the equation by $e^{-z/2}$ and defining $q \equiv \omega^2/(2NC^2)$, we arrive at the confluent hypergeometric differential equation,

$$zG''(z) + (1-z)G'(z) - [-N + 1/2]\,G(z) = 0$$

The general solution to this equation is,

$$G(z) = b_1\,{}_1F_1(a = -N + 1/2; b = 1; z) + b_2\,U(a = -N + 1/2; b = 1; z)$$

where ${}_1F_1(-N+1/2; 1; z)$ and $U(-N+1/2; 1; z)$ are the confluent hypergeometric functions of the first and second kind. We keep only the first solution since U diverges at $z = 0$. Because the confluent hypergeometric function of the first kind, ${}_1F_1(-N + 1/2; 1; z)$, is a polynomial in z, it converges only if it has a finite number of terms. This condition is satisfied when a is zero or a negative integer, and $b < a$ or $b > 0$. Thus,

$$-N + 1/2 = -n \Rightarrow N = n + 1/2, \quad \text{where } n = 0, 1, 2, 3..$$

Since $q = \omega^2/(2NC^2)$ and $C^2 = (4\pi^2\hbar^2\, E_0^2 h\, D)/(d^2m^2U)$ the eigenfrequencies are,

$$\omega_n^2 = 2NC^2q = (n + 1/2)\frac{8\pi^2\hbar^2\, E_0^2 h\, D}{d^2m^2U}q \tag{7.19}$$

and the eigenfunctions $\delta\rho$ are,

$$\begin{aligned}\delta\rho_n(\tilde{x}) =& e^{-\frac{\omega_n^2}{2NC^2}\tilde{x}}\,{}_1F_1(-N + 1/2; 1; \frac{\omega_n^2}{N\,C^2}\tilde{x}) \\ =& e^{-q\tilde{x}}\,{}_1F_1(-n; 1; 2q\tilde{x})\end{aligned} \tag{7.20}$$

Since $\delta\rho$ does not vanish at the boundary of the neutral strip, $\tilde{x} = x - h = 0$, we can conclude that there are finite fluctuations at the boundary of the neutral strip. Also, it is obvious that the spectrum has q dependence.

7.3 Long Wavelength, $h \ll \lambda$

Similar to the last two sections, we start by approximating the charge density ρ_0 to a simpler form,

$$\begin{aligned}
\rho_0(x) = \mathrm{sgn}(x)\,\Theta(|x|-h)E_0\sqrt{\frac{x^2-h^2}{d^2-x^2}} &= \mathrm{sgn}(x)\,\Theta(|x|-h)E_0\sqrt{\frac{(x-h)(x+h)}{(d-x)(d+x)}} \\
&= \mathrm{sgn}(\tilde{x})E_0\sqrt{\frac{\tilde{x}(\tilde{x}+2h)}{(d-\tilde{x}-h)(d+\tilde{x}+h)}} \\
&= \mathrm{sgn}(\tilde{x})E_0\sqrt{\frac{\tilde{x}^2+2h\tilde{x}}{d^2-\tilde{x}^2-2\tilde{x}h-h^2}} \\
&\approx \mathrm{sgn}(\tilde{x})E_0\sqrt{\frac{\tilde{x}^2}{d^2}}
\end{aligned}$$

In the limit of long wavelength, $\delta\rho(x')$ changes very slowly under the integration and consequently K_0 can be approximated as a delta function to convert the integral equation into a differential one. Therefore, Eq. 7.12 takes the form,

$$\omega^2\delta\rho(\tilde{x}) + 2\pi\frac{\hbar^2\pi}{m^2U}\frac{E_0^2}{d^2}\left[\frac{d}{d\tilde{x}}\tilde{x}^2\frac{d}{d\tilde{x}} - q^2\tilde{x}^2\right]D\delta\rho(\tilde{x}) = 0 \tag{7.21}$$

Eq. 7.21 is just the radial Schrödinger equation in 3D. By letting $2\pi^2\hbar^2E_0^2D/(m^2d^2U) = C'^2$ and dividing the equation by C'^2 we get,

$$\tilde{x}^2\frac{d^2}{d\tilde{x}^2}\delta\rho(\tilde{x}) + 2\tilde{x}\frac{d}{d\tilde{x}}\delta\rho(\tilde{x}) + \left[\frac{\omega^2}{C'^2} - q^2\tilde{x}^2\right]\delta\rho(\tilde{x}) = 0$$

let $\delta\rho(\tilde{x}) = r(\tilde{x})/\tilde{x}$ and $q\tilde{x} = \zeta$ to get,

$$\frac{d^2}{d\zeta^2}r(\zeta) + \frac{\omega^2}{C'^2\,\zeta^2}r(\zeta) = r(\zeta)$$

Eq. 7.22 has the form of one-dimensional Schrödinger equation with potential $-\omega^2/(C'^2\zeta^2)$ and energy -1. To regularize the singularity at $\zeta = 0$, we define a cutoff at $\zeta = qa$ such that the potential is finite at the origin. A solution to the Schrödinger equation with the regularized potential is obtained by using the WKB approximation through enforcing the Bohr-Sommerfeld condition,

$$\int_{\zeta_1}^{\zeta_2} d\zeta\sqrt{\frac{\omega^2}{C'^2\,\zeta^2} - 1} = \pi\left(n + \frac{1}{2}\right) \tag{7.22}$$

where ζ_1 and ζ_2 are the turning points at which the kinetic energy is zero and thus, the total energy is equal to the potential energy $E = -\omega^2/(C'^2\,\zeta^2) \Rightarrow 1 = \omega^2/(C'^2\,\zeta_2^2)$. Since

the integrand is an even function in ζ and the integration limits are $\zeta_2 = -\zeta_1 = \omega/C^{'}$ we can write the quantization condition as,

$$2\int_{qa}^{\omega/C^{'}} d\zeta \sqrt{\frac{\omega^2}{C'^2\,\zeta^2} - 1} = \pi\left(n + \frac{1}{2}\right) \tag{7.23}$$

where $\omega \gg C^{'}$ because the Bohr-Sommerfeld condition, Eq. 7.23, is satisfied in the classical region where the energy is greater than the potential energy $E > V(x) \Rightarrow -1 \gg -\omega^2/(C'^2\,\zeta^2)$ for all ζ; therefore, $1 \ll \omega/C'$. After simplifying the integrand in Eq. 7.23 by ignoring the 1 under the square root, integrating and taking $|\ln(qa)| \gg \ln(\omega/C')$, we solve for ω to obtain the eigenfrequencies,

$$\omega^2 = \frac{\pi^4 E_0^2 D}{2m^2 d^2 U \ln^2(qa)}\left(n + \frac{1}{2}\right)^2 \tag{7.24}$$

where $n = 0, 1, 2, 3....$ It is worth noting that the spectrum has weak dependence on the wavenumber q.

In conclusion, the three cases of the gated bilayer graphene showed similarities in that the spectrum was linear in E_0 indicating strong dependence on the magnitude and direction of the electric field, and showed differences in the wave number (q) dependence ranging from no dependence at all in the short wavelength limit to square-root proportionality in the intermediate limit. Also, the three cases showed different proportionality to parameters like d, D, h and U.

CHAPTER 8

CONCLUSION

Plasmon propagation in gapless and band gapped bilayer graphene was investigated to find the dependence of plasmon frequencies on the applied electric field E_0 and wave number q. Throughout the calculations, the width of the flake $2d$ was assumed much smaller than its length that was taken to be infinity, and the distance between graphene layers was ignored. The in-plane electric field E_0 induced charge density $\rho_0(x)$ producing a p-n junction along the length of the bilayer. The nonhomogeneous induced charge density along the flake's width enforced charge fluctuations to propagate along the length of the bilayer giving rise to one-dimensional plasmons.

The band structure of bilayer graphene was calculated quantum mechanically within the tight binding model in Chapter 2. In the non-gated bilayer graphene case, the energy was quadratic in momentum and the band structure was gapless. In gated bilayer graphene, the additional gate introduced a perpendicular electric field that broke the inversion symmetry between the two layers making one layer at a higher potential than the other one and consequently leading to the opening of a gap in the bilayer band structure. The energy dispersion relations in both cases were used in the derivation of the chemical potential in the Thomas-Fermi equation, and in the computation of the density of states and Fermi velocity in the hydrodynamic equation, Eq. 5.9.

Few constraints, $\sqrt{e/E_0} \ll \lambda$, d, had to be satisfied to allow the semiclassical description of charge carriers as continuous fluid of fermions. In the case of gated bilayer graphene an additional constraint, $E_0 > (U/ed)$, had to be satisfied to establish charge distribution across the flake. From the Thomas-Fermi integral equation we obtained the equilibrium charge density $\rho_0(x)$, Eq. 6.7 and Eq. 7.5. By substituting $\rho_0(x)$ into the hydrodynamics equations we set up the eigenvalue integro-differential equations, Eq. 6.15 and Eq. 7.12, that were analyzed for limiting cases.

In gapless bilayer graphene, we considered two limiting cases for the spectrum analysis. In the limit of short wavelength, an exact solution was found, Eqs. 6.26, 6.27, 6.32 and 6.33,

that exhibited pathological behavior, such as infinite oscillations very close to the p-n junction and continuous spectrum. The oscillatory behavior was regularized by introducing a cutoff at which the eigenfunction was set to zero. The introduced cutoff served to discretize the eigenfrequencies that showed very weak dependence on q, see Eq. 6.41. Unexpectedly, even modes of plasmons had higher energies than odd ones in the short wavelength limit. In the limit of long wavelength that order was reversed with the lowest mode was found to be even and gapless (vanishing eigenfrequency at zero wavenumber $q = 0$). The reversal of the order of even and odd modes in terms of frequency as we go from long wavelengths to short wavelengths limits was unusual; it was explained as a consequence of the greater decrease of the electric field in odd modes than in even ones in the intermediate range $\lambda \sim d$. That decrease in the electric field was due to the checkerboard pattern of charge distribution that was composed of sequence of quadrupoles (weaker electric field) in odd modes, and of two dipoles in even ones. More interesting was the finding that the first odd mode $(1-)$ is forbidden in the limit $q \to 0$, i.e., the first odd mode that could be established in that limit has three nodes across the width of the flake instead of just one. This odd mode $(1-)$ reappears as we go to shorter wavelengths. In both limits, the scaling factor was proportional to $\sqrt{E_0/(m\,d)}$ showing that plasmon frequencies can be controlled by modifying the magnitude of the applied electric field.

In the gated bilayer graphene, the integro-differential equation was much more complicated. The problem was approached by assuming that the width of the flake is much greater than the plasmon wavelength λ, the distance between the bilayer and the gate (D), and the width of the neutral strip $2h$. Three limiting cases were considered for different relative lengths of h, D and λ. In all cases the scaling was linear in E_0, see Eqs. 7.17, 7.19 and 7.24, indicating stronger dependence of plasmon frequency on the applied electric field in band gapped bilayer than in gapless case. Also, the three cases had different dependence on the wave number q ranging from no dependence at all to linear dependence.

APPENDIX A

DENSITY OF STATES IN 2D

Let's consider the $2p_z$ electrons in bilayer graphene at temperature $T = 0$ K as an example of a system of N electrons in the ground state. Because the electrons are fermions, every state is occupied by only one electron; hence, the N electrons occupy the lowest N states starting from the zero-point energy up to the Fermi energy ϵ_F . Occupied orbitals can be represented by points, in k-space, confined within a circle in 2D systems, see Fig. A.1, or within a sphere in 3D materials. The radius of that circle (sphere) is the Fermi wavevector k_F such that $\epsilon_F = \hbar^2 k_F^2/(2m)$, where $\hbar k_F$ is the Fermi momentum. The total number of occupied orbitals is the ratio between the area (volume) of the circle (sphere) in k-space πk_F^2, and the area (volume) occupied by each k-point $2\pi/A$. Thus, in bilayer graphene the number of electrons (or states)is,

$$N = 4\frac{\pi k_F^2}{(2\pi)^2/A} = \frac{A\,k_F^2}{\pi} \tag{A.1}$$

where A is the area of the two dimensional graphene lattice. The factor of four is due to the fact that each point within the circle in k-space represents one orbital that is occupied by four electrons; two to account for spin and two more electrons for two parabola below and above the x-axis in the bilayer graphene band structure . Therefore, the number density is,

$$n = \frac{N}{A} = \frac{k_F^2}{\pi} = \frac{p_F^2}{\pi\hbar^2} \tag{A.2}$$

where $n(x)$ and $p_F(x)$ are x dependent. Hence, in bilayer graphene the number density or equivalently charge density and Fermi momentum are functions of the distance from the p-n junction. The density of states is defined as the number of orbitals per unit energy range $d\epsilon$, i.e.,

$$\nu(\epsilon) = \frac{dN}{d\epsilon} \tag{A.3}$$

In monolayer graphene the density of states can be derived from Eqs. A.3 and Eq. 2.20 as follows,

$$N = \frac{A\,k_F^2}{\pi} = \frac{A\,\epsilon_F^2}{v_F^2\hbar^2\pi}$$

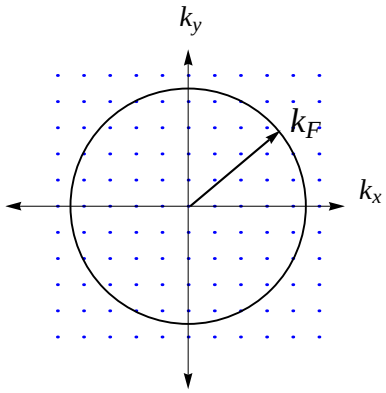

Figure A.1: k-space in 2D. Each point (k_x,k_y) inside the circle of radius k_F represents four filled orbitals, two orbitals to account for spin and two for the two parabola in the band structure of bilayer graphene

to obtain

$$\nu(\epsilon) = \frac{dN}{d\epsilon} = \frac{2A\,\epsilon_F}{v_F^2\hbar^2\pi} = \frac{2A\,v_F p_F}{v_F^2\hbar^2\pi} = \frac{2A\,p_F}{v_F\hbar^2\pi} \tag{A.4}$$

where we used Eq. 2.20 to substitute for the energy $\epsilon_F = v_F p_F$. Similarly, the density of states in bilayer graphene is,

$$\nu(\epsilon) = \frac{dN}{d\epsilon} = \frac{d}{d\epsilon}\frac{Ak_F^2}{\pi} = \frac{A}{\pi}\frac{d}{d\epsilon}\frac{2\,m\,\epsilon}{\hbar^2} = \frac{2\,m\,A}{\pi\hbar^2} = \frac{2A\,p_F}{v_F\hbar^2\pi} \tag{A.5}$$

where $\epsilon = p^2/2m$, see Eq. 2.37, and $m = p/v$.

APPENDIX B

EVALUATION OF INTEGRALS

B.1 Integral in Eq. 6.14

Multiply $\int_{-\infty}^{\infty} dy' \frac{e^{iqy'}}{\sqrt{(x-x')^2+(y-y')^2}}$ by $1 = e^{iq(y-y)}$ to obtain,

$$\int_{-\infty}^{\infty} dy' \frac{e^{iqy'}}{\sqrt{(x-x')^2+(y-y')^2}} = e^{iqy} \int_{-\infty}^{\infty} dy' \frac{e^{iq(y'-y)}}{\sqrt{(x-x')^2+(y-y')^2}}$$

$$= e^{iqy} \left[\int_{-\infty}^{\infty} dy' \frac{\cos[q(y'-y)]}{\sqrt{(x-x')^2+(y-y')^2}} + \underbrace{i \int_{-\infty}^{\infty} dy' \frac{\sin[q(y'-y)]}{\sqrt{(x-x')^2+(y-y')^2}}}_{0} \right]$$

$$= 2e^{iqy} \int_{0}^{\infty} dy' \frac{\cos[q(y'-y)]}{\sqrt{(x-x')^2+(y-y')^2}}$$

The second term in the second line vanishes because it is an odd function in y. let $|y-y'| = |x-x'|t \Rightarrow dy' = dt|x-x'|$ for some variable t, the integral becomes,

$$2e^{iqy} \int_{0}^{\infty} dt \frac{\cos[qt(x-x')]|x-x'|}{\sqrt{(x-x')^2+(y-y')^2}} = 2e^{iqy} \int_{0}^{\infty} dt \frac{\cos[qt(x-x')]}{\sqrt{1+t^2}} = 2e^{iqy} K_0(q|x-x'|) \tag{B.1}$$

where $K_0(x) = \int_0^{\infty} dt \cos(xt)/\sqrt{(t^2+1)}$.

B.2 Integral in Eq. 6.20

By differentiating the integral,

$$\int_{-\infty}^{\infty} d\xi' e^{i(k'-k)\xi'} = 2\pi\delta(k'-k)$$

we get,

$$\frac{\partial}{\partial k'} \int_{-\infty}^{\infty} d\xi' e^{i(k'-k)\xi'} = 2\pi \frac{\partial}{\partial k'} \delta(k'-k)$$

Because the integration is taken over ξ', the differentiation operator can operate on the integrand inside the integral sign. Therefore,

$$\int_{-\infty}^{\infty} d\xi' \xi' e^{i(k'-k)\xi'} = -2\pi i \frac{\partial}{\partial k'} \delta(k'-k) \tag{B.2}$$

B.3 Integral in Eq. 6.22

Because the integral $2i\int_0^\infty d\xi \sin[(k-k')\xi]$ does not have a determinate value, we use the substitution,

$$2i\int_0^\infty d\xi \sin[(k-k')\xi] = \int_0^\infty d\xi[e^{i(k-k')\xi} - e^{i(k'-k)\xi}]$$

and regularize the integrand by multiplying to it an infinitesimal exponentially decreasing term $e^{-\epsilon\xi}$ to obtain,

$$\begin{aligned}\lim_{\epsilon\to 0}\int_0^\infty d\xi[e^{i(k-k')\xi-\epsilon\xi} - e^{i(k'-k)\xi-\epsilon\xi}] &= \lim_{\epsilon\to 0}\left[\frac{e^{i(k-k')\xi-\epsilon\xi}}{i(k-k')-\epsilon} - \frac{e^{i(k'-k)\xi-\epsilon\xi}}{i(k'-k)-\epsilon}\right]_0^\infty \\ &= \lim_{\epsilon\to 0}\left[\frac{-1}{i(k-k')-\epsilon} + \frac{1}{i(k'-k)-\epsilon}\right] \\ &= \frac{-2}{i}\frac{1}{(k-k')} = \frac{2i}{(k-k')} \end{aligned} \tag{B.3}$$

B.4 Integral in Eq. 7.10

Multiply the integrand by $1 = e^{iq(y-y)}$ to obtain,

$$\begin{aligned}&\int_{-\infty}^\infty dy' \frac{e^{iqy't}}{\sqrt{(x-x')^2+(y-y')^2+4D^2}} = e^{iqy}\int_{-\infty}^\infty dy' \frac{e^{iq(y'-y)}}{\sqrt{(x-x')^2+(y-y')^2+4D^2}} \\ &= e^{iqy}\left[\int_{-\infty}^\infty dy' \frac{\cos[q(y'-y)]}{\sqrt{(x-x')^2+(y-y')^2+4D^2}} + \underbrace{i\int_{-\infty}^\infty dy' \frac{\sin[q(y'-y)]}{\sqrt{(x-x')^2+(y-y')^2+4D^2}}}_{0}\right] \\ &= 2e^{iqy}\int_0^\infty dy' \frac{\cos[q(y'-y)]}{\sqrt{(x-x')^2+(y-y')^2+4D^2}}\end{aligned} \tag{B.4}$$

The second term in the second line vanishes because it is an odd function in y. Let's define $|y-y'| = \sqrt{(x-x')^2+4D^2}\,t \Rightarrow dy' = dt\sqrt{(x-x')^2+4D^2}$ and use the relation $K_0(x) = \int_0^\infty dt \cos(xt)/\sqrt{(t^2+1)}$ to simplify Eq. B.4 to,

$$\begin{aligned}&2e^{iqy}\int_0^\infty dt \frac{\cos[qt\sqrt{(x-x')^2+4D^2}]\sqrt{(x-x')^2+4D^2}}{\sqrt{(x-x')^2+(y-y')^2+4D^2}} \\ &= 2e^{iqy}\int_0^\infty dt \frac{\cos[qt\sqrt{(x-x')^2+4D^2}]}{\sqrt{1+t^2}} = 2e^{iqy}K_0(q\sqrt{(x-x')^2+4D^2})\end{aligned}$$

Therefore,

$$\int_{-\infty}^\infty dy' \frac{e^{iqy'}}{\sqrt{(x-x')^2+(y-y')^2+4D^2}} = 2e^{iqy}K_0(q\sqrt{(x-x')^2+4D^2}) \tag{B.5}$$

APPENDIX C

COMPUTATION OF EIGEN-FUNCTIONS AND EIGENVALUES

In the limit of short wavelength, we obtained the integro-differential equation in k-space, see Section 6.3 Eq 6.23,

$$\lambda\,\delta\tilde{\rho}(q) = -P\int_{-\infty}^{\infty} dk\,\frac{\sqrt{1+k^2}\,\delta\tilde{\rho}'(k)}{k-q} \tag{C.1}$$

where $\lambda = \omega^2\, m\, d/(2\sqrt{2\pi}eE_0)$ and P stands for principle value. This equation is an eigenvalue problem, and in this section we introduce the detailed calculations to solve for the eigenfunctions and eigenfrequencies.

Let's write Eq. C.1 in terms of hyperbolic functions by making the following substitutions,

$$k = \sinh(u) \Rightarrow dk = \cosh(u)\,du \Rightarrow \frac{d\,\delta\tilde{\rho}(k)}{dk} = \frac{1}{\cosh(u)}\frac{d\,\delta\tilde{\rho}(u)}{du} = \frac{\delta\tilde{\rho}'(u)}{\cosh(u)},$$

and

$$q = \sinh(t).$$

Therefore, Eq.C.1 becomes,

$$\begin{aligned}\lambda\,\delta\tilde{\rho}(t) &= -P\int_{-\infty}^{\infty}\cosh(u)\,du\,\frac{\sqrt{1+\sinh^2(u)}\,\delta\tilde{\rho}'(u)}{\cosh(u)\,[\sinh(u)-\sinh(t)]}\\ &= -P\int_{-\infty}^{\infty} du\,\frac{\cosh(u)\,\delta\tilde{\rho}'(u)}{[\sinh(u)-\sinh(t)]}\end{aligned} \tag{C.2}$$

We propose two functions, for even and odd solutions, and insert them into the integro-differential equation to test if they actually work. Let's assume that $\delta\tilde{\rho}'$ takes the following forms,

$\delta\tilde{\rho}(u) = \cos(\alpha u)$ for even solutions $\Rightarrow \delta\tilde{\rho}'(u) = -\alpha\sin(\alpha u)$, and

$\delta\tilde{\rho}(u) = \sin(\alpha u)$ for odd solutions $\Rightarrow \delta\tilde{\rho}'(u) = \alpha\cos(\alpha u)$

In the following two sections we will prove that the proposed functions actually constitute a solution to Eq. C.1

C.1 Even Solutions

By inserting the even solution $\delta\tilde{\rho}(u) = \cos(\alpha u)$ into Eq. C.2 we obtain,

$$P\int_{-\infty}^{\infty} du\,\frac{\cosh(u)\,\delta\tilde{\rho}'(u)}{[\sinh(u)-\sinh(t)]} = -P\int_{-\infty}^{\infty} du\,\frac{\alpha\cosh(u)\,\sin(\alpha u)}{[\sinh(u)-\sinh(t)]}$$
$$= \frac{i\alpha}{2}\left[P\int_{-\infty}^{\infty} du\,\frac{\cosh(u)\,e^{i\alpha u}}{[\sinh(u)-\sinh(t)]} - P\int_{-\infty}^{\infty} du\,\frac{\cosh(u)\,e^{-i\alpha u}}{[\sinh(u)-\sinh(t)]}\right] \qquad \text{(C.3)}$$

To compute the first and second integrals, we perform contour integration. Therefore, we move to the complex plane where we take $z = u + iv$ and t as complex variables. The contour integral of the first term of Eq. C.3 in complex plane is taken over the upper half plane because $e^{i\alpha z} = e^{i\alpha(u+iv)} = e^{i\alpha u}e^{-\alpha\, v}$ vanishes as $v \to \infty$. Let's evaluate the first term in Eq. C.3,

$$\begin{aligned}\oint dz\,\frac{\cosh(z)\,e^{i\alpha z}}{[\sinh(z)-\sinh(t)]} &= \int_{C_1} dz\,\frac{\cosh(z)\,e^{i\alpha z}}{[\sinh(z)-\sinh(t)]} + \int_{C_2} dz\,\frac{\cosh(z)\,e^{i\alpha z}}{[\sinh(z)-\sinh(t)]} \\ &+ \underbrace{\int_{-\infty}^{t-\epsilon} du\,\frac{\cosh(u)\,e^{i\alpha u}}{[\sinh(u)-\sinh(t)]} + \int_{t+\epsilon}^{\infty} du\,\frac{\cosh(u)\,e^{i\alpha u}}{[\sinh(u)-\sinh(t)]}}_{I_1} \\ &= 2\pi i\sum \text{residues in upper half-plane} \qquad \text{(C.4)}\end{aligned}$$

where the first term is zero because the integrand vanishes over the infinite semicircle C_1, see Fig. C.1, $I_1 = P\int_{-\infty}^{\infty} du\,\cosh(u)\,e^{i\alpha u}/\,(\sinh(u)-\sinh(t))$ and the contour integral over C_2 is equal to $-i\pi e^{i\alpha t}$. Therefore, the expression of Eq. C.4 simplifies to,

$$-i\pi e^{i\alpha t} + I_1 = 2\pi i\sum_{n=1,2,3..} e^{i\alpha(t+2\,n\pi i)} + 2\pi i\sum_{n=0,1,2...} e^{i\alpha[(2n+1)\,\pi i - t]}$$

The first term on the L.H.S is the residue due to the singularity on the real axis and the second term is the principle value of the integral we want to evaluate. The R.H.S is the sum of residues due to the singular points inside the contour. Hence, I_1 becomes,

$$\begin{aligned} I_1 &= i\pi e^{i\alpha t} + 2\pi i\,e^{i\alpha t}\sum_{n=1,2,3..} e^{-2\,n\pi\alpha} + 2\pi i\,e^{-i\alpha t}\sum_{n=0,1,2...} e^{-(2n+1)\,\pi\alpha} \\ &= i\pi e^{i\alpha t} + 2\pi i\,e^{i\alpha t}\frac{e^{-2\pi\alpha}}{1-e^{-2\pi\alpha}} + 2\pi i\,e^{-i\alpha t}e^{-\pi\alpha}\left[\frac{1}{1-e^{-2\pi\alpha}}\right] \\ &= \frac{i\pi\,e^{i\alpha t}(e^{\pi\alpha} + e^{-\pi\alpha}) + 2\pi i\,e^{-i\alpha t}}{e^{\pi\alpha}-e^{-\pi\alpha}} \end{aligned} \qquad \text{(C.5)}$$

where we have used the geometric series

$$\sum_{n=0}^{\infty} x^n = 1/(1-x)$$

in the second line by replacing $x \to e^{-2\pi\alpha}$.

The second integral in Eq. C.3 is evaluated by taking the lower half contour C_3 because $e^{-i\alpha z} = e^{-i\alpha(u+iv)} = e^{-i\alpha u}e^{\alpha\, v}$ vanishes as $v \to -\infty$,

$$\begin{aligned}
\oint dz\, \frac{\cosh(z)\, e^{-i\alpha z}}{[\sinh(z) - \sinh(t)]} &= \int_{C_3} dz\, \frac{\cosh(z)\, e^{-i\alpha z}}{[\sinh(z) - \sinh(t)]} + \int_{C_2} dz\, \frac{\cosh(z)\, e^{-i\alpha z}}{[\sinh(z) - \sinh(t)]} \\
&+ \underbrace{\int_{-\infty}^{t-\epsilon} du\, \frac{\cosh(u)\, e^{-i\alpha u}}{[\sinh(u) - \sinh(t)]} + \int_{t+\epsilon}^{\infty} du\, \frac{\cosh(u)\, e^{-i\alpha u}}{[\sinh(u) - \sinh(t)]}}_{I_2} \\
&= 2\pi i \sum \text{residues in lower half-plane}
\end{aligned}$$

where the first term vanishes and $I_2 = P\int_{-\infty}^{\infty} du\, \cosh(u)\, e^{-i\alpha u}/\left(\sinh(u) - \sinh(t)\right)$. We obtain the following expression for I_2,

$$-i\pi e^{-i\alpha t} + I_2 = -2\pi i \sum_{n=0,1,2,3..} e^{-i\alpha(t - 2\, n\pi i)} - 2\pi i \sum_{n=0,1,2...} e^{-i\alpha[-(2n+1)\, \pi i - t]}$$

$$\begin{aligned}
\Rightarrow I_2 &= i\pi e^{-i\alpha t} - 2\pi i\, e^{-i\alpha t} \sum_{n=0,1,2,3..} e^{-2\, n\pi\alpha} - 2\pi i\, e^{i\alpha t} \sum_{n=0,1,2...} e^{-(2n+1)\, \pi\alpha} \\
&= i\pi e^{-i\alpha t} - 2\pi i\, e^{-i\alpha t}\left[\frac{1}{1 - e^{-2\pi\alpha}}\right] - 2\pi i\, e^{i\alpha t} e^{-\pi\alpha}\left[\frac{1}{1 - e^{-2\pi\alpha}}\right] \\
&= \frac{-i\, \pi e^{-i\alpha t}\, (e^{\pi\alpha} + e^{-\pi\alpha}) - 2\pi i\, e^{i\alpha t}}{e^{\pi\alpha} - e^{-\pi\alpha}} \qquad \text{(C.6)}
\end{aligned}$$

By subtracting the principle value I_2 from I_1,

$$\begin{aligned}
\Rightarrow I_1 - I_2 &= \frac{i\pi\, e^{i\alpha t}(e^{\pi\alpha} + e^{-\pi\alpha}) + 2\pi i\, e^{-i\alpha t}}{e^{\pi\alpha} - e^{-\pi\alpha}} - \frac{-i\, \pi e^{-i\alpha t}\, (e^{\pi\alpha} + e^{-\pi\alpha}) - 2\pi i\, e^{i\alpha t}}{e^{\pi\alpha} - e^{-\pi\alpha}} \\
&= \frac{i\, \pi\, e^{i\alpha t}\, [e^{\pi\alpha} + e^{-\pi\alpha} + 2] + i\, \pi\, e^{-i\alpha t}\, [e^{\pi\alpha} + e^{-\pi\alpha} + 2]}{e^{\pi\alpha} - e^{-\pi\alpha}} \\
&= \frac{i\, \pi\, \left[e^{i\alpha t} + e^{-i\alpha t}\right]\, \left[e^{\pi\alpha/2} + e^{-\pi\alpha/2}\right]^2}{e^{\pi\alpha} - e^{-\pi\alpha}}
\end{aligned}$$

and doing the following substitutions,

$$\begin{aligned}
&\left[e^{\pi\alpha/2} + e^{-\pi\alpha/2}\right]^2 = 4\cosh^2(\pi\alpha/2) \\
&e^{i\alpha t} + e^{-i\alpha t} = 2\cos(\alpha t) \\
&e^{\pi\alpha} - e^{-\pi\alpha} = 2\sinh(\pi\alpha) = 4\sinh(\pi\alpha/2)\cosh(\pi\alpha/2)
\end{aligned}$$

we find the solution to Eq. C.3 to be,

$$P\int_{-\infty}^{\infty} du\, \frac{\cosh(u)\, \delta\tilde{\rho}'(u)}{[\sinh(u) - \sinh(t)]} = \frac{i\, \alpha}{2}[I_1 - I_2] = \frac{-\pi\, \alpha}{\tanh(\pi\, \alpha/2)} \cos(\alpha\, t) \qquad \text{(C.7)}$$

where α can take any positive real number. The coefficient $-\pi\, \alpha/\tanh(\pi\, \alpha/2)$ is proportional to the eigenvalues and $\delta\tilde{\rho}(u) = \cos(\alpha u)$ constitute an infinite set of even eigenfunctions to the integro-differential equation.

C.2 Odd Solutions

By inserting the odd solution $\delta\tilde{\rho}(u) = \sin(\alpha u)$ into Eq. C.2 we obtain,

$$\begin{aligned} P\int_{-\infty}^{\infty} du\, \frac{\cosh(u)\,\delta\tilde{\rho}'(u)}{[\sinh(u)-\sinh(t)]} &= P\int_{-\infty}^{\infty} du\, \frac{\alpha\cosh(u)\,\cos(\alpha u)}{[\sinh(u)-\sinh(t)]} \\ &= \frac{\alpha}{2}\left[P\int_{-\infty}^{\infty} du\, \frac{\cosh(u)\,e^{i\alpha u}}{[\sinh(u)-\sinh(t)]} + P\int_{-\infty}^{\infty} du\, \frac{\cosh(u)\,e^{-i\alpha u}}{[\sinh(u)-\sinh(t)]}\right] \\ &= \frac{\alpha}{2}\,[I_1+I_2] \end{aligned} \tag{C.8}$$

The principle values were already evaluated in the last section. Therefore, by adding Eqs. C.5 and C.6,

$$\begin{aligned} I_1+I_2 &= \frac{i\pi\, e^{i\alpha t}(e^{\pi\alpha}+\,e^{-\pi\alpha}) + 2\pi i\, e^{-i\alpha t}}{e^{\pi\alpha}-e^{-\pi\alpha}} + \frac{-i\,\pi e^{-i\alpha t}\,(e^{\pi\alpha}+e^{-\pi\alpha}) - 2\pi i\, e^{i\alpha t}}{e^{\pi\alpha}-e^{-\pi\alpha}} \\ &= \frac{i\,\pi\, e^{i\alpha t}\,[e^{\pi\alpha}+e^{-\pi\alpha}-2] - i\,\pi\, e^{-i\alpha t}\,[e^{\pi\alpha}+e^{-\pi\alpha}-2]}{e^{\pi\alpha}-e^{-\pi\alpha}} \\ &= \frac{i\,\pi\,\left[e^{i\alpha t}-e^{-i\alpha t}\right]\left[e^{\pi\alpha/2}-e^{-\pi\alpha/2}\right]^2}{e^{\pi\alpha}-e^{-\pi\alpha}} \end{aligned}$$

and using the following substitutions,

$$\begin{aligned} \left[e^{\pi\alpha/2}-e^{-\pi\alpha/2}\right]^2 &= 4\sinh^2(\pi\alpha/2) \\ e^{i\alpha t}-e^{-i\alpha t} &= 2\,i\,\sin(\alpha t) \\ \left[e^{\pi\alpha}-e^{-\pi\alpha}\right] &= 4\sinh(\pi\alpha/2)\cosh(\pi\alpha/2) \end{aligned}$$

we obtain,

$$P\int_{-\infty}^{\infty} du\, \frac{\cosh(u)\,\delta\tilde{\rho}'(u)}{[\sinh(u)-\sinh(t)]} = \frac{\alpha}{2}[I_1+I_2] = -\pi\,\alpha\tanh(\pi\,\alpha/2)\sin(\alpha\,t) \tag{C.9}$$

where α can take any positive real number. The coefficient, $-\pi\,\alpha\tanh(\pi\,\alpha/2)$, is proportional to the eigenvalue corresponding to the odd eigenfunction $\delta\tilde{\rho}(u) = \sin(\alpha u)$ for some value of α.

C.3 Fourier Transform of Eigenfunctions

Because we are interested in the plasmon wave profile in real space we will perform the inverse Fourier transform on Eq. C.1. Therefore, the charge fluctuations in real space is,

$$\delta\rho_\alpha^+(\xi) = \int_{-\infty}^{\infty} \frac{dk}{\sqrt{2\pi}} e^{i\xi k}\tilde{\rho}_\alpha^+(k) \tag{C.10}$$

where the superscript + denotes even solutions,

$$\tilde{\rho}_\alpha^+(k) = \cosh(\pi\alpha/2)\cos\left(\alpha\,\mathrm{arcsinh}(k)\right) \tag{C.11}$$

where u is replaced with $\text{arcsinh}(k)$. Multiplying by the coefficient $\cosh(\pi\alpha/2)$ is justified in Section 6.3.1. Let $k = \sinh(x) \Rightarrow dk = \cosh(x)dx$ and integrate by parts to get,

$$\begin{aligned}\delta\rho^+_\alpha(\xi) &= \frac{\cosh(\pi\alpha/2)}{\sqrt{2\pi}} \int_{-\infty}^{\infty} \underbrace{dx\, e^{i\xi\, \sinh(x)} \cosh(x)}_{dg} \underbrace{\cos(\alpha x)}_{f} \\ &= \frac{\cosh(\pi\alpha/2)}{\sqrt{2\pi}} \left(\left[\frac{e^{i\xi \sinh(x)} \cos(\alpha x)}{i\xi} \right]_{-\infty}^{\infty} + \frac{\alpha}{i\xi} \int_{-\infty}^{\infty} dx e^{i\xi\, \sinh(x)} \sin(\alpha x) \right) \qquad \text{(C.12)}\end{aligned}$$

The first term vanishes, the second term is evaluated using contour integration. The contour taken to simplify the integral is plotted in Fig. C.1(b). Therefore, the second term becomes,

$$\begin{aligned}\oint dz\, e^{i\xi\, \sinh(z)} \sin(\alpha z) = \lim_{R\to\infty} \Bigg[&\int_{-R}^{R} dx\, e^{i\xi\, \sinh(x)} \sin(\alpha x) \\ &+ \int_{R}^{-R} dx\, e^{i\xi\, \sinh(x+i\pi/2)} \sin(\alpha[x + i\pi/2]) \Bigg] = 0 \qquad \text{(C.13)}\end{aligned}$$

The contour integral is zero because there are no poles inside the contour and thus has zero residue. Also, the integrals over the vertical sections of the contour vanish because the integrand decays like $e^{-\cosh(x)}$ as $x \to \pm\infty$. By taking $R \to \infty$ the integral over the real axis takes the form,

$$\begin{aligned}\int_{-\infty}^{\infty} dx\, e^{i\xi\, \sinh(x)} \sin(\alpha x) &= \int_{-\infty}^{\infty} dx e^{i\xi\, \sinh(x+i\pi/2)} \sin(\alpha[x + i\pi/2]) \\ &= \int_{-\infty}^{\infty} dx\, e^{-\xi\, \cosh(x)} \left[\sin(\alpha x)\cos(i\alpha\,\pi/2) + \sin(i\alpha\,\pi/2)\cos(\alpha\, x)\right] \\ &= 2\int_{0}^{\infty} dx\, e^{-\xi\, \cosh(x)} \sin(i\alpha\,\pi/2)\cos(\alpha\, x) \qquad \text{(C.14)}\end{aligned}$$

where we used the identity $\sinh(x + iy) = \sinh(x)\cos(y) + i\cosh(x)\sin(y)$. The first term in the second line vanishes because the integrand is an odd function in x. The second integrand can be integrated from 0 to ∞ since it is an even function. By substituting $\sin(i\alpha\pi/2) = i\sinh(\alpha\pi/2)$ and $\cos(\alpha\, x) = \cosh(i\alpha\, x)$, Eq. C.10 becomes,

$$\begin{aligned}\delta\rho^+_\alpha(\xi) &= \frac{2\alpha\cosh(\pi\alpha/2)}{\xi\sqrt{2\pi}} \int_{0}^{\infty} dx\, e^{-\xi\, \cosh(x)} \sinh(\alpha\,\pi/2)\cosh(i\alpha\, x) \\ &= \frac{\alpha\sinh(\pi\alpha)}{\xi\sqrt{2\pi}} \int_{0}^{\infty} dx e^{-\xi\, \cosh(x)} \cosh(i\alpha\, x) \qquad \text{(C.15)}\end{aligned}$$

where we used the identity, $2\sinh(\pi\alpha/2)\cosh(\pi\alpha/2) = \sinh(\pi\alpha)$. By substituting,

$$\int_{0}^{\infty} dx\, e^{-\xi\, \cosh(x)} \cosh(i\alpha\, x) = K_{i\alpha}(\xi)\ ,\ \ Re(\xi) > 0 \qquad \text{(C.16)}$$

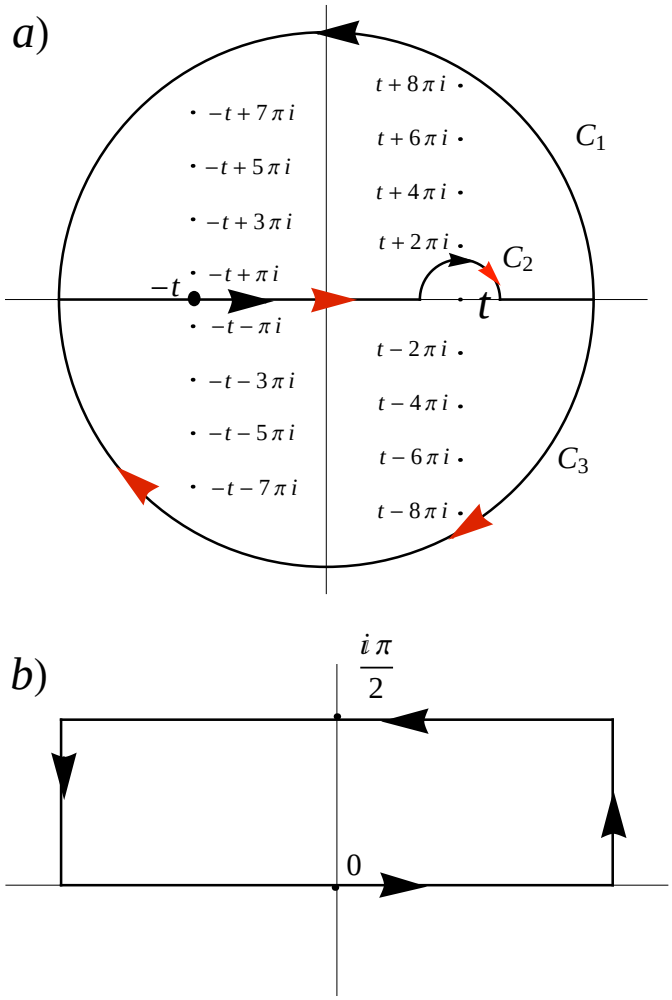

Figure C.1: Contours taken for calculating eigenfunctions and their inverse Fourier transform a) Three contours, C_1, C_2 and C_3, in the complex plane are used for the calculation of the integral Eq. C.1. The dots show singularities. b) Rectangular contour is traversed counter clockwise in the complex plane to evaluate the integral of Eq. C.10

the plasmon charge density in real space becomes,

$$\delta\rho_\alpha^+(\xi) = \frac{\alpha \sinh(\pi\alpha)}{|\xi|\sqrt{2\pi}} K_{i\alpha}(|\xi|) \tag{C.17}$$

The same procedure need not be repeated to find odd eigenfunctions in real space because even and odd solutions are related by Eq. 6.31.

REFERENCES

[1] Hubert B. Heersche, Pablo Jarillo-Herrero, Jeroen B. Oostinga, Lieven M. K. Vandersypen, and Alberto F. Morpurgo. Bipolar supercurrent in graphene. *Nature*, 446:56–59, 2006.

[2] C. Kittel. *Introduction to Solid State Physics, 7th edition.* John Wiley and Sons, United States of America, 1996.

[3] L. D. Landau and L. M. Lifshitz. *Quantum Mechanics Non-Relativistic Theory, Third Edition: Volume 3.* Butterworth-Heinemann, Russia, 1981.

[4] Edward McCann. Asymmetry gap in the electronic band structure of bilayer graphene. *Phys. Rev. B*, 74:161403–161407, 2006.

[5] E. Mishchenko. Many-body effects in the quasiparticle and collective properties of graphene. presentation, BYU Colloquium, Jan 26, 2011.

[6] E.G. Mishchenko, A.V. Shytov, and P. G. Silvestrov. Guided plasmons in graphene p-n junctions. *Phys. Rev. Lett*, 104:156806–1–156806–4, 2010.

[7] W. Luis Mochan. Plasmons. notes, Centro de Ciencias Fisicas, Universidad Nacional Autonoma de Mexico.

[8] Philip M. Morse and Herman Feshbach. *Methods Of Theoretical Physics.* McGraw-Hill Book Company, Inc, New York, 1953.

[9] A.H. Castro Neto, F. Guinea, N.M.R. Peres, K.S. Novoselov, and A.K. Geim. The electronic properties of graphene. *Review of Modern Physics*, 81:109–162, 2009.

[10] K. S. Novoselov, A. K. Geim, S. V. Morozov, D. Jiang, M. I. Katsnelson, I. V. Grigorieva, S. V. Dubonos, and A. A. Firsov. Two-dimensional gas of massless dirac fermions in graphene. *Nature*, 438:197–200, 2005.

[11] K. S. Novoselov, A. K. Geim, S. V. Morozov, D. Jiang, Y. Zhang, S. V. Dubonos, I. V. Grigorieva1, and A. A. Firsov. Electric field effect in atomically thin carbon films. *Science*, 306:666–669, 2004.

[12] Taisuke Ohta, Aaron Bostwick, Thomas Seyller, Karsten Horn, and Eli Rotenberg. Controlling the electronic structure of bilayer graphene. *Science*, 313:951–954, 2006.

[13] L. P. Pitaevskii and E.M. Lifshitz. *Physical Kinetics: Volume 10 (Course of Theoretical Physics).* Butterworth-Heinemann, Russia, 1981.

[14] A. D. Polyanin and A. V. Manzhirov. *Handbook of Integral Equations.* CRC Press, United States of America, 1998.

[15] T. A. Sedrakyan, E. G. Mishchenko, and M. E. Raikh. Planar array of semiconducting nanotubes in external electric field: Collective screening and polarizability. *Phys. Rev. B*, 74:235423–1–235423–9, 2006.

[16] Larry Spruch. Pedagogic notes on Thomas-Fermi theory (and on some improvements): atoms, stars, and the stability of bulk matter. *Rev. Mod. Phys*, 63:151–209, 1991.

[17] P. R. Wallace. The band theory of graphite. *Phys. Rev.*, 71:622–634, 1947.

[18] Feng Wang, Yuanbo Zhang, Chuanshan Tian, Caglar Girit, Alex Zettl, Michael Crommie, and Y. Ron Shen. Gate-variable optical transitions in graphene. *Science*, 320:206–209, 2008.

[19] J. R. Williams, L. DiCarlo, and C. M. Marcus. Quantum hall effect in a gate-controlled p-n junction of graphene. *Science*, 317:638–641, 2007.

[20] X. L. Yang, S. H. Guo, and F. T. Chan. Analytic solution of a two-dimensional hydrogen atom. i. nonrelativistic theory. *Physical Review A*, 43:1186–1196, 1991.

[21] Yuanbo Zhang, Yan-Wen Tan, Horst L. Stormer, and Philip Kim. Experimental observation of quantum Hall effect and Berry's phase in graphene. *Nature*, 438:201–204, 2005.

[22] Yuanbo Zhang, Tsung-Ta Tang, Caglar Girit, Zhao Hao, Michael C. Martin, Alex Zettl, Michael F. Crommie, Y. Ron Shen, and Feng Wang. Direct observation of a widely tunable bandgap in bilayer graphene. *Nature*, 459:820–823, 2009.